Reviews in Mineralogy & Geochemistry
Vol. 89 pp. 293-338, 2023

The Evolution of the Lunar Crust

Stephen M. Elardo[1,2,*], Carle M. Pieters[3,*], Deepak Dhingra[4], Kerri L. Donaldson Hanna[5,6], Timothy D. Glotch[7], Benjamin T. Greenhagen[8], Juliane Gross[9,10], James W. Head[3], Bradley L. Jolliff[11], Rachel L. Klima[8], Tomáš Magna[12], Francis M. McCubbin[10], Makiko Ohtake[13]

[1]The Florida Planets Lab, Department of Geological Sciences
University of Florida, Gainesville, FL 32611, USA
[2]Earth and Planets Laboratory, Carnegie Institution for Science
Washington, DC 20015, USA
[3]Department of Earth, Environmental, and Planetary Sciences
Brown University, Providence, RI 02912, USA
[4]Department of Earth Sciences, Indian Institute of Technology Kanpur
Kalyanpur, Kanpur 208016, Uttar Pradesh, India
[5]Atmospheric, Oceanic and Planetary Physics
University of Oxford, Oxford, UK
[6]Department of Physics, University of Central Florida
Orlando, FL 32816, USA
[7]Department of Geosciences, Stony Brook University
Stony Brook, NY 11794, USA
[8]Planetary Exploration Group, Johns Hopkins University Applied Physics Laboratory,
Laurel, MD 20723, USA
[9]Department of Earth and Planetary Sciences, Rutgers
The State University of New Jersey, Piscataway, NJ 08854 USA
[10]NASA Johnson Space Center, Houston, TX 77058, USA
[11]Department of Earth and Planetary Sciences and
the McDonnell Center for Space Sciences
Washington University in St. Louis, St. Louis, MO, 63130, USA
[12]Czech Geological Survey, Klárov 3
CZ-118 21 Prague 1, Czech Republic
[13]Institute of Space and Astronautical Science
Japan Aerospace Exploration Agency, 3-1-1 Yoshino-dai, Chuo-ku
Sagamihara, Kanagawa 252-5210, Japan

selardo@ufl.edu, carle_pieters@brown.edu

1. INTRODUCTION

1609 AD marked the beginning of the modern scientific exploration of the Moon's crust when Thomas Harriot and later Galileo Galilei made the first recorded maps of the nearside with telescopic observations. Galileo's observations in particular, using a more advanced telescope than was previously available, revealed lunar surface features and topography in detail, effectively refuting the view from Aristotle that the Moon was a perfect, translucent sphere. In 1840, John W. Draper made the first successful photographs of an astronomical object with his daguerreotype photos of the Moon. Increasingly higher quality images of the Moon, first with telescopes and later with spacecraft, served as the primary tool for exploring the Moon's crust (e.g., Baldwin 1963) until the first samples were returned to Earth by Neil A. Armstrong, Edwin E. "Buzz" Aldrin, and Michael Collins on July 24th 1969.

1529-6466/23/0089-0007$05.00 (print)
1943-2666/23/0089-0007$05.00 (online)
http://dx.doi.org/10.2138/rmg.2023.89.07

The return of samples by the American Apollo and Soviet Luna missions along with the first contemporaneous global observations of the crust naturally revolutionized what was known about the Moon and Earth's history. The rapidly-developed hypothesis of a lunar magma ocean (LMO; Smith et al. 1970; Wood et al. 1970) has endured over 50 years of scrutiny, and magma oceans have become the standard model for the differentiation of other terrestrial planets and large asteroids (e.g., Elkins-Tanton 2012). The giant impact hypothesis (Hartmann and Davis 1975; Cameron and Ward 1976) remains the model that best explains multiple observations about the state of the Earth-Moon system and the thermal state of the early Moon, though the details of the model continue to evolve (e.g., Canup 2004, 2012; Ćuk and Stewart 2012; Rufu et al. 2017; Lock et al. 2018; Nakajima and Stevenson 2018; Canup et al. 2023, this volume).

The Moon's anorthositic crust remains the most well-studied stagnant lid and the model of its formation via plagioclase flotation in the LMO has become a cornerstone for understanding crust formation on terrestrial planets and asteroids (e.g., Elkins-Tanton et al. 2005; Brown and Elkins-Tanton 2009; Vander Kaaden and McCubbin 2015) despite increasing evidence for complexity in its formation processes (Gaffney et al. 2023, this volume). Improvements in determining the ages of ferroan anorthosites (FANs) have presented issues for models of lunar formation, crustal petrogenesis, and crust formation on Earth. Newly dated and recently re-dated FANs have produced ages between 4.37 and 4.34 Ga and, in the context of the LMO model, this could be interpreted to represent the age of the Giant Impact or potentially a resetting event such as mantle overturn or a major impact (e.g., Borg et al. 2011, 2015; Boyet et al. 2015; Sio et al. 2020; Gaffney et al. 2023, this volume). This tight clustering of ages is significantly younger than previously determined and potentially less reliable ages (see Borg et al. 2015) for FANs in the ≥ 4.4 Ga range, and also presents issues for models of terrestrial crust formation. The oldest age yet measured for a zircon from the Jack Hills, Australia is 4.374 Ga (Valley et al. 2014), which suggests cool, wet conditions favorable to the development of continental crust at Earth's surface by that time (e.g., Wilde et al. 2001; Watson and Harrison 2005). Models have been proposed to reconcile these young lunar ages with petrologic observations (Elkins-Tanton et al. 2011; Maurice et al. 2020); however nearly identical isochron and model ages for the crust, mantle, and KREEP may be in conflict with protracted LMO crystallization models (e.g., Gaffney and Borg 2014; Borg et al. 2017). Recent advancements in understanding the formation of FANs and crustal chronology are reviewed in detail in Gaffney et al. (2023, this volume).

Most of lunar crustal evolution took place over the first ~500 Myr of lunar history during a period of high heat flux from the interior and high impact flux to the surface (Fig. 1). During this time major crust-building magmatic events created the lithologies of the magnesian-suite (Mg-suite), alkali-suite, silicic rocks, and at least some high-Al basalts. This was also a period of intense bombardment (Cohen et al. 2023; Hiesinger et al. 2023, both this volume), which effectively fractured much of the evolving crust and created a range of impact-derived lithologies. Although the most intense bombardment waned after ~500 Myr, the impact modification of the Moon's crust is ongoing. From ~3.9 Ga onward, the evolution of the crust was dominated by mare magmatism, secondary crust produced from re-melting of the mantle, and continued bombardment (Head et al. 2023, this volume), with both processes becoming less prominent with time. The peak in mare basaltic volcanic output occurred ~3.8–3.5 Ga, but the production of volumetrically significant flows continued sporadically until ~1.0 Ga (Hiesinger et al. 2000, 2011; Shearer et al. 2023, this volume) and small, isolated occurrences are suggested to be as young as 18 Ma (Braden et al. 2014), assuming certain crater retention properties.

Reviewing new understanding of and constraints on these periods of crustal evolution is the principal focus of this chapter through evidence extracted from ongoing and increasingly sophisticated studies of lunar samples as well as remarkable global and local compositional properties recently derived from a host of modern remote measurements. The first ~35 post-Apollo years of knowledge regarding the formation and evolution of the lunar crust are

well-summarized in *New Views of the Moon* (see Lucey et al. 2006; Shearer et al. 2006; Stöffler et al. 2006; Wieczorek et al. 2006). Since that time, new discoveries have been made by applying new and/or improved analytical techniques and ideas to long-studied samples (McCubbin et al. 2023, this volume) and new measurements of surface and atmospheric volatiles with modern instruments (Hurley et al. 2023, this volume). An international fleet of new missions including Kaguya/the Selenological and Engineering Explorer (SELENE), Chandrayaan-1, the Lunar Reconnaissance Orbiter (LRO), Chang'e-1, -2, -3, -4, and -5, including the Yutu 1 and 2 rovers, the Lunar Crater Observation and Sensing Satellite (LCROSS), the Gravity Recovery and Interior Laboratory (GRAIL), and the Lunar Atmosphere and Dust Environment Explorer (LADEE) have all returned rich new datasets and discoveries. Newly discovered lunar meteorites continue to provide a window into regions of the crust far from the restricted areas sampled in the 1970's (Joy et al. 2023, this volume). Here we review the past ~15 years of science regarding the evolution of the Moon's crust, during which time the planetary science community has witnessed a continuing renaissance in lunar science.

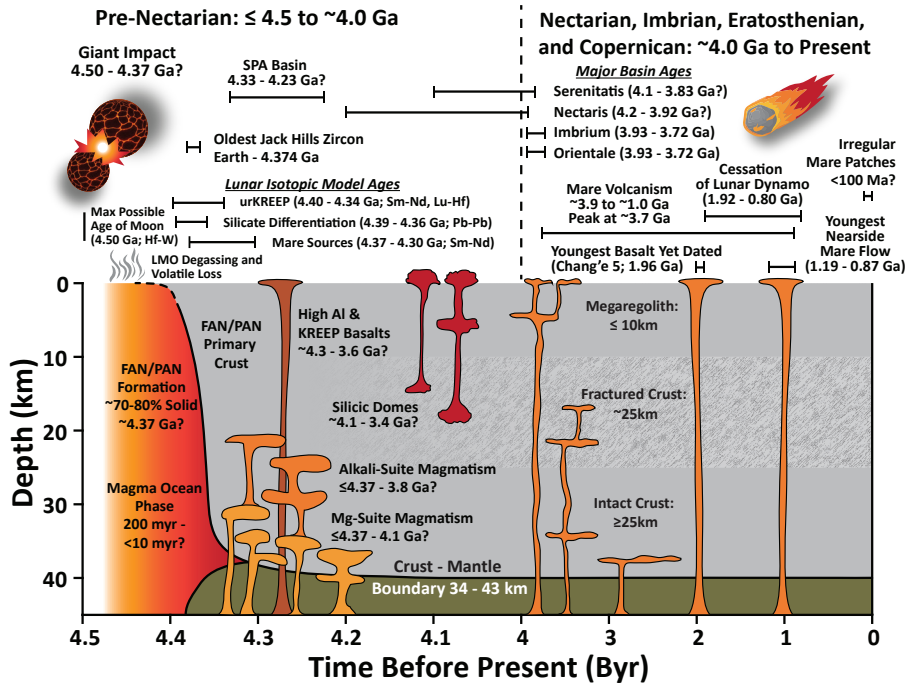

Figure 1. Schematic representation of the scale and age ranges for major events in the evolution of the lunar crust. Note the change in the time scale after 4 Ga. See text for references.

2. NEW SAMPLE OBSERVATIONS AND GLOBAL ASSESSMENTS

Since there are currently no known mantle xenoliths in the sample collection, all lunar samples represent either samples of the primary lunar crust, additions made to it, and/or modifications of it. Despite decades of studies, these samples are still revealing fundamental information about the composition and structure of the Moon and its geochemical and geophysical evolution from crust to core. The sample collection is continually expanding as new lunar meteorites are found and new missions such as Chang'e-5 return additional samples, giving lunar scientists access to regions of

the crust not visited by the Apollo and Luna missions. Additionally, observations from samples can now be placed in a global context by a tremendous increase in remote lunar observations. This is the result of data returned by a number of new missions sent to lunar orbit by an international community. The data from these missions bring new insights that complement and supplement both one another and sample observations. Each technical improvement in modern remote sensing instrumentation and data return has brought surprises along with a more sophisticated and deeper understanding of issues involved in crustal evolution of the Moon.

2.1. The global primary crust

The anorthositic composition of the Moon's primary crust has been established since the Apollo era through analyses of samples and remote observations. Investigations of fresh and relatively regolith-free locations using relatively high-spatial and -spectral resolution visible to near infrared (VNIR) spectrometers on orbiting spacecraft have unambiguously identified evidence for a global plagioclase-rich crust from the unique 1.25 mm absorption band of crystalline plagioclase (Ohtake et al. 2009; Pieters et al. 2009; Yamamoto et al. 2012b; Cheek et al. 2013; Donaldson Hanna et al. 2014). These regions have been identified as spectrally pure anorthosite, insofar as their spectra have minor to no detectable absorptions (near 1 and 2 mm) due to common mafic minerals, but nevertheless clearly exhibit the diagnostic 1.25 μm plagioclase absorption (Pieters et al. 2019). Ohtake et al. (2009) coined the acronym PAN (i.e., purest anorthosite) to describe regional anorthosite apparently with > 98 vol. % plagioclase. Although several orders of magnitude smaller in scale, there are FAN samples in the collection that support this observation.

PAN outcrops have been identified across the Moon and appear to be common in the Feldspathic Highlands Terrane (FHT; Jolliff et al. 2000) found primarily on the farside, where the thickest portions of the crust are observed (Yamamoto et al. 2012b; Donaldson Hanna et al. 2014). It is effectively nonexistent in the South-Pole Aitken (SPA) terrane. Global elemental and mineralogical maps show the surface composition of the farside FHT to be plagioclase-rich (> 80%) and poor in mafic materials (Prettyman et al. 2006; Crites and Lucey 2015; Peplowski et al. 2016). The small amount of mafic minerals that are observed in the FHT appear to be distinctly more magnesian than those observed on the lunar nearside highlands (Ohtake et al. 2012; Peplowski and Lawrence 2013; Crites and Lucey 2015). Thermal infrared spectral measurements of the largest PAN outcrops estimate the composition of the plagioclase observed as PAN to have a highly anorthitic composition (An# 94–98), consistent with FANs (Greenhagen et al. 2010; Donaldson Hanna et al. 2014), although more Na-rich compositions could possibly occur at a few sites (Greenhagen et al. 2010).

These distinctive PAN outcrops often are associated with some large craters with central peaks and massifs associated with basin-scale impacts (Fig. 2; Ohtake et al. 2009; Yamamoto et al. 2012b; Cheek et al. 2013; Kramer et al. 2013; Donaldson Hanna et al. 2014; Baker and Head 2015). The inner ring of Orientale represents perhaps the most pervasive regional exposure of PAN (Ohtake et al. 2009; Cheek et al. 2013). The remote identification of additional high albedo units with no detectable diagnostic absorptions (i.e., 'featureless') is thought to be shocked and/or altered forms of PAN (Cheek et al. 2013; Yamamoto et al. 2015; Pieters et al. 2018), although this has not been confirmed with current FAN samples. Low spatial resolution elemental abundance maps (Peplowski et al. 2016) suggest that the distribution of PAN/FAN in the upper crust might be more extensive than suggested solely from regional VNIR PAN detections. Combining the expected excavation depths of impact basins and craters with the GRAIL crustal thickness models (Wieczorek et al. 2013) suggests that the PAN/FAN primary crust layer could be ~50 km thick (Ohtake et al. 2009; Yamamoto et al. 2012b; Donaldson Hanna et al. 2014; Baker and Head 2015). The observations of PAN along the rings of such spatially large impact structures that would have uplifted materials from deep within the lunar crust suggest the original existence of a thick, global PAN/FAN layer. Examination of crustal

thickness where anorthositic materials and mafic minerals were identified in close proximity suggest that anorthosite, in particular PAN, is identified at all crustal thickness values while anorthositic materials in association with mafic minerals are more commonly found in regions with thinner crustal thickness values (Cahill et al. 2009; Donaldson Hanna et al. 2014).

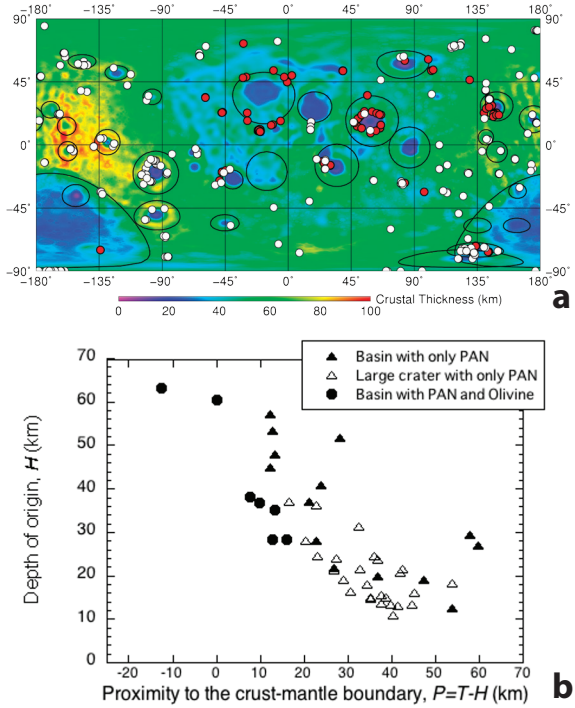

Figure 2. a) Example global distribution of pure anorthosite areas (PAN, **white dots**) and olivine-rich exposures (**red dots**) superimposed on a crustal thickness map (Yamamoto et al. 2012b). **Black circles** indicate location of major basins. **b)** Depth of origin of olivine and PAN-bearing materials at basin or craters as a function of crustal thickness.

2.2. Defining the Mg-suite: The earliest phase of post-LMO crust-building magmatism

All of the landed Apollo missions except Apollo 11 returned samples of coarse-grained plutonic rocks with a high Mg# (molar [Mg/Mg+Fe]x100) in mafic minerals, cumulus plagioclase, and mineral trace element compositions indicative of parental magmas with a signature of the KREEP reservoir (rich in potassium [K], rare earth elements [REE], phosphorus [P], and other geochemically-incompatible elements). These rocks, referred to as the Mg-suite, represent a period of magmatism contemporaneous with or immediately after the end of magma ocean crystallization that formed intrusions in the primary anorthositic crust (Fig. 1; e.g., Shearer et al. 2006, 2015b; Elardo et al. 2011, 2020; Carlson et al. 2014; Borg et al. 2017). These rocks have naturally become a primary focus of lunar science, as they provide a window into early crust-building processes and the thermal and chemical state of the Moon at the end of the LMO (Gaffney et al. 2023; Shearer et al. 2023, both this volume).

The sampled Mg-suite is composed of ultramafic, troctolitic, and noritic lithologies characterized by primitive olivine and pyroxene compositions ranging in Mg# from ~78 to 91, and up to 96 within rare spinel troctolites (e.g., Shearer et al. 2015b). Nearly all models for

Mg-suite petrogenesis require the contribution of three components of the bulk silicate Moon: 1) high-Mg# early magma ocean cumulates from the deep mantle to achieve magmas with a similarly high Mg#, 2) anorthosite from the crust to achieve plagioclase-saturated magmas, and 3) KREEP to achieve the trace element and isotopic characteristics of the parental magmas. In order to generate magmas from these three components, nearly all models for Mg-suite petrogenesis also include the mantle cumulate overturn process, which brings Mg-rich dunitic cumulates from the deep mantle to the base of the crust via mantle convection, presumably in close proximity to the evolving anorthositic crust and KREEP (see Shearer et al. 2015b).

It is useful to consider the defining characteristics of the Mg-suite in order to better place into context new observations from both the lunar samples and the available suite of remote observations of the crust. There may be other processes besides Mg-suite magmatism that produce lithologies with some of the same compositional characteristics. For example, fractional crystallization of a lunar magma with similar composition to many of the low-Ti picritic glasses collected by Apollo 15 will produce olivine and pyroxene cumulates with Mg#s similar to the same phases found in Mg-suite norites. Caution should be exercised in claiming discovery of new Mg-suite lithologies, given the scale of the processes needed to produce the Mg-suite and the implications a new discovery would have for physiochemical models of the early Moon.

Although the details of various Mg-suite petrogenetic models differ, there are defining characteristics of this episode of lunar magmatism that separate it from other episodes of magmatic activity on the Moon. As currently understood, Mg-suite lithologies are:

1. The products of crystallization from high-Mg#, plagioclase-saturated magmas, or magmas along the liquid line of decent from such parental magmas, that were generated by interaction of Mg-rich, and Al- and Ca-rich source rocks generally thought to be mixtures of deep LMO cumulates and crustal anorthosite.
2. Chronologically the oldest post-magma ocean igneous rocks. Recent high-fidelity isochron ages for Mg-suite rocks cluster around 4.37–4.34 Ga; however, the youngest date produced for an Mg-suite rock is ~4.1 Ga, which still predates most other lunar igneous activity.
3. The direct consequence of the geodynamic processes operating in the Moon's interior at or near the end of magma ocean crystallization. The two criteria above require, in some fashion, convective overturn of the mantle during the waning stages of or immediately after solidification of the magma ocean.

Some workers have argued that KREEP is a necessary component of Mg-suite magmatism and thus its geochemical signatures are a defining characteristic of Mg-suite rocks (e.g., Korotev 2000, 2005; Wieczorek and Phillips 2000; Shearer and Papike 2005), although this has been disputed. The role of KREEP is an active area of research in lunar science (e.g., Prissel et al. 2014; Treiman and Gross 2015; Elardo et al. 2020; Gross et al. 2020), which has implications for the extent of planetary-scale processes in the early Moon. Therefore, we do not include KREEP in this list of defining characteristics of the Mg-suite.

2.3. Mg-spinel-bearing lithologies

Lunar spinel-group minerals can be divided into two distinct populations: (1) chromite, ulvöspinel, and ilmenite found in crustal rocks such as troctolites, dunites, and pervasively in mare basalts; and (2) Mg-rich spinel in spinel troctolites (Papike et al. 1998; Gross and Treiman 2011; Elardo et al. 2012; Shearer et al. 2015b). Mg-Al-rich, Cr-poor spinel (Mg-spinel hereafter) is rare in the current lunar sample collections. Mg-spinel occurs primarily in a subset of troctolites and troctolitic cataclastites. Only two Mg-spinel-rich samples are known: a spinel-troctolite clast in 67435 with ~13 vol% Mg-spinel (Papike et al. 1998) and a unique

fragment of spinel-anorthositic troctolite in the regolith breccia ALHA81005 that contains ~30 vol. % Mg-spinel (see Fig. 3a,b; Gross and Treiman 2011), although it also occurs in trace abundances in other samples.

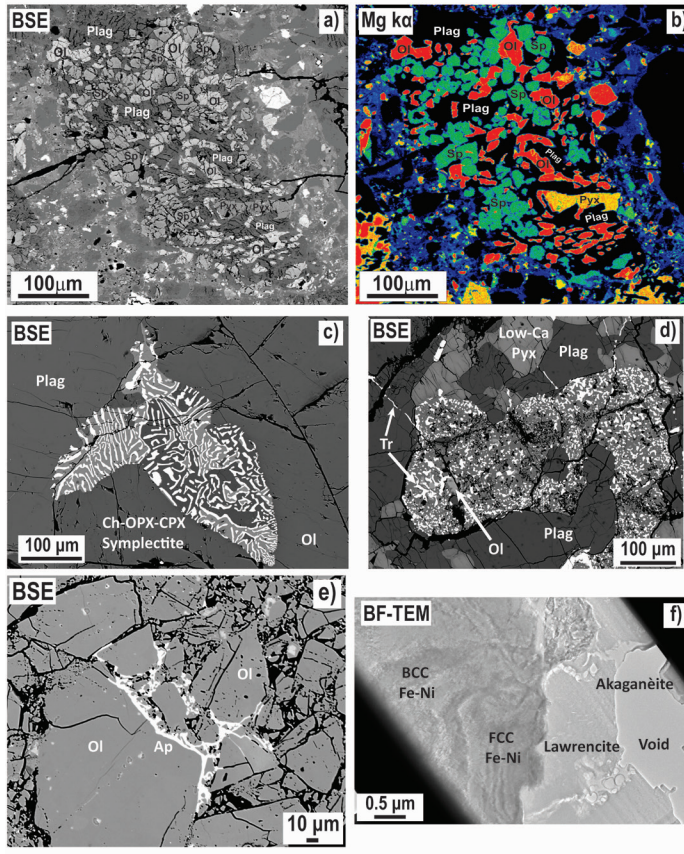

Figure 3. Backscattered electron (BSE) image **(a)** and Mg-Kα X-ray map **(b)** of a newly discovered Mg-spinel-rich clast in lunar meteorite ALHA 81005. BSE images of a chromite–OPX–CPX symplectite from Mg-suite troctolite 76535 **(c)**, sulfide (troilite) replacement textures in an Mg-suite clast in breccia 67016,294 **(d)**, and apatite (Ap) veining in Mg-suite dunite 72415 **(e)**. A bright-field TEM image of alteration volatile-rich alteration features in "rusty rock" 66095, wherein the void space is where akaganèite was lost during sample preparation, **(f)**.

A new lunar rock type was recognized using Moon Mineralogy Mapper (M^3) data, pink spinel anorthosite (PSA), identified by the presence of broad highly diagnostic absorptions near 2 and 3 µm (Pieters et al. 2011). PSA occurs as a distinct localized rock type on a scale up to a few kilometers only in anorthositic highland settings (Fig. 4) and exhibits no other detectable mafic minerals such as pyroxene or olivine. Identification criteria were discussed in detail by Pieters et al. (2014 and references therein) and at least 23 Mg-spinel-rich sites were identified globally. Some of the most prominent exposures are found in the central peaks of Theophilus, which also separately hosts abundant anorthosite and small areas of olivine (Dhingra et al. 2011; Pieters et al. 2014). Several additional Mg-spinel-rich sites were identified in a global survey of central peaks (Sun et al. 2017), although not all criteria were met for several locations.

All individual exposures of PSA are relatively small, typically a few hundred meters in extent, but regional clusters often exist (see images in Pieters et al. 2014). Confirmed PSA locations also include dispersed areas in terraced walls of a few large feldspathic craters and two areas of hypothesized non-mare volcanism. Notably, PSA is found along the inner ring of four major basins in areas of relatively low crustal thickness and thus appears to be originally associated with a lower crust origin, perhaps predating the basin-forming period (Pieters et al. 2014).

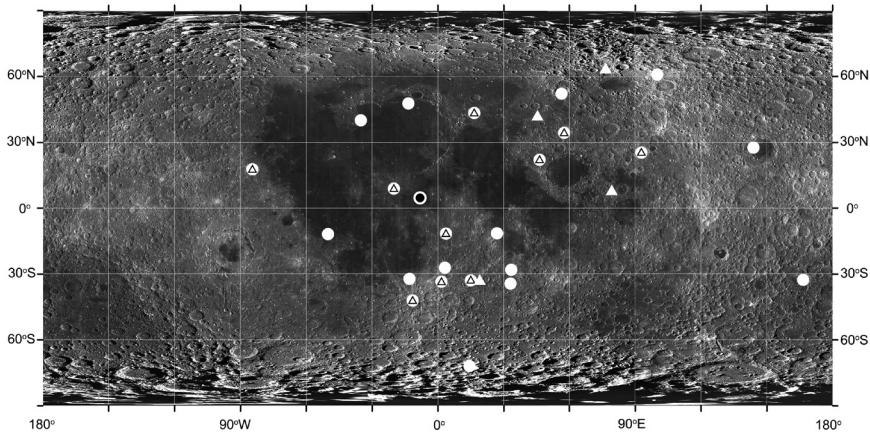

Figure 4. Distribution of Mg-spinel across the Moon displayed with oversized symbols. **White circles** indicate areas that meet the spectroscopic diagnostic criteria discussed in Pieters et al. (2014); the **white and black circle near the center** is one pyroclastic 'dark mantle' region that also contains abundant spinel (but different composition). **Triangles** indicate Mg-spinel bearing central peaks identified by Sun et al. (2017) that meet the diagnostic criteria. Although exposures of Mg-spinel are found associated with SPA and Moscoviense basins on the farside, the majority are associated with nearside terrain.

Several possible hypotheses for the petrogenesis of Mg-spinel-bearing lithologies based on exogenic or endogenic processes have been proposed. Although Yue et al. (2013) suggested that Mg-spinel might represent remnants of an impactor projectile that survived the impact process, other studies have suggested that Mg-spinel is an indicator of magma-wallrock interactions within the lunar crust (e.g., Gross and Treiman 2011; Pieters et al. 2011; Prissel et al. 2014, 2016). This mechanism increases the normative anorthite contents of initially plagioclase-undersaturated Mg-suite melts and eventually produces Mg-spinel that is consistent with the PSA observed remotely. Thermodynamic entropy calculations show that the assimilated anorthosites would need to be ~1300°C (Treiman et al. 2019) in order to facilitate anorthite dissolution without extensive co-crystallization of silicates that would drop the Mg# of the magma to unacceptably low values. Such hot anorthosite could arise by pre-heating from passage of earlier magma (Gross et al. 2014a), extreme crustal flexing due to tidal forces (Elkins-Tanton et al. 2011), or from impacts. However, an impact model is less likely as experimental studies have shown that simple melting and recrystallization of lunar surface materials would not produce PSA (Gross et al. 2014b).

2.4. Mafic components of crustal lithologies

2.4.1. Magnesian anorthosites and granulites. Magnesian anorthosites (distinguished from FANs) are found in both the Apollo sample collection and lunar meteorites, although their abundance in the crust relative to other crustal materials is still unknown. They contain mafic minerals with higher Mg#s than FANs and are more similar to some Mg-suite lithologies

in that regard (e.g., Lindstrom et al. 1984; Takeda et al. 2006; Treiman et al. 2010; Gross et al. 2014b). However, magnesian anorthosites do not exhibit the Na enrichment trend in plagioclase with decreasing Mg# that is found in the Mg-suite. Magnesian anorthosites fill in the compositional gap between the Mg-suite and the FAN-suite on a plot of Mg# of mafic silicates vs. An# (molar [Ca/Ca+Na+K]x100; Fig. 5), and the dated magnesian anorthosites appear to be contemporaneous with both suites (Takeda et al. 2006; Gross et al. 2014b; Borg et al. 2015). Although many magnesian anorthosites are recrystallized polymict clastic breccias and may not be representative of igneous lithologies, some appear to be primary igneous rocks. Analyses suggest that their major and trace element compositions cannot represent simple mixtures of FAN and KREEP-bearing Mg-suite rocks (Dreibus et al. 1977; Snyder et al. 1992; Korotev et al. 2003; Takeda et al. 2006; Treiman et al. 2010; Gross et al. 2014b), suggesting that they could represent a lunar crustal rock type not found in great abundance in the Procellarum KREEP Terrane (PKT; Jolliff et al. 2000). Consequently, the significance of magnesian anorthosites in the lunar crust is a topic of discussion and a number of origins remain possible. The magnesian anorthosites could provide evidence for an atypical Mg-suite component with distinctive chemistry, including an absence of KREEP (Korotev and Jolliff 2001; Korotev et al. 2003, 2006, 2012; Takeda et al. 2006; Shearer et al. 2015b; Gross et al. 2020). However, the lack of Na enrichment with decreasing Mg# in the magnesian anorthosites (Fig. 5) argues for an origin separate from the Mg-suite. One possibility is that magnesian anorthosites represent samples of the primary anorthositic LMO flotation crust (or reworked breccias with a large component of it) from the highlands outside the PKT. The Soviet Luna 20 mission returned samples with a highlands component dominated by magnesian anorthosite and not FAN (Korotev et al. 2003; Arai et al. 2008). These samples were collected near the Crisium basin and outside the continuous ejecta blanket of the Imbrium basin, which dominates the regions from which the Apollo rocks were sampled. Remote sensing observations have shown that average mafic minerals of the lunar highlands crust away from the PKT exhibit a higher Mg# than the those of the crust in the PKT, and this is especially true on the farside (e.g., Ohtake et al. 2012).

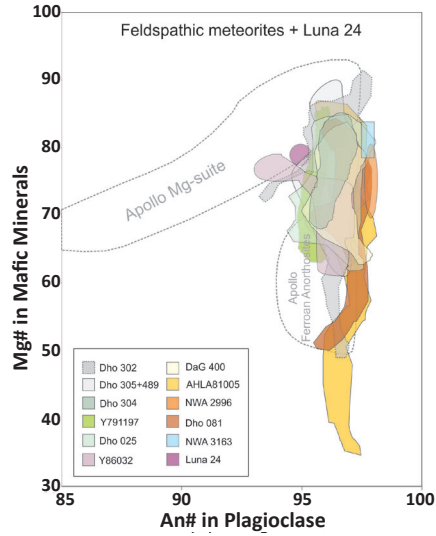

Figure 5. Plot of the Mg# of mafic minerals vs. the An# of plagioclase in lunar crustal samples. **White fields** denote the trends from Apollo Mg-suite and ferroan anorthosite sample suites. **Colored fields** denote the compositions ranges for Luna 24 samples and magnesian anorthosite and granulite clasts in newly discovered and/or studied feldspathic lunar meteorites. Figure after Gross et al. (2014).

Furthermore, feldspathic lunar meteorites, a generally random sampling of the global surface, show variable and on average higher Mg/Fe than breccias returned by Apollo, thus providing sample-based support for the inference from remote observations for a higher Mg# across the farside FHT crust (e.g., Korotev et al. 2003). However, a simple regolith mixing explanation can also account for the remote observations such that the surface of the farside FHT reflects crustal anorthositic breccias that naturally contain a component of the local equivalent of deep-seated Mg-suite but without a significant component from the more Fe-rich minerals of the PKT nearside megaregolith. Another possibility is that at least some magnesian anorthosites could be the products of the differentiation of impact melt sheets and seas produced by basin-scale impacts. Models of impact melt sheet differentiation indicate that if fractional crystallization of such melts occurs, it could potentially produce similar lithologies (Vaughan et al. 2013; Hurwitz and Kring 2014; Vaughan and Head 2014; Cassanelli and Head 2016).

Granulites are, in general, polymict clastic breccias that recrystallized during prolonged annealing, forming granulitic textures with equigranular and rounded grains (Warner et al. 1977; Lindstrom and Lindstrom 1986; Pernet-Fisher and Joy 2022) and contain slightly less plagioclase component (70–80%) than anorthosites. Many granulites have ages as old as ~4.3 Ga (James and Hammarstrom 1977; Warner et al. 1977; McLeod et al. 2016), which indicates that at least some examples of this rock type formed prior to the last major basin-forming epoch, and likely originated from the early-formed crust (e.g., Takeda et al. 2006; Arai et al. 2008). Granulites also include impact melt breccias, which have a range of formation ages (Cohen et al. 2000; 2005). They are chemically distinct in having major element mineral compositions (i.e., Mg#) similar to Mg-suite rocks and magnesian anorthosites but contain no trace of KREEP component (Warner et al. 1977; Lindstrom and Lindstrom 1986; Korotev and Jolliff 2001; Treiman et al. 2010). Apollo granulites are divided into more ferroan types (mineralogically similar to FANs) and magnesian types, which have a very high Th/Sm ratio indicative of derivation from a yet unaccounted end-member (Korotev and Jolliff 2001; Korotev et al. 2003). Granulites that are thought to originate from the farside appear to be chemically distinct from the Apollo types (Treiman et al. 2010). These observations suggest that the lunar crust represented by the Apollo collection is characteristic of only a part of the nearside highlands, whereas the magnesian anorthosites and Mg-granulites may better represent typical highland materials, although the relative abundances of Mg-anorthosites and granulites in the crust need to be better quantified (Takeda et al. 2006; Arai et al. 2008).

2.4.2. Olivine-bearing lithologies. Modern VNIR spectroscopic instruments in lunar orbit have clearly identified multiple surface areas with olivine-rich spectral features. They are globally distributed (Fig. 2a) across the surface both on the nearside and the farside (Yamamoto et al. 2010; Isaacson et al. 2011; Dhingra et al. 2015). These areas lack the paired absorptions near 1 and 2 μm that are characteristic of pyroxene, and olivine is identified as the most abundant mafic silicate mineral phase by its strong and highly diagnostic multicomponent absorption near 1050 nm.

A large number of olivine-rich sites have been found on or near basin rings (Fig. 2a). Estimates of mineral modal abundances suggest some of these rocks could be dunitic in composition (Yamamoto et al. 2010) and might represent mantle excavated from depth by basin-forming impacts. However, as discussed above, for craters and basins that have exposed PAN and olivine, an anti-correlation can be seen between local crustal thickness estimates and the approximate original depth of any mafic compositions observed (Fig. 2b). A few Apollo samples are categorized as dunite, but analyses show that they are likely not derived from the lunar mantle, but are rather the products of fractional crystallization of intrusive magmas (Shearer et al. 2015a; 2015b). Many, if not most, olivine-rich lithologies detected remotely are almost certainly troctolite (i.e., plagioclase + olivine) based on variations in olivine band strength across locations within the same morphology (e.g., the central peak of Copernicus; Dhingra et al. 2015). Such areas suggest lower crustal magmatic intrusions.

However, some olivine-bearing exposures within the same crater can exhibit different morphological character and geologic context hinting at possibly different origins (Dhingra et al. 2015). This observation has important implications for assigning mantle origin for multiple olivine-bearing exposures around lunar basins. Detailed high-resolution geologic context is needed to further understand the likely origin of these exposures. Most lunar olivine-rich areas have been confirmed by independent VNIR instruments (Spectral Profiler [SP] on Kaguya; Moon Mineralogy Mapper [M^3] on Chandrayaan-1). However, the thermal infrared data from the LRO Diviner Lunar Radiometer Experiment can only place an upper limit of olivine present at these sites (< 90 wt.%; Arnold et al. 2016). The olivine in the identified olivine-rich sites has yet to be sampled and its origin remains an important question to be resolved.

2.4.3. OPX and pigeonite-bearing lithologies. The mafic component of the lunar highlands, as characterized from orbit, is dominated by low-Ca pyroxene, typically Mg-rich orthopyroxene and pigeonite. This was broadly recognized from Earth-based telescopic surveys (Pieters 1986, 1993; Hawke et al. 2003) and later in more detail with Clementine analyses (e.g., Tompkins and Pieters 1999; Cahill et al. 2009; Crites et al. 2015). The higher spatial and spectral resolution of modern instruments, including the M^3 on Chandrayaan-1 and the Multiband Imager (MI) and SP on Kaguya, have provided a more detailed view of the specific composition and geological context of low-Ca pyroxene in the crust. In addition to being present at low (< 5%) abundance within soils of the anorthositic crust, more prominent concentrated exposures of low-Ca pyroxenes are found in and/or around major impact basins, including the SPA and the Imbrium basins (Pieters et al. 2001; Isaacson and Pieters 2009; Klima et al. 2011; Nakamura et al. 2012; Moriarty et al. 2013; Lucey et al. 2014; Ohtake et al. 2014; Moriarty and Pieters 2015). The presence of low-Ca pyroxene both stratigraphically above and below the FAN/PAN zone in the upper crust suggests a lower crustal origin, which provided extensive low-Ca pyroxene-bearing anorthositic breccia debris from the basin impact period of early lunar history. It has also been suggested that some of the low-Ca pyroxene observed throughout the highland crust may be scattered upper mantle debris, excavated by the largest lunar impacts, including the impact that produced SPA, and then distributed further through regolith gardening over billions of years (e.g., Lucey et al. 2014; Crites et al. 2015; Melosh et al. 2017).

In low-Ca pyroxenes, the band positions of the 1 and 2 μm absorptions are controlled primarily by crystallographic effects determined by the ratio of Fe to Mg, with both absorption bands shifting to longer wavelengths as Fe and Ca substitute for Mg. Thus, band position can be used to assess the overall Fe content of the pyroxenes. Based on M^3 data, the band positions of most of the broadly-distributed low-Ca pyroxenes associated with anorthositic crust suggest an average pyroxene with moderate amounts of Fe (Mg# of 50–75) (e.g., Matsunaga et al. 2008; Klima et al. 2011), although a few selected locations exhibit shorter wavelength bands consistent with an average higher Mg content (Mg# > 80) (e.g., Nakamura et al. 2009; Klima et al. 2011). One prominent such high-Mg exposure is found in the Montes Alpes region, where large massifs associated with the Imbrium impact are located (Klima et al. 2017). Some of these blocks appear to exhibit gabbroic and olivine-rich compositions in direct contact with the high-Mg, low-Ca pyroxenes, suggesting that such lithologies sometimes coexist at depth in the lunar crust, potentially as layered mafic intrusions near the base of the crust.

2.5. The distribution of Th in the global lunar crust

Radioactive elements such as Th, K, and U, which are concentrated in KREEP, produce gamma-ray fluxes high enough to be measured from orbit. The first global maps of Th abundances were produced by Lunar Prospector Gamma Ray Spectrometer (LPGRS) by Lawrence et al. (1998). More recently, gamma ray spectrometers have flown on both Kaguya/SELENE (KGRS) and Chang'e-1 (CGRS). Both instruments have refined Th abundance maps consistent with earlier work (e.g., Kobayashi et al. 2010; Wang et al. 2016). Kobayashi et al. (2012) found that the Moon's two regions of lowest Th abundance are located near the

equator on the lunar farside in the FHT, regions which also have the greatest crustal thickness. The highest Th abundances are associated with the KREEP-rich mare basalts on the lunar nearside, especially around Oceanus Procellarum. Jolliff et al. (2000) used LP-GRS bins with greater than ~3.5 ppm Th to define the extensive PKT found on the lunar nearside. In contrast, the FHT is characterized by very low Th abundances and dominates the northern farside highlands. The SPA basin terrane is intermediate, somewhat elevated compared to the FHT but significantly lower than the PKT. These relations are readily recognized in Th global maps.

A number of localized regions outside the PKT exhibit Th abundances that are anomalous compared to their surrounding terranes. The most prominent of these features is an isolated Th hotspot in the farside FHT (Lawrence et al. 1999, 2003) and that includes the Compton-Belkovich Volcanic Complex (CBVC). The CBVC is an area of highly reflective terrain that contains numerous domes, irregular depressions, and pyroclastic deposits consistent with explosive silicic volcanism (Jolliff et al. 2011; Wilson et al. 2015; Clegg-Watkins et al. 2017; Head and Wilson 2017). The highest Th abundances on the farside are relatively close to the Imbrium antipode within SPA and might suggest it has been delivered by an external event (Haskin et al. 1998; Lawrence et al. 1999), although Moriarty et al. (2021) alternatively proposed that the high Th abundances are related to upper mantle exposures in SPA. Another farside high-Th example is an area ENE of the 50 km Dewar Crater which shows elevated Th abundances coincident with a region of elevated FeO abundance, one of the few locations outside of the PKT that has abundances similar to nearside mafic impact melt breccias (Lawrence et al. 2003). Lawrence et al. (2008) suggested this geochemical anomaly could be associated with high-Th cryptomare, which is rare on the farside.

2.6. The non-mare interior of the South Pole-Aitken Basin

The largest and oldest recognized impact basin on the Moon is the ~2500 km SPA basin that dominates the southern lunar farside. SPA has not been filled with mare basalts as have nearside basins, allowing examination of the mineralogy of its interior impact products (Pieters et al. 2001; Ohtake et al. 2014; Moriarty and Pieters 2018), including extensive impact melt and excavated breccia. These SPA data from independent missions and instruments all provide consistent results: the principal mafic lithology excavated and exposed by the SPA basin-forming impact is dominated by Mg-rich low-Ca pyroxene (Melosh et al. 2017). The systematic compositional variations across SPA are shown schematically in Fig. 6. Exposure of olivine is quite rare across SPA, whereas the innermost non-mare deposits contain more Ca- and Fe-rich pyroxene (Ohtake et al. 2014; Moriarty and Pieters 2015, 2018; Uemoto et al. 2017). LMO Crystallization models (see Gaffney et al. 2023, this volume) predict abundant olivine being sequestered in the deep mantle before plagioclase appears in the crystallization sequence (~70–80% crystallization). The combined remote sensing data for SPA interior, along with multiple assessments of the megaregolith that is largely derived from basin ejecta, exhibit a preponderance of Mg-rich pyroxene lithologies. Thus, the lower crust and upper mantle that was tapped by large basins early in crustal evolution is characterized as being dominated by Mg-rich pyroxene with minor Ca-rich pyroxene, but only local areas of olivine/troctolite. These components dominate the anorthositic megaregolith debris resulting from the heavy bombardment that occurred during the first ~500 Ma of lunar crust evolution.

2.7. Non-mare silicic magmatism

Silicic (or felsic) magmatism is discussed in detail by Shearer et al. (2023, this volume) and is summarized here within the context of crustal evolution. In addition to a connection with KREEP (Taylor et al. 1980), samples of silicic/granitic crustal rocks are believed to be the product of late-stage secondary or even tertiary (e.g., partial melting of secondary crust) magmatism relative to other crustal components such as the FANs, magnesian anorthosites, Mg-suite, and alkali-suite (Fig. 1). The first suggestion of non-mare volcanism observed on

the Moon was made during the Apollo era, where observations of "red spots" (relatively bright regions of the Moon with increasing reflectance throughout the VNIR) were interpreted as a result of high-viscosity silicic volcanism (Whitaker 1972a; Malin 1974; Head et al. 1978; Head and McCord 1978; Chevrel et al. 1999). Most non-mare volcanics are located in the PKT, although the CBVC is on the lunar farside (Jolliff et al. 2000). However, all show evidence for elevated Th abundances of ~20–80 ppm (Lawrence et al. 1999, 2000, 2003, 2007; Hagerty et al. 2006, 2009; Glotch et al. 2011). Silicic clasts in the Apollo sample collection generally have Th abundances > 60 ppm (Seddio et al. 2013).

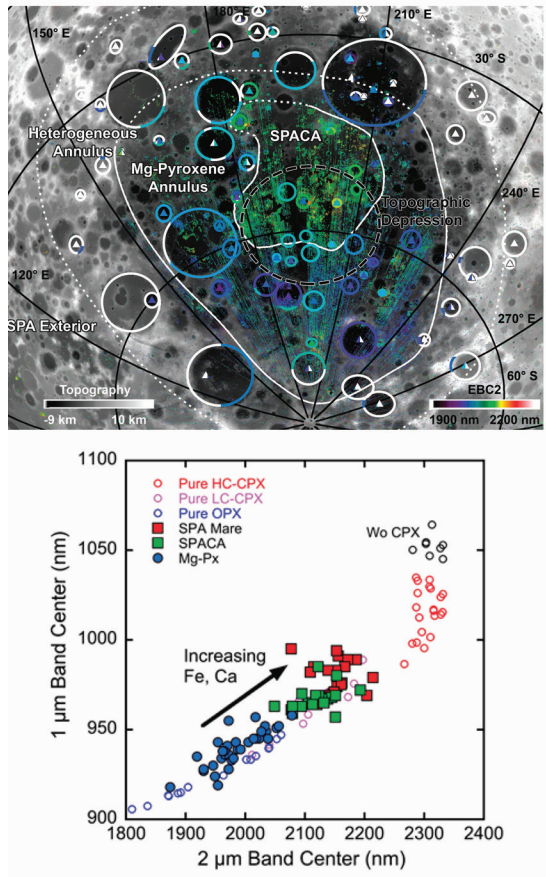

Figure 6. Mineralogy observed across South Pole-Aitken basin (after Moriarty and Pieters, 2018). (**Top**) Schematic distribution of SPA mafic mineralogy based on observed pyroxene composition (**blue**: Mg-rich; **green-yellow**: increasing Fe and Ca). Regular observed compositional annuli across the basin are labeled. Location of the topographic deepest part of the basin is outlined. (**Bottom**) Shift of pyroxene diagnostic absorption band center as Fe and Ca substitute for Mg (after Moriarty and Pieters, 2018). **Open circles** are pure pyroxenes measured in the laboratory (Klima et al. 2007, 2011b). **Filled symbols** are example M3 spectra across SPA.

Recent results from the Diviner Lunar Radiometer Experiment (Glotch et al. 2010, 2011; Jolliff et al. 2011; Ashley et al. 2016; Boyce et al. 2017) have demonstrated that many, but not all, of these areas display thermal IR spectral characteristics (short wavelength Christiansen Feature) that are consistent with dacite or rhyolite compositions. These include the Gruithuisen

Domes, Mairan Domes, Hansteen Alpha (HA), the CBVC, and Lassell Massif. The central peak and some ejecta of Aristarchus crater also show similar Diviner characteristics, suggesting the excavation of a silicic pluton. Crater counting of the proposed silicic volcanic domes suggested ages between 3.38 and 4.07 Ga (Wagner et al. 2002, 2010). By contrast, the dated silicic samples are generally older, falling into two groups with ages > 4.3 Ga and ~3.9 Ga (Fig. 1).

Observations of what appear to be viscous volcanic domes (e.g., Head and McCord 1978) have led to concepts for the origin of silicic rocks in the crust. For example, basaltic underplating coupled with partial melting of "fertile" rocks such as KREEP basalt or its intrusive equivalents has been proposed (Hagerty et al. 2006; Gullikson et al. 2016). Although silicate-liquid immiscibility (SLI) has been demonstrated to have occurred on a small scale, it is unclear whether this process could occur on a scale large enough to produce large features such as the Gruithuisen Domes (Hagerty et al. 2006). Nevertheless, late-stage SLI on a small scale might have been involved in the formation of small domes and bulges. An unsolved issue is the degree and range of silica enrichment exhibited at the volcanic sites (Clegg-Watkins et al. 2017).

The topographic and morphologic expressions of the silicic volcanic complexes exhibit striking diversity. The Gruithuisen Domes are the largest of the volcanic constructs, with each over 10 km across and ~1.7–1.8 km high (Tran et al. 2011; Ivanov et al. 2016). The Mairan Domes range in size with the largest volcanic constructs being on the order of 5–8 km base widths and at least 800 m heights, one with a distinctive summit depression (Glotch et al. 2011). The CBVC is a broad dome, ~25 × 35 km across and about 500 m high, with an irregular central depression interpreted to be a collapse caldera. This volcanic complex has a range of volcanic constructs, with the largest dome or cone having a base width of ~4 × 6.5 km, an elevation ~550 m, and a small summit depression (Jolliff et al. 2011; Walcek et al. 2016). The HA complex is a rough-textured triangular mound ~25 km on a side, the margins of which stand ~700 m above the surrounding mare surface (Boyce et al. 2017). Unlike others in this group, the HA complex is riddled with exposures of Mg-spinel (Pieters et al. 2014).

Many of the small domes or bulges also feature distinctive dense boulder populations, which suggests formation from relatively silicic and viscous lavas. Overall, the compositions indicated by remote sensing are consistent with low-FeO felsic materials (Clegg-Watkins et al. 2017). Unfortunately, no direct link has yet been possible between the small fragments of highly silicic samples returned by the Apollo astronauts and the larger regions tentatively identified as silicic non-mare volcanism from remote sensing data.

2.8. Mare volcanism and evolution of secondary crust

2.8.1. Newly discovered meteoritic mare basalt samples. Mare basaltic magmatism represents the predominant form of endogenous secondary crust building activity for most of lunar history (Fig. 1). The broad peak in mare magmatism, based on sample dating and extended by crater counting studies of mare units, was between 3.9–3.1 Ga (e.g., Hiesinger et al. 2011), but may have continued until as recently as ~18 Ma (Braden et al. 2014). A number of newly discovered basaltic meteorites have expanded the age and compositional ranges represented in the sample collection. Interestingly, basaltic lunar meteorites fall into narrow compositional and age ranges (Joy et al. 2023, this volume). All mare basaltic meteorites are low- or very-low Ti mare basalts except for one high-Al basalt sample (Northwest Africa [NWA] 4898; Li et al. 2016) and one high-Ti basalt clast (Dhofar 1428; Zhuqing et al. 2018). Additionally, with the exception of NWA 4898 (3.58 Ga; Gaffney et al. 2008), the basaltic lunar meteorites cluster in two age bins of ~3.8–3.9 Ga and ~2.9–3.1 Ga. These factors indicate the basaltic lunar meteorites sample a limited range of the broad diversity of mare basalts present on the lunar surface. Conversely, the 1.96 Ga basalts recently returned by the China National Space Agency's Chang'e-5 mission appear to sample an intermediate Ti (~5.7 wt.% TiO_2) mare basalt unit (Che et al. 2021; Hu et al. 2021; Li et al. 2021; Tian et al. 2021).

NWA 032/479, NWA 4734, NWA 8632, and LaPaz Icefield (LAP) 02205 and its five pairings are compositionally-nearly identical, relatively evolved low-Ti mare basalts with overlapping crystallization ages ranging from 2.93–3.02 Ga (Rankenburg et al. 2007; Borg et al. 2009; Elardo et al. 2014; Fagan et al. 2018). It is likely that these meteorites sample flows from the same volcanic complex and can be source-crater paired (Zeigler et al. 2005; Elardo et al. 2014). NWA 032/479, NWA 4734, and the LAP meteorites are enriched in incompatible trace elements compared to most mare basalts (Fagan et al. 2002; Zeigler et al. 2005; Anand et al. 2006; Day et al. 2006; Joy et al. 2006; Hill et al. 2009; Elardo et al. 2014), which has led to the suggestion that they have interacted with the KREEP reservoir. However, geochemical characteristics and isotopic compositions suggest that this is likely not the case. These three basalts have high Ti/Sm and Cl-poor apatite, which are both inconsistent with KREEP (Elardo et al. 2014). Additionally, the depleted initial Nd isotopic composition of NWA 032 precludes involvement of the enriched KREEP reservoir. Alternatively, Elardo et al. (2014) argued that the geochemical features of these basalts can be generated by low-degree partial melting of the lunar mantle.

NWA 032/479 and NWA 8632 are some of the only basaltic samples in the lunar sample collection that record evidence of dynamic magma chamber processes. Elardo and Shearer (2014) documented oscillatory chemical zoning patterns in major and minor elements in both pyroxene and olivine phenocrysts in NWA 032, and Fagan et al. (2018) documented oscillatory zoning patterns in minor elements in olivine phenocrysts in NWA 8632. Analyses of these patterns indicated that they formed during cooling and fractionation of a compositionally-zoned and convecting magma chamber (Elardo and Shearer 2014). Elardo and Shearer (2014) inferred that the compositional zoning and convection in the chamber may have been driven by heat loss to the cold lunar crust at 2.93 Ga, which is the crystallization age of NWA 032/479 (Borg et al. 2009). Evidence for fractional crystallization in the magma chamber before eruption is supported by high-temperature and -pressure experiments (Elardo et al. 2015).

Northeast Africa (NEA) 003 is a lunar meteorite that contains an unbrecciated low-Ti basalt clast (lithology A) and a basaltic regolith breccia (lithology B; Haloda et al. 2009). It is similar to the Apollo 15 low-Ti basalts in major element compositions; however, it is one of the most incompatible trace element depleted mare basalts yet discovered, has no Eu anomaly, and a chondritic initial Nd isotopic composition, indicative of derivation from a primitive mantle source. High-temperature and -pressure experiments and modeling from Elardo et al. (2015) indicated NEA 003-A may be sourced from one of the deepest sources for a crystalline mare basalt, possibly from depths > 215 km, and approaching the source depths for the picritic glasses. The young age of NEA 003-A (3.09 Ga; Haloda et al. 2009) relative to other low-Ti basalts in the Apollo collection demonstrates that it represents another newly sampled mare basalt unit.

NWA 4898 is the first high-Al mare basalt in the lunar meteorite collection and is distinct from the high-Al basalts collected during Apollo. Its bulk composition and preliminary initial Nd isotopic composition indicate that, unlike the Apollo 14 high-Al basalts (e.g., Neal and Kramer 2006), it is not the result of interaction with the KREEP reservoir (Gaffney et al. 2008; Greshake et al. 2008; Fernandes et al. 2009b; Li et al. 2016). Additionally, a preliminary Rb–Sr isochron from Gaffney et al. (2008) suggested an age of 3.58 Ga indicating that NWA 4898 may be significantly younger than the Apollo 14 high-Al basalts, thus extending the timespan recorded in the sample collection over which high-Al basalts were added to the lunar crust.

Miller Range (MIL) 05035 is a coarse-grained low-Ti gabbroic lunar meteorite with low abundances of incompatible trace elements (e.g., 0.28 ppm Th) and almost no negative Eu anomaly (Joy et al. 2008; Liu et al. 2009). Its age (3.80 Ga; Nyquist et al. 2007) and bulk composition suggest that MIL 05035 is paired with Asuka-881757 and is the coarse-grained equivalent of Yamato-793169 (Koeberl et al. 1993; Warren and Kallemeyn 1993; Joy et al. 2008; Fernandes et al. 2009a; Liu et al. 2009; Arai et al. 2010). MIL 05035 is also similar in composition to the basaltic component of regolith breccia Meteorite Hills (MET) 01210.

On the basis of these compositional similarities and textural variations indicating differing cooling rates and degrees of crystal accumulation between these meteorites, Joy et al. (2008) proposed that these four meteorites are sourced from different levels of a thick lava flow, where MIL 05035 and Asuka-881757 sample the coarse-grained regions deep within the flow, Yamato-793169 samples the more quickly cooled, fine-grained upper regions of the flow, and MET 01210 samples the regolith breccia formed in part from samples of the thick underlying lava flow. Arai et al. (2010) suggested that the low irradiation history and immaturity of the MET 01210 regolith breccia may indicate these meteorites sample a cryptomare unit, which could potentially make these samples important for understanding early magmatic activity on the Moon, as cryptomare does not appear to be well-represented in the sample collection.

2.8.2. Young olivine-rich high-titanium basalts. Modern crater size–frequency distribution analyses have identified several large areas of unsampled basalts in the lunar nearside mare that are substantially younger than the maria from which the Apollo and Luna samples were collected (Hiesinger et al. 2023, this volume). Both gamma-ray and optical remote sensing approaches identify these young basalts as relatively Ti-rich (Pieters 1978; Kato et al. 2017b). However, near infrared spectroscopy also shows that their mafic mineral composition is different from the familiar Apollo 11 and 17 Ti-rich basalts. The young Ti-rich basalts located in Imbrium and Procellarum are exceptionally olivine-rich, with their mafic mineral content requiring ~30% olivine (Pieters et al. 1980; Staid et al. 2011). The Chang'e-3 landing site is located on the edge of one such mare exposure (Ling et al. 2015; Xiao et al. 2015). Any model of the evolution of nearside mare basalt source regions must be able to account for the elevated TiO_2 content together with abundant olivine that is pervasively present in extensive flows of distinctly young mare basalts on the western nearside. These basalts were recently sampled in the Mons Rümker region and returned to Earth by Chang'e-5 sample return mission (Qian et al. 2018; Che et al. 2021; Hu et al. 2021; Li et al. 2021; Tian et al. 2021).

2.8.3. Irregular mare patches—Compositions and ages. Braden et al. (2014) documented the presence of 70 small topographic anomalies with irregular morphologies. Terming these irregular mare patches (IMPs), they analyzed the largest, Ina, an enigmatic 2 x 3 km surface formation in the central nearside whose presence was known since the Apollo era (Whitaker 1972b; El-Baz 1974; Strain and El-Baz 1980). Ina has been interpreted to represent very young surface activity (e.g., Schultz et al. 2006 suggested ~10 Ma). Using LROC data, Braden et al. (2014) compiled impact crater size–frequency distributions that were interpreted to indicate that Ina was ~ 33 Myr in age, and that the other two largest IMPs (Sosigenes and Cauchy 5) were ~18 and ~58 Myr in age, respectively. They described the populations of IMPs as relatively small (100 m to 5 km maximum dimensions) and characterized by two types of deposit: (1) rough, topographically uneven deposits displaying a range of block densities, and (2) smooth-textured, mound-like deposits with almost no blocks. Smooth mound deposits exhibit lobate steep-sloped margins and contacts between the units are characterized by an abrupt slope change. An LROC high resolution image of Ina can be seen in Fig. 11 in Head et al. (2023, this volume). Braden et al. (2014) showed that the smooth deposits are higher in elevation, concluding that they are generally superposed on the rough deposits, and interpreted the morphology of both to be consistent with small volcanic eruptions within the last ~100 Myr.

Wilson and Head (2017) followed a different line of reasoning while documenting the effects of low lunar gravity and negligible atmospheric pressure on late-stage volcanic eruptions on the Moon. Lunar versions of hawaiian and strombolian explosive activity would lead to distinct products in the terminal stages of lunar eruptions (unusual mounds and hummocky, blocky floors of small-shield summit pit crater floors). Wilson and Head (2017) concluded that as the rise rate of ascending lunar magma slows to zero, volatiles exsolve in the dike or lava lake to form a very vesicular foam. As the dike begins to close, extremely vesicular magma is released. Stresses in the vesicular and porous lava crust produce fractures through which the

foam extrudes to form convex mounds. The physical properties of these solidified foams can inhibit typical impact crater formation and regolith development, factors that could lead to an artificially young crater retention age. Qiao et al. (2017, 2018) explored this model for the formation of the larger IMPs, such as Ina, Sosigenes, and Cauchy 5. However, an impediment for this model is that lunar magmas are depleted in magmatic volatiles (e.g., H_2O) compared to terrestrial magmas (McCubbin et al. 2015a) and a relatively high volatile load may have been needed to produce magmatic foams. The origin and absolute age of the IMPs, and thus the timing of the end of lunar mare basalt volcanism and implications for the thermal evolution of the Moon (Spohn et al. 2001; Ziethe et al. 2009; Laneuville et al. 2013), remain issues of great significance and ongoing debate.

2.8.4. Pyroclastic deposits. Lunar pyroclastic deposits have several fundamentally different modes of origin that resulted in distinct modes of occurrence. Large regional pyroclastic deposits (> 1000 km^2) have been extensively mapped and characterized (Pieters et al. 1973; Gaddis et al. 1985, 1998, 2000, 2003; Weitz et al. 1998; Gustafson et al. 2012). Most are very dark and Ti-rich. Although both high- and low-Ti volcanic glasses are identified in Apollo samples, low-Ti regional deposits have been difficult to confidently identify with remote sensing because they are not dark and not easily distinguished from orbit. The sampled Apollo 15 and 17 volcanic glasses are associated with regional deposits and have been shown to be some of the most primitive mantle melts in the sample collection. For most of these large regional pyroclastic deposits it is difficult to identify specific vents, but the various glassy deposits appear homogeneous on a regional scale with remote sensors. At many (but not all) of the nearside regional pyroclastic deposits, detection of hydration has been made from orbit that may be linked to the mantle-derived water in these volcanic glasses (Li and Milliken 2017; Milliken and Li 2017). Only one regional dark pyroclastic deposit (Sinus Aestuum) exhibits distinct and abundant Fe- or Cr-rich spinel (Sunshine et al. 2010; Yamamoto et al. 2013; Pieters et al. 2014; Weitz et al. 2017). Unfortunately, nothing similar has been found in the limited range of returned or meteoritic samples. In contrast to the regional deposits, smaller localized pyroclastic deposits are also observed and are usually associated with discrete vents along fractures formed in large highland craters that exhibit anomalously shallow floors. These floor-fractured craters commonly occur near a mare-highland boundary and are hypothesized to host a subsurface volcanic sill with dikes that produces the local deposits (Head and Wilson 1979; Jozwiak et al. 2012, 2015; Wilson and Head 2018).

2.9. Constraints on crustal evolution from non-traditional stable isotopes

One of the biggest advances in all of geochemistry in the past ~20 years has been in the field of stable isotope geochemistry, where advances such as the widespread availability of multiple collector inductively-coupled plasma mass spectrometry (MC-ICP-MS) have opened up the periodic table to high-precision measurements of non-traditional stable isotopes. Variations in non-traditional stable isotopes have the potential to be immensely powerful in recording the physiochemical conditions of a wide range of planetary processes due to their wide-ranging geochemical properties and affinities. Lunar samples have become targets for non-traditional stable isotope analyses and recent results interpreted in the context of Moon formation and other magmatic processes are reviewed elsewhere in this volume (Canup et al. 2023; McCubbin et al. 2023; Shearer et al. 2023, all this volume). However, crustal samples have remained rather under-explored while the major focus was dedicated to mare basalts for the purpose of estimating the composition of the bulk silicate Moon (BSM). Nevertheless, some crustal rocks have been studied and interpreted as the geochemical complement to the lunar mantle. Although some information is already available for elemental and isotope systematics of Li, Mg, Si, K, Cl, Fe, Zn, Ga, Rb, and other less utilized stable isotope systems, a detailed exploration of their relevance for further constraining the lunar crust history remains to be unraveled with future targeted studies.

2.9.1. Lithium. Magna et al. (2006) reported a low Li abundance (< 1 ppm) and isotopically heavy Li (δ^7Li = 8.9‰) in pristine ferroan anorthosite 62255. The overall Li-poor and ^{7}Li-enriched character of lunar anorthositic crust has been corroborated more recently by analysis of new lunar meteorite find Oued Awlitis 001 (Ferrière et al. 2017). Five highland samples were analyzed by Seitz et al. (2006), but their uniformly brecciated character, a large variation in Li abundance (6.6–48.8 ppm), and δ^7Li (1.9 to 18.4‰), combined with intra-sample heterogeneity (e.g., vastly different analytical results for two specimens of 15445; Seitz et al. 2006), preclude any clear insights into lunar crustal evolution. If systematically heavy Li isotope compositions are confirmed with future analyses of a larger sample suite, this could suggest (1) entirely different behavior of Li during differentiation of primordial magmatic crust on the Moon vs. Earth (cf., isotopically light Li in Earth's crust; Tomascak et al. 2016), and/or (2) kinetic isotope fractionation during prolonged cooling of lunar crust, with sizeable Li fractionation given their ability to diffuse rapidly in silicate systems.

2.9.2. Magnesium. The first high-precision Mg isotope data for highland rocks displayed δ^{26}Mg values from −0.34 to −0.18‰, similar to those of low-Ti mare basalts, highland soils, and regolith breccias (Sedaghatpour et al. 2013). This range largely encompassed the variation reported for all lunar lithologies, apart from high-Ti mare basalts (Shearer et al. 2023, this volume) and indicates that formation of primary and secondary mafic crust on Moon was not accompanied by any sizeable Mg isotope fractionation, whereas on Earth a marginal difference exists between the primitive mantle and magmatic crust (Teng 2017). An extended dataset of lunar lithologies presented by Sedaghatpour and Jacobsen (2019) included anorthosites, Mg-suite samples, breccias with granite, and several others. In particular, anorthosites 60015 and 60025 depart towards positive δ^{26}Mg up to 0.08‰, and these isotope anomalies were suggested to reflect Mg isotope fractionation due to crystallization of plagioclase from LMO. Alternative explanations could involve slight mineralogical heterogeneity at a sample scale or kinetic isotope exchange at sub-solidus temperatures, a process that has widely been observed to be coupled with Fe isotopes. Future detailed investigations may establish Mg isotope links to temperatures and duration of crystallization and post-emplacement heating.

2.9.3. Silicon. Armytage et al. (2012) reported δ^{30}Si values for five FANs and norites, and Zambardi et al. (2013) reported data for one norite. Unlike Mg, the mean δ^{30}Si = −0.27 ± 0.10‰ of these crustal samples is identical, though with a slightly larger variation, to other lunar reservoirs analyzed (mare basalts, volcanic glasses) and by inference the BSM. Although broadly similar in Si isotope systematics, FANs show marginally higher δ^{30}Si values (−0.28 to −0.20‰) with the highest δ^{30}Si found for pristine FAN 60025. Only noritic anorthosite 67955 shows somewhat lighter Si isotope signature (δ^{30}Si = −0.34‰) and this is unlikely to be caused by meteoritic contamination (Armytage et al. 2012). Therefore, it may be that Si isotopes are marginally fractionated between lunar crust and mantle but new data for a greater diversity of highland rocks are required to address this preliminary observation.

2.9.4. Sulfur. Although S is not a non-traditional stable isotope system, S abundances and isotope data are somewhat sparse for crustal rocks. Rees and Thode (1974), Kerridge et al. (1975), and Des Marais (1983) reported on coupled S contents and δ^{34}S values in anorthosites and breccias. Sulfur abundances were 145–1165 ppm S and δ^{34}S varied between −0.2 ± 0.3‰ and +1.1 ± 0.3‰ in anorthosites, which is generally consistent with the range in δ^{34}S for indigenous lunar S (Wing and Farquhar 2015). Impact melt breccias had similar ranges in S contents and isotope compositions. Gibson and Moore (1974) reported on S abundances in Mg-suite rocks (norites, dunites). For dunite 72415, they found only 44 ppm S whereas norites had 720–945 ppm S. Unfortunately, high-precision S isotope data are not widely available for lunar crustal rocks, which could help establish their mutual relationship and significance for early LMO evolution (cf., new data for mare basalts; Wing and Farquhar 2015). Shearer et al. (2012) reported δ^{34}S values between –1.0 and –3.3 ‰ for secondary troilite replacement veins

in FAN and Mg-suite clasts from Apollo 16 (Fig. 3). Such negative $\delta^{34}S$ values point to either a previously unrecognized S reservoir or, more likely, fractionation processes associated with volatile element transport and crustal alteration.

2.9.5. Iron. The first Fe isotope data for lunar crustal lithologies come from Poitrasson et al. (2004) for norite 77215, KREEP basalt 15386, and three FANs. Weyer et al. (2005) added data for KREEP basalt 15386 as well as some KREEP-rich breccias. Wang et al. (2015) reported on Fe isotope systematics in dunite 72415, troctolite 76535, and a number of meteoritic feldspathic breccias. Sossi and Moynier (2017) extended the existing dataset with new Fe isotope determinations in 72415, troctolite 76535, and four norites. Several important observations can be made for lunar crustal rocks. Firstly, crustal rocks have heavy $\delta^{57}Fe$ compositions relative to chondrites and, excluding the outlying extremely light dunite 72415, have a more limited range in $\delta^{57}Fe$ compared with mare basalts (Poitrasson et al. 2004; Weyer et al. 2004; Liu et al. 2010; Sossi and Moynier 2017). Secondly, Mg-suite samples have a lighter average Fe isotopic composition ($\delta^{57}Fe < 0.13‰$) than FANs ($\delta^{57}Fe > 0.18‰$). Whether this difference is a consequence of variations in parental magma composition and/or mineral–melt isotope fractionation remains to be resolved. Thirdly, $\delta^{57}Fe$ for troctolite 76535 is consistent for different aliquots measured in different laboratories and is in the range of norites. This may, in part, attest to sample homogeneity, although we note that a recent report by Poitrasson et al. (2019) indicated possible variation among different sub-samples. Finally, a systematically light Fe isotope composition in dunite 72415 ($\delta^{57}Fe < -0.50‰$) (Wang et al. 2015; Sossi and Moynier 2017) has been reported, making this sample an outlier among lunar igneous rocks. Although it has been suggested that this light isotope signature may, after some inter-diffusion corrections, reflect isotopically light melts from which Mg-suite cumulates were sourced (Wang et al. 2015), Sossi and Moynier (2017) disputed this interpretation and suggested major element zoning in dunite 72415 is greater than should be expected given its large grains size and slow cooling rates, which is suggestive of later alteration. Shearer et al. (2015b) documented some potential secondary alteration features in 72415, which may point to a post-crystallization origin for its anomalous $\delta^{57}Fe$ value. A recent study by Prissel et al. (2018) supported the origin of light Fe isotope composition in 72415 as resulting from kinetic effects via diffusion of Fe into high-Mg olivine crystals.

Lunar crustal rocks are one of the suites that have been used to estimate the $\delta^{57}Fe$ of the BSM. Although the $\delta^{57}Fe$ of the BSM has been variously estimated at ~+0.10 to +0.14‰ (Wiesli et al. 2003; Poitrasson et al. 2004; Weyer et al. 2004; Liu et al. 2010) based on data for low-Ti mare basalts, Sossi and Moynier (2017) considered the Mg-suite as the sample suite most likely to record the $\delta^{57}Fe$ of the BSM due to their high Mg#'s and the origin of their parental magmas, in part, from the earliest LMO cumulates. They estimated the $\delta^{57}Fe$ of the BSM to be $+0.07 \pm 0.02‰$. Poitrasson et al. (2019) broadly followed this approach using a larger set of new and compiled $\delta^{57}Fe$ values for Mg-suite rocks and anorthosites, showing a 1.2‰ variation. In dunite 72415 and anorthosite 60025, in particular, the negative $\delta^{57}Fe$ values could be explained by diffusion-driven Fe isotope fractionation related to olivine. Specifically, the $\delta^{57}Fe$ varies by ~0.6‰ for 60025, apparently caused by sample heterogeneity on an allocation scale. The available highlands data led Poitrasson et al. (2019) to derive $\delta^{57}Fe$ of BSM, and by inference bulk Moon (if no Fe isotope fractionation between silicate part and core is considered) at $\sim 0.094 \pm 0.035‰$. However, high-temperature and pressure isotope exchange experiments have demonstrated Fe isotope fractionation during core formation at lunar conditions (Shahar et al. 2015; Elardo and Shahar 2017; Elardo et al. 2019).

Elardo et al. (2019) noted that Mg-suite parental magmas have been contaminated by KREEP, whereby analyses of KREEP basalts have shown to have a $\delta^{57}Fe$ fractionated to positive values, most likely through extensive fractionation in the LMO. This would make the Mg-suite unlikely to record the $\delta^{57}Fe$ of the BSM, as its Fe is sourced from multiple reservoirs,

including KREEP. Alternatively, they suggested that the Apollo 15 green glasses are most likely to record the δ^{57}Fe of the BSM, after correction for fractionation during partial melting. The estimates of the δ^{57}Fe of the green glass source region (–0.10 ± 0.05‰) are consistent with predictions of the δ^{57}Fe of the BSM based on core formation models.

2.9.6. Copper. Day et al. (2019) reported δ^{65}Cu values for two breccia fragments from the 'Rusty Rock' 66095 and observed no distinctive differences compared to the range reported for lunar basalts (Herzog et al. 2009). Sequential leaching and etching of the fragments has revealed only slight variations in δ^{65}Cu. A residue of one anorthosite fragment following H_2O leaching returned δ^{65}Cu of 0.59‰, similar to that of breccia fragments (0.70–0.79‰). Copper isotope systematics of a wider range of Mg-suite lithologies and anorthosites thus remains to be investigated in the future.

2.9.7. Potassium. Modern MC-ICP-MS K isotopic analyses have facilitated a reduction in analytical uncertainties by roughly an order of magnitude (Wang and Jacobsen 2016; Parendo et al. 2017). Wang and Jacobsen (2016) and Tian et al. (2020) analyzed a suite of lunar rocks of various petrologic types. The crustal rocks investigated included FAN 60015, Mg-suite norite 77215, and a range of breccias. Tian et al. (2020) argued that the relatively homogenous $\delta^{41}K = -0.07 \pm 0.09$‰ of mare basalts represents the δ^{41}K of the BSM. This value is distinctly heavier than the δ^{41}K inferred for the bulk silicate Earth (BSE) and chondrites, which led Wang and Jacobsen (2016) and Tian et al. (2020) to argue that K isotopic fractionation accompanied volatile deletion of the Moon during the giant impact, resulting in higher δ^{41}K values of the BSM relative to the BSE. Tian et al. (2020) further argued that a second phase of K isotopic fractionation occurred through LMO degassing of K, likely as KCl. They showed that some KREEP-rich rocks crustal have higher δ^{41}K values than the mare basalt average, indicating that KREEP may have a more fractionated δ^{41}K than the BSM due to degassing of KREEP during the terminal stages of the LMO (Fig. 1). A few crustal breccias, however, have extremely low δ^{41}K down to −2.60‰, which Tian et al. (2020) interpreted as light K deposited in the crustal environment due to degassing. Still, these isotope variations should be combined with thermodynamic calculations to assess K loss from LMO under lunar conditions (cf., a marginal loss of K from silicate melts on Earth; Jiang et al. 2019).

2.9.8. Zinc. Much like K, Zn is a potentially important isotopic system for understanding volatile depletion processes on the Moon due to its volatile nature, either at the time of lunar origin or during other episodes of magmatic degassing (e.g., Paniello et al. 2012; Day and Moynier 2014; Kato et al. 2015; Dhaliwal et al. 2018; Wimpenny et al. 2018, 2019; Day et al. 2020). However, Zn isotope data for lunar crustal samples are fairly sparse. A significant range in Zn abundances and isotopic compositions has been found for FANs (0.6–75 ppm, δ^{66}Zn from −11.4 to +4.2‰;) (Kato et al. 2015), which is larger than the range for other lunar rocks, with the exception of impact melt breccia 66095, with bulk-rock δ^{66}Zn of −13.7‰ (Day et al. 2017). Day et al. (2017) and Kato et al. (2015) interpreted the heavy Zn isotopic compositions in lunar samples, including mare basalts, as evidence for evaporation of significant portion of Zn from the LMO and light isotopic values as evidence of re-condensation of Zn at lunar surface. The least affected FAN, 15415, has a Zn abundance of 0.6 ppm and heavy δ^{66}Zn of +4.2‰, which may reflect the pristine anorthositic crustal value. In contrast, cataclastic anorthosite 65315 has a high Zn abundance of 75 ppm and a light δ^{66}Zn of −11.4‰. This, combined with other FAN data, provides evidence supporting isotopically light Zn derived from Zn-rich vapor (Kato et al. 2015). The Mg-suite rocks dunite 72415 and norite 77215 show similar enrichments in heavy Zn isotopes, suggesting they have not been contaminated by vapor deposition of light Zn. Day et al. (2020) reported on Zn elemental and isotope data for three norites and one troctolite, all with uniformly elevated δ^{66}Zn between 2.5 and 9.3‰ compared to mare basalts, which have δ^{66}Zn values between 1.2 and 1.9‰. They modelled heavy Zn isotope signature as a consequence of evaporative loss during later stages of LMO.

These data support the depletion of the Moon in volatiles following the giant impact and/or during LMO evolution (Kato et al. 2015). A precise chronology of FAN and Mg-suite rocks combined with Zn elemental and isotope measurements could thus place strong constraints on the timing of volatile depletion within the context of the LMO model.

2.9.9. Gallium. The first available Ga isotopic data for lunar crustal samples reported by Kato and Moynier (2017) have two interesting features: (1) Mg-suite norite 77215 has a δ^{71}Ga value identical to the mean Ga isotope composition of mare basalts, and (2) FANs show a range of δ^{71}Ga values from −0.47 to +0.85‰. Moreover, Ga appears to be significantly depleted in the Moon compared to Earth (e.g., Kato et al. 2017a), with Ga contents generally lower than 4 ppm irrespective of lithology (Neal 2001; Magna et al. 2006; Kato and Moynier 2017). The participation of early LMO cumulates in the origin of Mg-suite rocks suggests that the low Ga abundance in 77215 (1.5 ppm) can be considered a primary feature of their rocks. In contrast, low Ga concentrations (0.5–1.9 ppm) and variable δ^{71}Ga values in FANs may reflect volatilization and re-condensation at the lunar surface rather than a Ga-depleted source in continuously crystallizing LMO (Kato and Moynier 2017). A more extensive set of Mg-suite samples, anorthosites, and mare basalts may provide further constraints on Ga systematics in the lunar crust and its relationship to mare basalt sources.

2.9.10. Rubidium. A preliminary report of the stable Rb isotopic composition of lunar samples focused on mare basalts. However, a single δ^{87}Rb datum for Mg-suite norite 77215 is identical to mean δ^{87}Rb value for low-Ti and high-Ti mare basalts (Pringle and Moynier 2017). Overall, the current available stable Rb isotopic data for lunar samples show them to be heavier than the average composition of terrestrial samples, although it should be noted that chondrites span a large range that encompasses the range in both the lunar and terrestrial data. Pringle and Moynier (2017) argued that the isotopically heavier lunar data are indicative of fractionation during the giant impact or during LMO stage. However, more Rb stable isotopic data are needed for both crustal and basaltic samples before any definitive conclusions can be drawn.

2.9.11. Titanium. KREEP-rich lunar materials appear to carry heavy stable Ti isotope systematics although the samples were so far limited to three KREEP-rich breccias, one KREEP-rich basalt, and a meteorite (Greber et al. 2017; Kommescher et al. 2020). Extensive ilmenite segregation has been suggested based on experimental data. Given the yet unconstrained δ^{49}Ti of true crustal samples, an exact role of LMO solidification, and its link to mineralogy, and stable Ti isotope systematics of distinct mantle and crustal reservoirs awaits future work.

2.9.12. Chromium. Sossi et al. (2018) provided stable δ^{53}Cr data for four norites, one troctolite, and one dunite. The δ^{5}Cr values in latter two samples were suggested to reflect that of their Mg-suite parent magma (~ −0.3‰) whereas increasingly heavier Cr isotope compositions reflect the cumulate nature of norites with chromite accumulation and the important role of orthopyroxene in Cr isotope fractionation.

2.10. Magmatic volatiles (H, F, and Cl) and their isotopes in the lunar crust

Earth and the Moon have many geochemical similarities, but one of the most striking differences between the two bodies is the degree of volatile-depletion in the Moon relative to Earth. Nevertheless, the abundance, distribution, and isotopic composition of volatile elements in lunar samples, particularly H and Cl, have been under intense study since ~2008. These studies were motivated by the discovery of endogenous H in pyroclastic volcanic glasses (Saal et al. 2008; Hauri et al. 2011) and in apatite from a wide range of samples (Boyce et al. 2010; McCubbin et al. 2010a,b; Greenwood et al. 2011). Moreover, the discovery of highly fractionated isotopic compositions of H and Cl further revealed the important roles that volatiles have played in the thermochemical evolution of the Moon and provide important constraints on the nature of crust formation (Sharp et al. 2010; Greenwood et al. 2011; Saal et al. 2013; Tartèse et al. 2013, 2014; Barnes et al. 2014, 2016a,b; Füri et al. 2014; Shearer et

al. 2014; Boyce et al. 2015; Potts et al. 2018). Although variations of hydrated species on the surface can now be detected remotely (see review in Hurley et al. 2023, this volume), returned samples are required for the detailed analyses of volatiles reviewed here.

Hydrogen, Cl, C, N, F, and S are all considered magmatic volatiles and are also considered geochemically volatile elements, which describes any element with a 50% condensation temperature below 1300 K (see McCubbin et al. 2023, this volume). Here we focus on differences in the abundance, distribution, and isotopic compositions of H and Cl between the lunar crust and the lunar mantle to constrain the geological processes that led to the formation and subsequent evolution of the lunar crust. Volatiles in lunar samples have been measured in glasses (Saal et al. 2008, 2013; Füri et al. 2014; Wetzel et al. 2015; Greenwood et al. 2017), melt inclusions (Hauri et al. 2011; Saal et al. 2013; Chen et al. 2015; Ni et al. 2017), apatite (Patiño Douce and Roden 2006; Boyce et al. 2010, 2015; McCubbin et al. 2010a,b, 2011, 2015a; Sharp et al. 2010; Greenwood et al. 2011; Barnes et al. 2013, 2014, 2016a,b; Tartèse et al. 2013, 2014a,b; Elardo et al. 2014; Robinson and Taylor 2014; Treiman et al. 2014, 2016; Robinson et al. 2016; Potts et al. 2018), and nominally anhydrous minerals (Hui et al. 2013, 2017; Mills et al. 2017). However, apatite is the only phase that has been analyzed in a wide range of lunar crustal rocks, in part because it occurs in nearly all lunar rock types.

2.10.1. Relative abundances of H, F, and Cl in the lunar interior. Apatite contains H, F, and Cl in its crystal structure, and substantial efforts have been put forth to characterize apatite as a quantitative magmatic hygrometer (Mathez and Webster 2005; Boyce et al. 2014; Li and Hermann 2015; McCubbin et al. 2015b; Li and Hermann 2017; Webster et al. 2017; McCubbin and Ustunisik 2018; Riker et al. 2018). Although considerable work remains before apatite is a quantitative hygrometer, relative abundances of F, Cl, and H in apatite can be used to infer their relative abundances in the melt from which apatite formed (e.g., McCubbin et al. 2013, 2016). Based on the apatite compositions in lunar samples (Fig. 3 in McCubbin et al. 2023, this volume) the relative abundances of F, Cl, and H in mare basalts differs from those of the Mg- and alkali-suite (McCubbin et al. 2011, 2015a). Mare basalt magmas are inferred to have been depleted in Cl relative to F and H, whereas crustal magmas are inferred to have been enriched in Cl relative to F and H. This observation has been interpreted as a fundamental difference between the relative abundances of volatiles in the lunar mantle, reflected by mare basalts, and the relative abundances of volatiles in urKREEP (where the prefix ur refers to the primordial, LMO liquid KREEP), reflected by Mg- and alkali-suite rocks (McCubbin et al. 2015a). The heterogeneous distribution of volatiles in the lunar interior is thought to arise from crystallization of the LMO during which F and H are more compatible than Cl in the nominally anhydrous mantle phases (Aubaud et al. 2004; Hauri et al. 2006; O'Leary et al. 2010; Beyer et al. 2012). Consequently, the urKREEP composition is more reflective of the relative abundances of volatiles in the BSM with $Cl > H_2O \approx F$. However, this model also levies a requirement that less than 1% LMO liquid is trapped in the cumulate mantle, which is on the low end of most estimates (Snyder et al. 1992; Elkins-Tanton and Grove 2011; Charlier et al. 2018).

2.10.2. Chlorine isotopes in the lunar crust. Chlorine enrichment in the lunar crust relative to the mantle is also accompanied by differences in the Cl isotopic composition between the crust and mantle. It was noted that $\delta^{37}Cl$ values of apatite in low-Ti mare basalts, including KREEP basalts, were positively correlated with the bulk rock abundances of incompatible trace elements (ITE; Boyce et al. 2015; Barnes et al. 2016b). Furthermore, the upper end of the values exhibited by low-Ti mare basalts was similar to all of the $\delta^{37}Cl$ values of apatite from the KREEP-rich crustal rocks (Boyce et al. 2015; McCubbin et al. 2015a; Barnes et al. 2016b), which are thought to have volatiles sourced almost exclusively from the KREEP reservoir (McCubbin et al. 2015a). These studies estimated that the KREEP reservoir has a $\delta^{37}Cl$ value of ≥ 25‰ (Boyce et al. 2015; McCubbin et al. 2015a; Barnes et al. 2016b) whereas the lunar mantle is estimated to have a $\delta^{37}Cl$ value of approximately 0‰ (Sharp et al. 2010; Boyce et al. 2015, 2018b; Barnes et al. 2016b), similar to terrestrial rocks and chondrites (Sharp et al. 2007, 2013b).

The Cl isotopic composition of KREEP is thought to result from the loss of metal chlorides from either the LMO (Boyce et al. 2015) or directly from degassing of urKREEP (Barnes et al. 2016b). Data from only the low-Ti mare basalts and the KREEP-rich crustal rocks are consistent with both models, although magma ocean degassing has also been implicated to explain the Cl isotopic composition of eucrites (Sarafian et al. 2017b) as well as other stable isotopic systems in lunar rocks. In contrast, Cl isotopic and bulk rock ITE systematics in high-Al and high-Ti mare basalts may not show the same trends as those reported in low-Ti basalts (Potts et al. 2018; Barnes et al. 2019). Additional data are needed to evaluate these two proposed hypotheses for the origin of elevated Cl isotopic compositions in KREEP-rich samples.

Paradoxically, both models to explain the elevated Cl isotopic composition of the lunar crust imply that the KREEP reservoir, which is enriched in Cl relative to F and H, is enriched in the heavier isotope of Cl through a Cl-loss process (i.e., degassing). Consequently, either Cl was highly enriched in urKREEP relative to F and H to a degree that Cl loss did not affect the relative abundances of Cl, H, and F, or F and H were also lost by a similar mechanism as Cl and the KREEP reservoir represents the end state of all loss processes. Experimental data on degassing of volatiles from lunar melts under vacuum supports the latter scenario (Ustunisik et al. 2011, 2015), although a combination of both possibilities cannot be ruled out.

2.10.3. Hydrogen isotopes in the lunar crust. Hydrogen isotopic compositions have been measured in nearly every rock type returned from the Apollo missions and in numerous lunar phases, including apatite, pyroclastic glasses, melt inclusions, and nominally anhydrous phases. Unlike Cl isotopic compositions, H isotopic compositions of lunar samples, for the most part, do not exhibit systematic variations. Therefore, there are far fewer constraints on the interpretations of H isotopic data. This is complicated further by the fact that H and D diffusion are fast relative to all other volatile stable isotopic systems that have been studied on the Moon, so re-equilibration is relatively rapid and closure temperatures are generally lower (Zhang and Stolper 1991; Baker 2008; Zhang and Ni 2010; Zhang et al. 2010; Gaetani et al. 2012; Bucholz et al. 2013; Boyce et al. 2018a). Consequently, H isotopic compositions are highly susceptible to resetting or modification via secondary processes such as degassing and assimilation (Greenwood et al. 2011; Sharp et al. 2013a; Tartèse and Anand 2013; Tartèse et al. 2014a; McCubbin et al. 2015a; Treiman et al. 2016). In fact, the lunar regolith is enriched in H from the solar wind with an H isotopic composition nearing the theoretical minimum of –1000 ‰ (Robert et al. 2000), and degassing of H_2 from lunar magmas can drive H isotopic compositions of a residual melt to values >1000 ‰ (Sharp et al. 2013a; Tartèse and Anand 2013). Furthermore, samples with low abundances of H and long exposure ages are susceptible to modifications of their H-isotopic composition through spallation, so cosmic-ray exposure corrections are necessary prior to the interpretation of H isotopic data (Saal et al. 2008, 2013; Liu et al. 2012; Barnes et al. 2014; Füri et al. 2014, 2017; Stephant and Robert 2014; Singer et al. 2017). Some of these corrections in δD values are in the range of 2000‰ to 4000‰ (Saal et al. 2013; Singer et al. 2017).

Nonetheless, a few studies have observed systematic variations in H isotopic compositions within subsets of sample types that have been used to understand the H isotopic composition of the Moon, including the crust. Olivine-hosted melt inclusions in the pyroclastic orange glass 74220 are the most H-rich glasses that have been analyzed, and these data have been used to infer that the mantle has an H-isotopic composition that is indistinguishable from carbonaceous chondrites (Saal et al. 2013), similar to many other terrestrial bodies in the solar system, including Earth (Alexander et al. 2012; Sarafian et al. 2014, 2017a). Similarly, apatite from KREEP basalts and KREEP-rich Mg-suite rocks also indicate an H isotopic composition for the Moon that is similar to Earth (Barnes et al. 2014; Tartèse et al. 2014a). In contrast to the Cl-isotopic systematics of the Moon, there is not a clear distinction between the inferred H isotopic composition of the lunar mantle and crust. We caution, however, that the large variations in H isotopic composition exhibited by many phases in lunar samples indicates that there is substantial uncertainty regarding

the H isotopic composition of the BSM, the variation in H isotopic compositions within the lunar interior, and the origin of H that has been measured in lunar samples.

2.11. Alteration of the lunar crust

2.11.1. Endogenous alteration. One of the primary issues in documenting and understanding secondary alteration in the lunar crust is recognizing the effects of alteration in a low f_{O_2}, water-poor environment. Unlike more oxidizing, water-rich environments such as those in Earth's crust or even the martian crustal environment in the past, the lunar crust does not contain minerals such as serpentinite, chlorite, iron hydroxides, and clays that are usually indicative of water-rich alteration. However, a number of studies have found textural and geochemical evidence for secondary alteration of the lunar crust.

Treiman et al. (2014) documented fluorapatite grains up to 1 mm in length in granulitic breccia 79215, a rock with low abundances of K and REEs, suggesting a decoupling of P from the KREEP reservoir. Although apatite had low REE abundances and a high F/Cl ratio, its Cl and H isotopic compositions were highly fractionated, with $\delta^{37}Cl = 32.7 \pm 1.6‰$ and δD between +350 and +750‰. The KREEP reservoir is REE-rich and has a low F/Cl ratio, but has highly fractionated $\delta^{37}Cl$ and δD (McCubbin et al. 2015a). Treiman et al. (2014) argued that the apatite grains in 79215 were deposited by a P- and halogen-rich vapor likely sourced from a nearby KREEP-rich reservoir. This vapor mobilized P and the halogens, but not the more refractory REEs and other incompatible lithophile elements enriched in KREEP, thus the apatite that was deposited in 79215 inherited the $\delta^{37}Cl$ and δD of KREEP but not its enrichment in incompatible elements. Treiman et al. (2014) suggested the heat source for the formation of this metasomatic vapor phase would most likely be an impact, but the mobilized elements were ultimately derived from lunar reservoirs. Shearer et al. (2015b) also documented apatite in Mg-suite dunite 72415 with textures suggesting a secondary origin. The apatite in 72415 had a vein-like morphology (Fig. 3e), filling in cracks within olivine grains. Although Shearer et al. (2015b) only documented apatite texture, its morphology is suggestive of formation from a metasomatic fluid or vapor, or possibly remobilization by re-melting of phosphate in the rock.

In three Mg-suite and FAN clasts (67016,294; 67016,297; and 67915,150), olivine has been partially or totally replaced by troilite and low-Ca pyroxene (Fig. 3d; Norman 1982; Lindstrom and Salpas 1983; Norman et al. 1995). Troilite veins crosscut the clasts, but not the host breccia, indicating alteration prior to brecciation. Various S-rich vapor/fluid-based models were proposed to explain the alteration, wherein heat was derived from either magmatic activity in the crust or impacts, and the S-rich vapor/fluid was either the product of degassing of crustal magma bodies or remobilization of sulfides in the crust or regolith (Haskin and Warren 1991; Papike et al. 1991; Colson 1992; Haskin et al. 1993; Norman et al. 1995). Shearer et al. (2012) concluded that magmatic intrusions into the crust supplied the heat for alteration and that S was sourced from either the intrusive magma body or troilite present in crustal rocks. Their measurements of the sulfur isotope composition of the troilite in the alteration assemblage showed a negative $\delta^{34}S$ between –1.0 ‰ and –3.3 ‰, which is uncharacteristic for lunar troilite. Shearer et al. (2012) suggested that these light isotopic compositions were indicative of fractionated S derived from a S-bearing vapor phase that interacted with and altered Mg-suite and FAN plutons.

The polymict impact melt breccia 66095 is often referred to as the "rusty rock" due to its rust-colored alteration assemblage on metal grains and adjacent silicates (Fig. 3f). The alteration assemblage of lawrencite, akaganéite, sphalerite, stanfieldite, hematite, goethite, and an amorphous phase has been attributed to either fumarolic activity on the lunar surface, oxidation in the Apollo capsule crew cabin either during transit back from the Moon or during recovery after splashdown, or alteration during curatorial processing and storage (El Goresy et al. 1973; Taylor et al. 1973, 1974; Epstein and Taylor 1974; Friedman et al. 1974). Shearer et al. (2014) revisited the rusty rock with transmission electron microscopy and Cl isotope

analyses in an attempt to distinguish between lunar and terrestrial alteration models. Although they found complex alteration assemblages (e.g., Fig. 3f), highly fractionated $\delta^{37}Cl$ values, and the nano-scale stratigraphy of the assemblages pointed to deposition of the lawrencite and transformation of troilite to sphalerite by a metal-chloride-bearing fumarolic vapor at ~600 °C, which also transported other elements such as Zn, Cu, Pb, and Fe. Stanfieldite was deposited at a higher temperature. Shearer et al. (2014) argued that the origin of akaganéite was more ambiguous and there were likely multiple episodes of alteration, including reactions occurring on Earth, which may have formed hematite, goethite, and the amorphous phase. Additionally, Day et al. (2017) argued for vapor deposition as a key process of secondary volatile enrichment acting on Moon's surface through Zn isotopic analysis of 66095. Their data showed progressive Zn enrichments in bulk 66095 (up to ~400 ppm) and leachates (up to ~12,040 ppm), paralleled by the lightest Zn isotopic compositions observed for any lunar rock to date. These Zn enrichments and light Zn signature are not paralleled by distinctive Cu and Fe isotope signatures, indicating temperatures at which Zn, but not Cu and Fe, is condensed from the gas phase below 900°C (Day et al. 2019).

Elardo et al. (2012) examined Mg-suite troctolite 76535 with a focus on symplectite assemblages (Fig. 3c) consisting of chromite and two pyroxenes. Although their origin was controversial, symplectites in 76535 had previously been thought to form from the reaction of cumulus chromite with olivine and plagioclase or due to the diffusion of chromium out of olivine during slow cooling. However, Elardo et al. (2012) argued based on the low Cr contents of melt inclusion pyroxenes, the sporadic distribution of symplectites, and relict grain boundaries within symplectites that they are likely the product of infiltration metasomatism from a basaltic melt, which deposited chromite along cracks and grain boundaries. The metasomatic introduction of chromite triggered the symplectite forming reaction with olivine and plagioclase.

2.11.2. Impact modification of the lunar crust. Impact bombardment is by far the most prevalent secondary alteration process in the lunar crustal rocks, spanning spatial scales from grain boundaries to impact melt seas, and effectively producing secondary and possibly tertiary crust. Nevertheless, from a global perspective, fundamental signatures remain in a local and regional context. Impact melt is observed across the Moon at many fresh craters, identified by its morphological, compositional, and textural properties. Despite the enormous energy involved in large-scale impact melting, recent work has provided strong evidence for the preservation of mineralogical heterogeneity within impact melt (Ohtake et al. 2009; Dhingra et al. 2013, 2015), emphasizing the fact that impact melting does not necessarily produce a homogeneous product on the scale of complex craters. There is also no diagnostic spectroscopic signature that can be used to identify impact melt. Although it was anticipated that quenched, Fe-bearing glass would be seen in remote measurements of impact melt as the surface quickly cooled, such a signature has not been readily confirmed. Laboratory spectroscopic measurements of lunar samples that have acquired a component of impact melt while on the lunar surface (Tompkins and Pieters 2010) typically exhibit properties of micro-crystalline products, and the signature of quenched Fe-bearing glass is relatively rare.

Without being placed in context, remote observations of mafic minerals in slowly cooled impact melt are indistinguishable from primary or secondary crustal materials, highlighting the importance of careful evaluation of geologic context. For example, Dhingra et al. (2015) found that strong olivine signatures in a dark (possibly impact melt) streamer along the northern wall of Copernicus crater is apparently unrelated to the abundant, bright olivine found in the central peaks. With high spatial resolution spectral data, impact melt can sometimes be identified covering other features of a complex crater, such as part of the crystalline central peak at Jackson crater (Ohtake et al. 2009; Osinski et al. 2011; Dhingra et al. 2017). One debated but unresolved issue is whether the large impact melt volumes produced by basins could give rise to layered lithologies by differentiation (Hurwitz and Kring 2014; Spudis et al. 2014; Vaughan

and Head 2014; Uemoto et al. 2017). White et al. (2020) observed a large baddeleyite grain in troctolite 76535 that exhibits microstructural features indicative of inversion from cubic ZrO. Since cubic ZrO is only stable at temperatures of >2100 °C and low pressures, or at magmatic temperatures and pressures >20 GPa, and since there is no evidence of shock up to >20 GPa in 76535, White et al. (2020) suggested an impact melt origin for the rock (i.e., very high temperatures at low pressures). However, given the preponderance of evidence for the origin of 76535 as a magmatic cumulate, it is possible that the baddeleyite grain observed by White et al. (2020) may have been inherited by the 76535 parental magma.

3. NEW INSIGHTS INTO THE EVOLUTION OF THE LUNAR CRUST

3.1. The significance of PAN in the global crust

One of the more significant findings in recent years has been the direct detection of pure anorthosite with < 2–3 vol. % mafic minerals (PAN). Such highly pure anorthosite is rare on Earth and it is found mainly in massif anorthosites. In the lunar environment, PAN could potentially be the result of extremely efficient density-driven separation of plagioclase from pyroxene and Fe-rich residual LMO melt (Dygert et al. 2017), which is expected after the crust became thick and thermally insulating, and the speed of the crustal growth slowed allowing more efficient separation during late stages of LMO solidification (e.g., Piskorz and Stevenson 2014). The global exposure of PAN outcrops associated with basins and large craters suggests that coherent blocks of PAN occur within the megaregolith debris over a depth range of 3–30 km (Ohtake et al. 2009; Donaldson Hanna et al. 2014). An example of remnant uplifted massive PAN can be seen along the innermost ring of the Orientale basin (Cheek et al. 2013). Understanding the formation and extent of the global PAN layer and its relation to other crustal lithologies with more detailed modern remote sensing would provide deeper insight into models of crustal formation and evolution.

The lunar sample collection reflects the presence of pure anorthosites as a component of the crust and mountain-sized outcrops of PAN are now readily observed. A compilation of modal mineral abundance data for the Apollo samples by Warren (1993) showed that there are many anorthosite samples or clasts that have a PAN composition and that low-mafic anorthosites are the most abundant component among the ferroan anorthosite suite as counted by the sample number or by the sample weight. For example, the large anorthosites 15415 (269 g) and 60015 (4.6 kg) both contain modal abundances of > 98 modal % plagioclase.

One estimation of the bulk mineral composition of the highland crust from current lunar samples suggests the crust contains an average mafic mineral abundance of around 10–20 wt.% (e.g., Warren 1990). Ejecta from basin impacts such as the impact melt breccias found at all Apollo landing sites were mixtures of crustal anorthosite, other components, and mare basalt, and are significantly more mafic than anorthosite, with bulk compositions that are typically noritic to gabbronoritic (Ryder and Wood 1977; Wieczorek et al. 2006). Surface soils developed on the megaregolith as sensed from orbit are also more mafic than pure anorthosite.

Feldspathic brecciated lunar meteorites, which are estimated to be derived from < 1 km in depth (Warren 1994), also contain more mafic components than PAN on average, reflecting the upper few km of the highlands surface as a mixed megaregolith zone. Although pure anorthosite clasts are relatively rare in meteoritic feldspathic regolith breccias (Korotev et al. 2010), a pristine pure anorthosite lithology was recently reported in the Dhofar 479 feldspathic meteorite group (Nagaoka et al. 2014). These observations lend sample-based support to the observation of PAN as a dominant component of the primary lunar crust, although it is difficult to place quantitative constraints on the average amount of PAN in the global crust using samples due to the very limited extent of sampling across the highland crust. The combined remote sensing information to date indicates the FHT of the lunar farside is the most anorthositic (least mafic) crustal region.

3.2. The Mg-suite: A global or regional crust-building event?

The extent of early Mg-suite crust-building magmatism on the Moon has bearing on planet-scale models of lunar evolution. Production of Mg-suite magmas seems to require rapid overturn of the initial mantle cumulate pile concurrent with or immediately after the end of LMO crystallization based on the concordant ages of FANs and Mg-suite rocks. High-Mg# olivine-dominated cumulates that form early during LMO crystallization are required in Mg-suite formation models, which in turn requires their rapid ascent from the deep mantle through density-driven convection, or that late-stage processes (possibly post-LMO) prolong the closure of isotopic systems in FANs. However, the Sm–Nd and Lu–Hf model ages of both KREEP and mare basalt source region formation are concordant with isochron ages from FAN and Mg-suite samples (Rankenburg et al. 2006; Gaffney and Borg 2014; McLeod et al. 2014; Borg et al. 2015; Boyet et al. 2015; Shearer et al. 2023, this volume), and show that KREEP and mare sources were derived from chondritic, undifferentiated reservoirs. This strongly points to rapid formation of all three reservoirs (crust, mantle, and KREEP) rather than a Moon-wide re-equilibration event.

Since convective mantle overturn is expected to occur globally, it could be argued that Mg-suite magmatism should be a global event. Remote sensing data have been used to argue that outcrops of Mg-suite lithologies occur globally based on the identification of Mg-rich mafic minerals across the lunar crust. Prissel et al. (2014) conducted experiments where a hypothetical KREEP-free Mg-suite parental magma was reacted with anorthite and showed that Mg-spinel is produced. They used these results to suggest that Mg-spinel-rich outcrops observed across the lunar surface (e.g., Pieters et al. 2011, 2014) may be the result of magma-wallrock interactions and therefore that Mg-spinel anorthosite outcrops could represent Mg-suite lithologies. Collectively, the cumulative observations of Mg-rich pyroxene, olivine, and spinel that is distributed globally point to a widespread component(s) of the global lower crust with minerals that are more Mg-rich than the mafic components found in FANs.

Studies of the Apollo Mg-suite samples have typically led to the conclusion that KREEP is a necessary component of Mg-suite magmas and that this episode of magmatism was confined to the PKT (e.g., Korotev 2000, 2005; Wieczorek and Phillips 2000; Shearer and Papike 2005). Radiogenic heat production from KREEP is thought to be a driving force for melting Mg-suite source rocks with a relatively high melting temperature. Mg-suite rocks found among the Apollo samples have been shown to have formed from KREEP-enriched parental magmas on the basis of elevated REE concentrations in their silicate minerals and the occurrence of REE-rich phosphates (Jolliff et al. 1993; Papike et al. 1994, 1996; Snyder et al. 1995; Shervais and McGee 1998; Shearer and Papike 2005; Elardo et al. 2012). Conversely, some Mg-rich igneous clasts found in lunar meteorites appear to lack such a relationship. Lunar meteorites provide a much broader, albeit random, sampling of the Moon compared to the Apollo samples (Korotev 2005) and therefore have the potential to sample Mg-suite lithologies from outside the PKT. Some lunar meteorites contain fragments of troctolitic material that have some major element similarities to the Apollo Mg-suite, such as high Mg#s in mafic minerals. However, in contrast to the Apollo troctolites, these meteoritic troctolitic materials show little to no KREEP component (e.g., Takeda et al. 2006; Treiman et al. 2010; Gross et al. 2014b, 2020; Treiman and Gross 2015). One possibility is that these lithologies represent KREEP-poor Mg-suite rocks sourced from the crust outside the PKT. The relationship between Mg-suite rocks in Apollo sample collection and KREEP-rich parent magmas may be a special consequence of rocks that occur within the PKT (Korotev 2000), and may reflect a non-uniform distribution of urKREEP that was assimilated by early crustal magmas in the PKT. However, without additional information such as crystallization ages and isotopic compositions for such clasts it is difficult to definitively link these samples with Mg-suite magmatism as opposed to other episodes of lunar magmatism or large-scale impact melt crystallization.

Recent experimental studies have come to differing conclusions. Prissel et al. (2014, 2016) used experiments designed to simulate magma-wallrock interactions and to quantify spinel–liquid equilibrium to argue that Mg-spinel anorthosites observed remotely could be representative of Mg-suite lithologies largely absent in the Apollo collection. They suggested that the Mg-rich, Cr-poor Mg-suite parental magmas were the best candidates to produce Mg-rich spinel alongside high Mg# silicates, as is observed in remote sensing studies (e.g., Pieters et al. 2011, 2014). Alternatively, Elardo et al. (2020) conducted a series of high-temperature experiments and heat production calculations on model Mg-suite source region compositions to assess the influence of KREEP on Mg-suite melt production. Their results showed that KREEP has a dramatic effect on melt production, resulting in ~4–13× more Mg-suite melt production solely from melting point depression, and their radiogenic heat production calculations showed that source regions with greater than 20–25 % KREEP would increase in temperature, contributing to further melting, whereas sources with less KREEP would cool over time. These results suggest that post-magma ocean Mg-suite crust building should have been concentrated on the nearside and be far less abundant (or absent) on the farside.

3.3. Composition of the deep crust

The composition of the lower crust can be examined through an analysis of the composition of central peaks of large impact craters, which are predicted to expose materials that resided 5–20 km deep prior to the impact, depending on the size of the crater. Such an endeavor, however, depends on stochastic geologic events (geologic location, prior impact history, crater age) as well as on the analytical approach and quality of data utilized. Consequently, diverse results appear in the literature.

Most analyses of central peaks using a variety of global remotely sensed data indicate that the lower crust is more mafic rich than the more feldspathic upper crust (Cahill et al. 2009; Tompkins and Pieters 2010; Sun et al. 2017). In addition, concentrations of olivine bearing lithologies are often associated with some (but not all) basins that excavate to near the modeled crust/mantle boundary (see Fig. 2 and Yamamoto et al. 2012a). Similarly, the integrated survey by Donaldson Hanna et al. (2014) clearly showed the origin of mafic-bearing crustal lithologies to be deeper and closer to the crust/mantle boundary than that of the widespread crustal crystalline plagioclase (i.e., PAN). In contrast, a separate analysis applied a multi-component mineral mixture model approach, designed to compute and estimate bulk mineralogy, to Kaguya MI data of 34 central peaks, but found no systematic variation with depth (Lemelin et al. 2015). Although noritic breccias with Mg-rich mafic minerals dominate the bulk of basin ejecta deposited globally as the mega-regolith, it is interesting to note that some data suggest that shallow and intermediate crustal zones (up to a few km) may harbor a distinct high-Ca pyroxene component (Ogawa et al. 2011; Crites and Lucey 2015). Additionally, the study of central peaks for deriving crustal composition at various depths requires careful analysis of impact melt that may cover several peaks (e.g., Ohtake et al. 2009; Dhingra and Pieters 2011; Osinski et al. 2011; Dhingra et al. 2014, 2017). The exclusion of impact melt components from compositional analyses of central peaks along with an assessment of regional impact history is necessary for estimates of crustal stratigraphic composition.

3.4. Mafic components of the global primary crust

Determining the nature and origin of mafic components in the crust is an area where it is challenging to merge sample and remote sensing observations. The scale of sample lithology measurements in the laboratory and those of surface lithologies measured remotely often differ by a factor of ~10^6. The detection of PAN in remote data, for example, indicates that mountain-sized areas of pure crystalline anorthosite are present with essentially no detectible mafic minerals. Small amounts of mafic minerals can exist as clumps embedded in the anorthosite,

but must be very limited in number and cannot be intimately or finely dispersed across the anorthosite (Ohtake et al. 2009; Cheek et al. 2013). Conversely, it is often difficult to determine how representative the mineralogy of mm-sized clasts is of their original host lithologies or in some cases whether such clasts are representative of igneous rocks or impact-derived lithologies.

Global remote sensing data appear to suggest the presence of Mg-rich pyroxene in some of the highly feldspathic areas of the highlands, especially in the FHT of the northern farside (Jolliff et al. 2000; Ohtake et al. 2012; Peplowski and Lawrence 2013; Crites and Lucey 2015). Although rare in the Apollo sample collection (e.g., Lindstrom et al. 1984), some lunar meteorites, which can represent the global lunar surface beyond the Apollo sites, have been shown to contain anorthosite with magnesian-rich mafic minerals (Takeda et al. 2006; Treiman et al. 2010; Gross et al. 2014b), leading to the suggestion that such primary crustal 'magnesian' anorthosite could be widespread. Remote sensing data indicate the FeO abundance (Jolliff et al. 2000) and Mg# of pyroxenes (Ohtake et al. 2012) are negatively correlated for surfaces across the nearside to a region of highest average pyroxene Mg# on the farside near the center of FHT. The areas exhibiting the highest mafic mineral Mg# (75 to 81) have the lowest mafic mineral abundance as well as lowest bulk FeO (Ohtake et al. 2012). In remote measurements of the feldspathic highlands, the amount of bulk FeO and MgO both are necessarily correlated with the abundance of mafic minerals present (largely pyroxene and olivine) and thus both oxides are anti-correlated with the abundance of plagioclase. Abundances of FeO, dependent on the amount of mafic minerals present, is estimated by optical approaches and measured by nuclear approaches. MgO is also dependent largely on the amount of mafic minerals present, but is not optically active and is also currently difficult to measure with nuclear techniques (e.g., γ-rays, neutrons). The Mg# of the mafic minerals present can be measured with remote optical techniques (e.g., IR, visible light spectra) but is a relatively small effect on the bulk MgO composition which is largely controlled by the total abundance of mafic minerals and plagioclase in the mixture.

The fragments of anorthositic materials found in lunar samples provide tangible evidence that an apparent continuum in the Mg# of both Fe-rich and Mg-rich minor components exists in crustal lithologies. There are a number of possibilities for the origin of these mafic components during crustal evolution. One possibility is that these components represent the incorporation of mafic magmas to the global lunar crust. Mg-suite magmas are the lithologies in the sample collection that best fit this scenario. Currently, candidate Mg-suite lithologies are best identified remotely by the presence and composition of Mg-rich pyroxene, olivine, and spinel present in highly feldspathic materials. However, an Mg-suite origin for these mafic components is uncertain. It remains to be resolved whether the KREEP reservoir is necessary for the origin of the important Mg-suite crustal component. Furthermore, hypothesized intrusive magmatism and crustal underplating in the farside highlands on a scale that could affect the composition of essentially the entire FHT would also be expected to result in extrusive volcanism, at least sporadically, which is not observed. Remote compositional analyses indicate that the mega-regolith, a mixture of feldspathic products of the crustal column (and perhaps the upper mantle) redistributed by basins, contains pervasive components of Mg-rich pyroxene on a global scale.

Of great interest is whether the observed higher Mg# mafic components associated with some anorthosites are a feature of the primary LMO anorthositic flotation crust. At least some such samples of anorthosites and granulites (Lindstrom et al. 1984; Korotev et al. 2003; Takeda et al. 2006; Gross et al. 2014b; Shearer et al. 2015b) could represent either relatively pristine or reworked samples of primary anorthositic crust, possibly from the FHT. An LMO origin is potentially consistent with major element chemistry of these lithologies, particularly the lack of a Na enrichment trend in the plagioclase. The Mg#s of their mafic minerals and the An#s of their plagioclase essentially follow the trend defined by the FANs, but extend this trend to higher Mg#s (Fig. 5). For example, an experimental study by Nekvasil et al. (2015)

showed that the pseudo-azeotrope found in the albite-anorthite system (Lindsley 1969) is also present in model LMO silicate liquid compositions. This liquidus topology results in a reaction between plagioclase and olivine melt components at pressures above 0.35 GPa (> 70 km in the Moon) that inhibits or reverses the typical Na enrichment trend in plagioclase with decreasing temperature. This reaction resulted in reverse Na zoning in plagioclase in their experiments, which can explain why FANs and magnesian anorthosites do not exhibit the more typical Na enrichment trend that Mg- and alkali-suite samples do (Fig. 5). Determining the nature of these two trends and their geologic context with a combination of remote, targeted *in-situ,* experimental, and sample data is an important challenge for the future.

If the primary anorthositic crust is indeed shown to have a hemispheric asymmetry in Mg# of mafic minerals co-crystalizing with plagioclase, then the simple LMO model of plagioclase saturation in a global, homogeneous magma ocean cannot be fully correct. Asymmetric crust formation beginning on the farside was initially proposed by Warren and Wasson (1980) to explain the concentration of KREEP on the nearside. Loper and Werner (2002) suggested that this concentration of early-formed plagioclase on the farside may be the result of tilted convection in the LMO oriented toward the farside by a thermal gradient induced by radiation from the nearby still-hot Earth. Early-formed plagioclase should incorporate mafic minerals with a higher Mg# than later-formed plagioclase, the latter of which would concentrate on the nearside in asymmetric crystallization (Gaffney et al. 2023, this volume). Targeted new sample studies along with high-quality remotely sensed-data obtained with modern sensors are clearly needed to elucidate the composition of the primary anorthositic crust and what any asymmetries in composition reveal about crustal formation and evolution processes.

3.5. Composition of the crust/mantle exposed by SPA and other basins

The composition of the SPA interior analyzed by remote sensing VNIR spectroscopy (see Fig. 6) suggests that Mg-rich, low-Ca pyroxene is a major mineral component with plagioclase of material exposed in this terrane (Ohtake et al. 2014; Moriarty and Pieters 2015; Uemoto et al. 2017; Moriarty and Pieters 2018). However, the origin of this Mg-rich pyroxene lithology is not simple. Impact models have suggested that large impacts, such as the one that generated the SPA basin, must have sampled the Moon's upper mantle and inevitably melted, mixed, and ejected large quantity of mantle material. Melosh et al. (2017) concluded that the low-Ca pyroxene observed in spectral data of SPA was derived not from the lower crust, but rather largely from the Moon's upper mantle. Magma ocean crystallization models have predicted that the Moon's upper mantle should be pyroxene-rich and olivine-poor pre-cumulate overturn (Taylor and Jakeš, 1974; Snyder et al. 1992; Elardo et al. 2011; Charlier et al. 2018; Rapp and Draper 2018). If the mantle under SPA did not experience extensive overturn of the cumulate pile, then the widespread occurrence of low-Ca pyroxene in SPA ejecta would be consistent with a mantle origin (e.g., Moriarty et al. 2021).

On the other hand, multiple analyses of remote sensing data have consistently indicated that the upper kilometers of mega-regolith, derived largely from the cumulative product of multiple large basin ejecta deposits during early crustal evolution, are globally dominated by anorthositic norite breccias (i.e., plagioclase with a small amount of Mg-pyroxene; Pieters 1986; Hawke et al. 2003; Petro and Pieters 2008; Lucey et al. 2014). This indicates that SPA is simply the largest and oldest basin to excavate and redistribute deep-seated Mg-rich lithologies, and potentially mantle materials. Olivine is a minor component and almost absent in SPA (Figs. 2, 6). The pervasive noritic megaregolith dominates surface materials and appears to be superimposed on what remains of the FAN/PAN primary crust (Hawke et al. 2003; Cheek et al. 2013; Donaldson Hanna et al. 2014).

It should be noted that if differentiation of a vast interior SPA impact melt sheet/sea is possible, models of the fractional crystallization process indicate that some of the lithologies observed remotely within SPA could result (Hurwitz and Kring 2014; Vaughan and Head 2014). Ultimately, the mafic components produced by melt sheet differentiation would have been controlled by the composition of the target lithologies incorporated into that melt sheet by the SPA impact. Therefore, if the observed noritic lithologies in SPA are impact melt sheet differentiates, it would indicate that the original components of the lower crust and/or upper mantle were likely generally noritic in bulk composition, as supported by SPA melt sheet differentiation models (Hurwitz and Kring 2014).

4. UNRESOLVED QUESTIONS AND FUTURE DIRECTIONS

Lunar science community has made enormous progress since the publication of *New Views of the Moon* in 2006. Missions making new high-quality observations, the discovery of new meteorites, and the emergence of novel and improved analytical techniques have significantly advanced our understanding of the fundamental crustal evolutionary processes. However, new discoveries continue and the resolution of old mysteries have led to challenging new questions, some of which, were not even possible to recognize 15 years ago. In the coming decades, diverse new samples from targeted sites and more advanced remote compositional analyses providing detailed geologic context, will be the key components for expanding our understanding of planetary crust formation and evolution. Here we highlight several major unresolved questions regarding the evolution of the lunar crust that offer fruitful directions for such integrated inquiry in the future:

What is the true chronological history of the lunar crust?

Sample isochron and reservoir model ages indicate that FANs, the Mg-suite, mare basalt sources, and KREEP formed essentially contemporaneously. Whether these ages are true formation ages or rather represent later events and how this chronology bears on the expected chronology from geochemical requirements must be resolved. Chronological studies of farside crustal samples, which may represent the most primitive lunar crust, will be needed in the future.

What is the cause of the hemispherical asymmetries in the lunar crust?

It has been known for decades that the sampled lunar nearside differs substantially from the farside. The nearside has significantly thinner crust on average and hosts the overwhelming majority of mare basalt deposits and KREEP-rich lithologies. A comprehensive model for the origin of these differences and how they relate to the lunar magma ocean and primary crust formation is lacking. Samples and detailed remote compositional analyses of the lunar farside crust, especially from the FHT, SPA, and sparse farside mare basalts will be essential to unraveling the origin of these fundamental crustal asymmetries.

What is the role of large impacts and the contribution of impact melt deposits in early crustal evolution?

The late heavy bombardment clearly shaped the character of the evolving crusts of the Earth-Moon system. The current incomplete assessment and sampling of early lunar crustal components cannot resolve the relative importance of initial post-magma ocean solidification products and possibly cotemporaneous extensive basin impact melt deposits (and their potential differentiation). A targeted sample return to the largest and oldest impact basin (SPA) combined with detailed remote observations of possible SPA impact melt deposits has been a high science priority for decades in order to understand the role of large impacts in shaping the early crust and the timing of the late heavy bombardment.

What is the extent, timing, and duration of secondary crust formation on the Moon?

The Apollo/Luna/Chang'e and basaltic meteorite sample collection does not contain examples of the youngest basaltic lava flows on the lunar surface. Crater statistics studies have revealed volcanic deposits dating to ~1 Ga and the tantalizing occurrences of IMPs, some of which might be as young as ~18 Myr. Sample return from these sites would reveal the most recent evolution of the crust, the impact history of not only the Moon but the whole inner solar system, and the thermal and chemical evolution of the lunar mantle.

Is KREEP required for Mg-suite magmatism and was the Mg-suite a global or regional magmatic event?

Remote observations have detected Mg-rich lithologies potentially consistent with -e rocks across the global lunar crust. Additionally, clasts have been discovered in lunar meteorites that hint at the same conclusion. However, no definitive, undisputed Mg-suite samples have been found in lunar meteorites derived from outside the PKT while experimental studies point to an important role of KREEP in producing Mg-suite magmas. Resolution of this dilemma has implications for the history of crustal evolution and relates to the extent of early planetary scale processes.

What is the origin of the alkali-suite and silicic lithologies, and how abundant are these lithologies in the crust?

There are currently only limited samples of the alkali-suite and silicic lithologies available for study in the sample collection. However, silicic lithologies, sometimes occurring as domes and/or volcanic complexes, have been detected via remote observations. Although models exist for their petrogenesis, the origins of these lithologies remain enigmatic, as does their relative abundance and importance as components of the crust.

What is the composition, vertical extent, mode of formation, and relationship between PAN and FAN?

Recent remote analyses have shown that local areas across large regions of the lunar crust consist of very pure anorthosite, PAN, allowing a rough estimation of its original lateral and vertical occurrences throughout the crust. The true extent and composition of minor mafic minerals associated with the origin of PAN anorthosite and the relationship to sampled ferroan anorthosite (FAN), however, remain to be addressed. A related challenge for understanding these two forms of crustal anorthosites is the current difficulty of detecting and understanding the character and distribution of shocked plagioclase across the lunar surface, and a thorough assessment of impact effects on the primary crust and how they affect remote observations is essential.

ACKNOWLEDGMENTS

S.M.E. acknowledges support from NASA Solar System Workings grant 80NSSC19K0752. C.M.P. appreciated SSERVI support through NNA14AB01A. J.G acknowledges support from NASA Solar System Workings grant 80NSSC19K0558. FMM was supported by NASA's planetary Science Research Program during this work. T.M. contributed through the Strategic Research Plan of the Czech Geological Survey (DKRVO/ČGS 2018-2022). T.D.G. was supported by the Diviner Lunar Radiometer Science Team and the RIS^{4}E node of NASA's Solar System Exploration Research Virtual Institute (SSERVI). R. L. K was supported by NASA LDAP grant NNX16AN50G. R.L.K and B.T.G appreciated SSERVI support through NNA14AB02A.

REFERENCES

Alexander CMOD, Bowden R, Fogel ML, Howard KT, Herd CDK, Nittler LR (2012) The provenances of asteroids, and their contributions to the volatile inventories of the terrestrial planets. Science 337:721–723

Anand M, Taylor LA, Floss C, Neal CR, Terada K, Tanikawa S (2006) Petrology and geochemistry of LaPaz Icefield 02205: A new unique low-Ti mare-basalt meteorite. Geochim Cosmochim Acta 70:246–264

Arai T, Takeda H, Yamaguchi A, Ohtake M (2008) A new model of lunar crust: Asymmetry in crustal composition and evolution. Earth, Planets and Space 60:433–444

Arai T, Hawke BR, Giguere TA, Misawa K, Miyamoto M, Kojima H (2010) Antarctic lunar meteorites Yamato-793169, Asuka-881757, MIL 05035, and MET 01210 (YAMM): Launch pairing and possible cryptomare origin. Geochim Cosmochim Acta 74:2231–2248

Armytage R, Georg R, Williams H, Halliday A (2012) Silicon isotopes in lunar rocks: Implications for the Moon's formation and the early history of the Earth. Geochim Cosmochim Acta 77:504–514

Arnold J, Glotch T, Lucey P, Song E, Thomas I, Bowles N, Greenhagen B (2016) Constraints on olivine-rich rock types on the Moon as observed by Diviner and M^3: Implications for the formation of the lunar crust. J Geophys Res: Planets 121:1342–1361

Ashley J, Robinson M, Stopar J, Glotch T, Hawke BR, van der Bogert C, Hiesinger H, Lawrence S, Jolliff B, Greenhagen B (2016) The Lassell massif—A silicic lunar volcano. Icarus 273:248–261

Aubaud C, Hauri EH, Hirschmann MM (2004) Hydrogen partition coefficients between nominally anhydrous minerals and basaltic melts. Geophys Res Lett 31:L20611

Baker DR (2008) The fidelity of melt inclusions as records of melt composition. Cont Min Petrol 156:377–395

Baker DM, Head JW (2015) Constraints on the depths of origin of peak rings on the Moon from Moon Mineralogy Mapper data. Icarus 258:164–180

Baldwin RB (1963) The Measure of the Moon. [Chicago] University of Chicago Press

Barnes JJ, Franchi IA, Anand M, Tartèse R, Starkey NA, Koike M, Sano Y, Russell SS (2013) Accurate and precise measurements of the D/H ratio and hydroxyl content in lunar apatites using NanoSIMS. Chem Geol 337–338:48–55

Barnes JJ, Tartèse R, Anand M, McCubbin FM, Franchi IA, Starkey NA, Russell SS (2014) The origin of water in the primitive Moon as revealed by the lunar highlands samples. Earth Planet Sci Lett 390:244–252

Barnes JJ, Kring DA, Tartèse R, Franchi IA, Anand M, Russell SS (2016a) An asteroidal origin for water in the Moon. Nat Commun 7:11684

Barnes JJ, Tartèse R, Anand M, McCubbin FM, Neal CR, Franchi IA (2016b) Early degassing of lunar urKREEP by crust-breaching impact(s). Earth Planet Sci Lett 447:84–94

Barnes JJ, Franchi IA, McCubbin FM, Anand M (2019) Multiple reservoirs of volatiles in the Moon revealed by the isotopic composition of chlorine in lunar basalts. Geochim Cosmochim Acta 266:144–162

Beyer C, Klemme S, Wiedenbeck M, Stracke A, Vollmer C (2012) Fluorine in nominally fluorine-free mantle minerals: Experimental partitioning of F between olivine, orthopyroxene and silicate melts with implications for magmatic processes. Earth Planet Sci Lett 337:1–9

Borg LE, Gaffney AM, Shearer CK, DePaolo DJ, Hutcheon ID, Owens TL, Ramon E, Brennecka G (2009) Mechanisms for incompatible element enrichment on the Moon deduced from the lunar basaltic meteorite Northwest Africa 032. Geochim Cosmochim Acta 73:3963–3980

Borg LE, Connelly JN, Boyet M, Carlson RW (2011) Chronological evidence that the Moon is either young or did not have a global magma ocean. Nature 477:70–72

Borg LE, Gaffney AM, Shearer CK (2015) A review of lunar chronology revealing a preponderance of 4.34–4.37 Ga ages. Meteorit Planet Sci 50:715–732

Borg LE, Connelly JN, Cassata WS, Gaffney AM, Bizzarro M (2017) Chronologic implications for slow cooling of troctolite 76535 and temporal relationships between the Mg-suite and the ferroan anorthosite suite. Geochim Cosmochim Acta 201:377–391

Boyce JW, Liu Y, Rossman GR, Guan Y, Eiler JM, Stolper EM, Taylor LA (2010) Lunar apatite with terrestrial volatile abundances. Nature 466:466–469

Boyce JW, Tomlinson SM, McCubbin FM, Greenwood JP, Treiman AH (2014) The lunar apatite paradox. Science 344:400–402

Boyce JW, Treiman AH, Guan Y, Ma C, Eiler JM, Gross J, Greenwood JP, Stolper EM (2015) The chlorine isotope fingerprint of the lunar magma ocean. Sci Adv 1:e1500380

Boyce JM, Giguere TA, Hawke BR, Mouginis-Mark PJ, Robinson MS, Lawrence SJ, Trang D, Clegg-Watkins RN (2017) Hansteen Mons: An LROC geological perspective. Icarus 283:254–267

Boyce JW, Baker MB, Guan Y, Macris CA (2018a) Hydrogen diffusion in apatite. 49th Lunar Planet Sci Conf Abst #2492

Boyce JW, Kanee SA, McCubbin FM, Barnes JJ, Bricker H, Treiman AH (2018b) Chlorine isotopes in the low-Ti basalts, and the early loss of volatiles from the Earth–Moon system. Earth Planet Sci Lett 500:205–214

Boyet M, Carlson RW, Borg LE, Horan M (2015) Sm–Nd systematics of lunar ferroan anorthositic suite rocks: Constraints on lunar crust formation. Geochim Cosmochim Acta 148:203–218

Braden SE, Stopar JD, Robinson MS, Lawrence SJ, van der Bogert CH, Hiesinger H (2014) Evidence for basaltic volcanism on the Moon within the past 100 million years. Nat Geosci 7:787–791

Brown SM, Elkins-Tanton LT (2009) Compositions of Mercury's earliest crust from magma ocean models. Earth Planet Sci Lett 286:446–455
Bucholz CE, Gaetani GA, Behn MD, Shimizu N (2013) Post-entrapment modification of volatiles and oxygen fugacity in olivine-hosted melt inclusions. Earth Planet Sci Lett 374:145–155
Cahill J, Lucey P, Wieczorek M (2009) Compositional variations of the lunar crust: Results from radiative transfer modeling of central peak spectra. J Geophys Res: Planets 114:E09001
Cameron AGW, Ward WR (1976) The origin of the Moon. Lunar Sci 7:120–122
Canup RM (2004) Dynamics of lunar formation. Annu Rev Astron Astrophys 42:441–475
Canup RM (2012) Forming a Moon with an Earth-like composition from a giant impact. Science 338:1052–1055
Canup RM, Righter K, Dauphas N, Pahlevan K, Ćuk M, Lock SJ, Stewart ST, Salmon J, Rufu R, Nakajima M, Magna T (2023) Origin of the Moon. Rev Mineral Geochem 89:53–102
Carlson RW, Borg LE, Gaffney AM, Boyet M (2014) Rb–Sr, Sm–Nd and Lu–Hf isotope systematics of the lunar Mg-suite: The age of the lunar crust and its relation to the time of Moon formation. Phil Trans R Soc A 372:20130246
Cassanelli JP, Head JW (2016) Did the Orientale impact melt sheet undergo large-scale igneous differentiation by crystal settling? Geophys Res Lett 4:11156–11165
Charlier B, Grove TL, Namur O, Holtz F (2018) Crystallization of the lunar magma ocean and the primordial mantle–crust differentiation of the Moon. Geochim Cosmochim Acta 234:50–69
Che X, Nemchin A, Liu D, Long T, Wang C, Norman MD, Joy KH, Tartèse R, Head J, Jolliff B, Snape JF (2021) Age and composition of young basalts on the Moon, measured from samples returned by Chang'e-5. Science 374:887–890
Cheek LC, Donaldson Hanna K, Pieters C, Head J, Whitten J (2013) The distribution and purity of anorthosite across the Orientale basin: New perspectives from Moon Mineralogy Mapper data. J Geophys Res: Planets 118:1805–1820
Chen Y, Zhang YX, Liu Y, Guan YB, Eiler J, Stolper EM (2015) Water, fluorine, and sulfur concentrations in the lunar mantle. Earth Planet Sci Lett 427:37–46
Chevrel SD, Pinet PC, Head JW (1999) Gruithuisen domes region: A candidate for an extended nonmare volcanism unit on the Moon. J Geophys Res: Planets 104:16515–16529
Clegg-Watkins R, Jolliff B, Watkins M, Coman E, Giguere T, Stopar J, Lawrence S (2017) Nonmare volcanism on the Moon: Photometric evidence for the presence of evolved silicic materials. Icarus 285:169–184
Cohen B, Swindle T, Kring D (2000) Support for the lunar cataclysm hypothesis from lunar meteorite impact melt ages. Science 290:1754–1756
Cohen BA, Swindle TD, Kring DA (2005) Geochemistry and ^{40}Ar–^{39}Ar geochronology of impact-melt clasts in feldspathic lunar meteorites: Implications for lunar bombardment history. Meteorit Planet Sci 40:755–777
Cohen BA, van der Bogert CH, Bottke WF, Curran NM, Fassett CI, Hiesinger H, Joy KH, Mazrouei S, Nemchin A, Neumann GA, Norman MV, Zellner NEB (2023) Impact history of the Moon. Rev Mineral Geochem 89:373–400
Colson RO (1992) Mineralization on the Moon? Theoretical consideration of Apollo 16 "rusty rocks", sulfide replacement in 67016 and surface-correlated volatiles on lunar volcanic glasses. Proc 22th Lunar Planet Sci Conf: 427–436
Crites ST, Lucey PG (2015) Revised mineral and Mg# maps of the Moon from integrating results from the Lunar Prospector neutron and gamma-ray spectrometers with Clementine spectroscopy. Am Mineral 100:973–982
Crites ST, Lucey PG, Taylor GJ (2015) The mafic component of the lunar crust: Constraints on the crustal abundance of mantle and intrusive rock, and the mineralogy of lunar anorthosites. Am Mineral 100:1708–1716
Ćuk M, Stewart ST (2012) Making the Moon from a fast-spinning Earth: A giant impact followed by resonant despinning. Science 338:1047–1052
Day JMD, Moynier F (2014) Evaporative fractionation of volatile stable isotopes and their bearing on the origin of the Moon. Philos Trans R Soc A 372: 20130259
Day JMD, Taylor LA, Floss C, Patchen AD, Schnare DW, Pearson DG (2006) Comparative petrology, geochemistry, and petrogenesis of evolved, low-Ti lunar mare basalt meteorites from the LaPaz ice field, Antarctica. Geochim Cosmochim Acta 70:1581–1600
Day JMD, Moynier F, Shearer CK (2017) Late-stage magmatic outgassing from a volatile-depleted Moon. PNAS 114:9547–9551
Day JMD, Sossi PA, Shearer CK, Moynier F (2019) Volatile distributions in and on the Moon revealed by Cu and Fe isotopes in the 'Rusty Rock' 66095. Geochim Cosmochim Acta 266:131–143
Day JMD, Moynier F, Sossi PA, Wang K, Meshik AP, Pravdivtseva OV, Pettit DR (2020) Moderately volatile element behaviour at high temperature determined from nuclear detonation. Geochem Perspect Lett 13:54–60
Des Marais DJ (1983) Light element geochemistry and spallogenesis in lunar rocks. Geochim Cosmochim Acta 47:1769–1781
Dhaliwal JK, Day JMD, Moynier F (2018) Volatile element loss during planetary magma ocean phases. Icarus 300:249–260
Dhingra D, Pieters C (2011) Mineralogical diversity of impact melts on central peak of Tycho and its vicinity. Annual Meeting of the Lunar Exploration Analysis Group 1646:11
Dhingra D, Pieters CM, Boardman JW, Head JW, Isaacson PJ, Taylor LA (2011) Compositional diversity at Theophilus Crater: Understanding the geological context of Mg-spinel bearing central peaks. Geophys Res Lett 38:L11201
Dhingra D, Pieters CM, Head JW, Isaacson PJ (2013) Large mineralogically distinct impact melt feature at Copernicus crater–Evidence for retention of compositional heterogeneity. Geophys Res Lett 40:1043–1048

Dhingra R, Dhingra D, Carlson L (2014) Evaluating the extent of impact melt on central peaks of lunar complex impact craters. 45th Lunar Planet Sci Conf Abst #1754
Dhingra D, Pieters CM, Head JW (2015) Multiple origins for olivine at Copernicus crater. Earth Planet Sci Lett 420:95–101
Dhingra D, Head JW, Pieters CM (2017) Geological mapping of impact melt deposits at lunar complex craters Jackson and Tycho: Morphologic and topographic diversity and relation to the cratering process. Icarus 283:268–281
Donaldson Hanna KL, Cheek L, Pieters C, Mustard J, Greenhagen B, Thomas I, Bowles N (2014) Global assessment of pure crystalline plagioclase across the Moon and implications for the evolution of the primary crust. J Geophys Res: Planets 119:1516–1545
Dreibus G, Kruse H, Spettel B, Wänke H (1977) The bulk composition of the moon and the eucrite parent body. Proc 8th Lunar Planet Sci Conf: 211–227
Dygert N, Lin JF, Marshall EW, Kono Y, Gardner JE (2017) A low viscosity lunar magma ocean forms a stratified anorthitic flotation crust with mafic poor and rich units. Geophys Res Lett 44:11282–11291
El-Baz F (1974) "D-Caldera": New Photographs of a Unique Feature. Apollo 17 Preminary Science Report:30-13–30-17
El Goresy A, Ramdohr P, Pavićević M, Medenbach O, Müller O, Gentner W (1973) Zinc, lead, chlorine and FeOOH-bearing assemblages in the Apollo 16 sample 66095: origin by impact of a comet or a carbonaceous chondrite? Earth Planet Sci Lett 18:411–419
Elardo SM, Shahar A (2017) Non-chondritic iron isotope ratios in planetary mantles as a result of core formation. Nat Geosci 10:317–321
Elardo SM, Shearer CK (2014) Magma chamber dynamics recorded by oscillatory zoning in pyroxene and olivine phenocrysts in basaltic lunar meteorite Northwest Africa 032. Am Mineral 99:355–368
Elardo SM, Draper DS, Shearer CK (2011) Lunar magma ocean crystallization revisited: Bulk composition, early cumulate mineralogy, and the source regions of the highlands Mg-suite. Geochim Cosmochim Acta 75:3024–3045
Elardo SM, McCubbin FM, Shearer CK (2012) Chromite symplectites in Mg-suite troctolite 76535 as evidence for infiltration metasomatism of a lunar layered intrusion. Geochim Cosmochim Acta 87:154–177
Elardo SM, Shearer CK, Fagan AL, Borg LE, Gaffney AM, Burger PV, Neal CR, Fernandes VA, McCubbin FM (2014) The origin of young mare basalts inferred from lunar meteorites Northwest Africa 4734, 032, and LaPaz Icefield 02205. Meteorit Planet Sci 49:261–291
Elardo SM, Shearer CK, Kaaden KEV, McCubbin FM, Bell AS (2015) Petrogenesis of primitive and evolved basalts in a cooling Moon: Experimental constraints from the youngest known lunar magmas. Earth Planet Sci Lett 422:126–137
Elardo SM, Shahar A, Mock TD, Sio CK (2019) The effect of core composition on iron isotope fractionation between planetary cores and mantles. Earth Planet Sci Lett 513:124–134
Elardo SM, Laneuville M, McCubbin FM, Shearer CK (2020) Early crust building enhanced on the Moon's nearside by mantle melting-point depression. Nat Geosci 13:339–343
Elkins-Tanton LT (2012) Magma oceans in the inner Solar System. Annu Rev Earth Planet Sci 40:113–139
Elkins-Tanton LT, Hess PC, Parmentier EM (2005) Possible formation of ancient crust on Mars through magma ocean processes. J Geophys Res: Planets 110:E12S01
Elkins-Tanton LT, Grove TL (2011) Water (hydrogen) in the lunar mantle: Results from petrology and magma ocean modeling. Earth Planet Sci Lett 307:173–179
Elkins-Tanton LT, Burgess S, Yin QZ (2011) The lunar magma ocean: Reconciling the solidification process with lunar petrology and geochronology. Earth Planet Sci Lett 304:326–336
Epstein S, Taylor HP (1974) D/H and $^{18}O/^{16}O$ ratios of H_2O in the 'rusty' breccia 66095 and the origin of 'lunar water'. Proc 5th Lunar Planet Sci Conf:1839–1854
Fagan TJ, Taylor GJ, Keil K, Bunch TE, Wittke JH, Korotev RL, Jolliff BL, Gillis JJ, Haskin LA, Jarosewich E, Clayton RN, Mayeda TK, Fernandes VA, Burgess R, Turner G, Eugster O, Lorenzetti S (2002) Northwest Africa 032: product of lunar volcanism. Meteorit Planet Sci 37:371–394
Fagan AL, Gross J, Ramsey S, Turrin B (2018) Northwest Africa 8632—Recording Young Lunar Volcanism. 49th Lunar Planet Sci Conf: Abst # 2984
Fernandes VA, Burgess R, Morris A (2009a) ^{40}Ar–^{39}Ar age determinations of lunar basalt meteorites Asuka 881757, Yamato 793169, Miller Range 05035, La Paz Icefield 02205, Northwest Africa 479, and basaltic breccia Elephant Moraine 96008. Meteorit Planet Sci 44:805–821
Fernandes VA, Korotev RL, Renne PR (2009b) ^{40}Ar–^{39}Ar ages and chemical composition for lunar mare basalts: NWA 4734 and NWA 4898. 40th Lunar Planet Sci Conf:Abstract #1045
Ferrière L, Meier M, Assis Fernandes V, Fritz J, Greshake A, Barrat J-A, Böttger U, Bouvier A, Brandstätter F, Busemann H (2017) The unique crowdfunded Oued Awlitis 001 Lunar Meteorite–A consortium overview. 48th Lunar Planet Sci Conf Abst #1621
Friedman I, Hardcastle KG, Gleason JD (1974) Water and carbon in rusty lunar rock 66095. Science 185:346–349
Füri E, Deloule E, Gurenko A, Marty B (2014) New evidence for chondritic lunar water from combined D/H and noble gas analyses of single Apollo 17 volcanic glasses. Icarus 229:109–120
Füri E, Deloule E, Trappitsch R (2017) The production rate of cosmogenic deuterium at the Moon's surface. Earth Planet Sci Lett 474:76–82
Gaddis LR, Pieters CM, Hawke BR (1985) Remote sensing of lunar pyroclastic mantling deposits. Icarus 61:461–489

Gaddis L, Rosanova C, Hare T, Hawke B, Coombs C, Robinson M (1998) Small lunar pyroclastic deposits: a new global perspective. 29th Lunar Planet Sci Conf: Abst #1807
Gaddis LR, Hawke B, Robinson MS, Coombs C (2000) Compositional analyses of small lunar pyroclastic deposits using Clementine multispectral data. J Geophys Res: Planets 105:4245–4262
Gaddis LR, Staid MI, Tyburczy JA, Hawke BR, Petro NE (2003) Compositional analyses of lunar pyroclastic deposits. Icarus 161:262–280
Gaetani GA, O'Leary JA, Shimizu N, Bucholz CE, Newville M (2012) Rapid reequilibration of H_2O and oxygen fugacity in olivine-hosted melt inclusions. Geology 40:915–918
Gaffney AM, Borg LE (2014) A young solidification age for the lunar magma ocean. Geochim Cosmochim Acta 140:227–240
Gaffney AM, Borg LE, DePaolo DJ, Irving AJ (2008) Age and isotope systematics of Northwest Africa 4898, a new type of highly-depleted mare basalt. 39th Lunar Planet Sci Conf Abst #1877
Gaffney AM, Gross J, Borg LE, Donaldson Hanna KL, Draper DS, Dygert N, Elkins-Tanton LT, Prissel KB, Prissel TB, Steenstra ES, van Westrenen W (2023) Magmatic evolution I: Initial differentiation of the Moon. Rev Mineral Geochem 89:103–145
Gibson E, Moore G (1974) Sulfur abundances and distributions in the valley of Taurus-Littrow. Proc 5th Lunar Planet Sci Conf:1823–1837
Glotch TD, Lucey PG, Bandfield JL, Greenhagen BT, Thomas IR, Elphic RC, Bowles N, Wyatt MB, Allen CC, Hanna KD, Paige DA (2010) Highly silicic compositions on the Moon. Science 329:1510–1513
Glotch TD, Hagerty JJ, Lucey PG, Hawke BR, Giguere TA, Arnold JA, Williams JP, Jolliff BL, Paige DA (2011) The Mairan domes: Silicic volcanic constructs on the Moon. Geophys Res Lett 38:L21204
Greber ND, Dauphas N, Puchtel IS, Hofmann BA, Arndt NT (2017) Titanium stable isotopic variations in chondrites, achondrites and lunar rocks. Geochim Cosmochim Acta 213:534–552
Greenhagen BT, Lucey PG, Wyatt MB, Glotch TD, Allen CC, Arnold JA, Bandfield JL, Bowles NE, Donaldson Hanna KL, Hayne PO, Song, E, Thomas IR, Paige, DA (2010) Global silicate mineralogy of the Moon from the Diviner Lunar Radiometer. Science 329:1507–1509
Greenwood JP, Itoh S, Sakamoto N, Warren P, Taylor L, Yurimoto H (2011) Hydrogen isotope ratios in lunar rocks indicate delivery of cometary water to the Moon. Nat Geosci 4:79–82
Greenwood JP, Sakamoto N, Itoh S, Warren PH, Singer JA, Yanai K, Yurimoto H (2017) The lunar magma ocean volatile signature recorded in chlorine-rich glasses in KREEP basalts 15382 and 15386. Geochem J 51:105–114
Greshake A, Irving AJ, Kuehner SM, Korotev RL, Gellissen M, Palme H (2008) Northwest Africa 4898: a new high-alumina mare basalt from the Moon. 39th Lunar Planet Sci Conf: Abst #1631
Gross J, Treiman AH (2011) Unique spinel-rich lithology in lunar meteorite ALHA81005: Origin and possible connection to M^3 observations of the farside highlands. J Geophys Res: Planets 116(E10):E10009
Gross J, Treiman AH, Mercer CN (2014a) Lunar feldspathic meteorites: Constraints on the geology of the lunar highlands, and the origin of the lunar crust. Earth Planet Sci Lett 388:318–328
Gross J, Isaacson PJ, Treiman AH, Le L, Gorman JK (2014b) Spinel-rich lithologies in the lunar highland crust: Linking lunar samples with crystallization experiments and remote sensing. Am Mineral 99:1849–1859
Gross J, Hilton A, Prissel TC, Setera JB, Korotev RL, Calzada-Diaz A (2020) Geochemistry and petrogenesis of Northwest Africa 10401: A new type of the Mg-suite rocks. J Geophys Res: Planets 125:e2019JE006225
Gullikson AL, Hagerty JJ, Reid MR, Rapp JF, Draper DS (2016) Silicic lunar volcanism: Testing the crustal melting model. Am Mineral 101:2312–2321
Gustafson JO, Bell JF, Gaddis L, Hawke B, Giguere TA (2012) Characterization of previously unidentified lunar pyroclastic deposits using Lunar Reconnaissance Orbiter Camera data. J Geophys Res: Planets 117:E00H25
Hagerty JJ, Lawrence DJ, Hawke BR, Vaniman DT, Elphic RC, Feldman WC (2006) Refined thorium abundances for lunar red spots: Implications for evolved, nonmare volcanism on the Moon. J Geophys Res: Planets 111:E06002
Hagerty JJ, Lawrence D, Hawke B, Gaddis LR (2009) Thorium abundances on the Aristarchus plateau: Insights into the composition of the Aristarchus pyroclastic glass deposits. J Geophys Res: Planets 114:E04002
Haloda J, Tycova P, Korotev RL, Fernandes VA, Burgess R, Thoni M, Jelenc M, Jakes P, Gabzdyl P, Kosler J (2009) Petrology, geochemistry, and age of low-Ti mare-basalt meteorite Northeast Africa 003-A: A possible member of the Apollo 15 mare basaltic suite. Geochim Cosmochim Acta 73:3450–3470
Hartmann WK, Davis DR (1975) Satellite-sized planetesimals and lunar origin. Icarus 24:504–515
Haskin LA, Warren PH (1991) Chemistry. *In*: Lunar Sourcebook: A user's guide to the Moon. Heiken G, Vaniman DT, French BM (eds) Cambridge University Press, Cambridge, p 357–474
Haskin LA, Colson RO, Vaniman DT, Gillett SL (1993) A geochemical assessment of possible lunar ore formation. Resources of Near-Earth Space, p 17–50
Haskin LA, Korotev RL, Rockow KM, Jolliff BL (1998) The case for an Imbrium origin of the Apollo thorium-rich impact-melt breccias. Meteorit Planet Sci 33:959–975
Hauri EH, Gaetani GA, Green TH (2006) Partitioning of water during melting of the Earth's upper mantle at H_2O-undersaturated conditions. Earth Planet Sci Lett 248:715–734
Hauri EH, Weinreich T, Saal AE, Rutherford MC, Van Orman JA (2011) High pre-eruptive water contents preserved in lunar melt inclusions. Science 333:213–215

Hawke BR, Peterson C, Blewett D, Bussey D, Lucey P, Taylor G, Spudis P (2003) Distribution and modes of occurrence of lunar anorthosite. J Geophys Res: Planets 108:5050

Head JW, McCord TB (1978) Imbrian-age highland volcanism on Moon—Gruithuisen and Mairan Domes. Science 199:1433–1436

Head JW, Wilson L (1979) Alphonsus-type dark-halo craters-Morphology, morphometry and eruption conditions. Proc 10th Lunar Planet Sci Conf, p 2861–2897

Head JW, Wilson L (2017) Generation, ascent and eruption of magma on the Moon: New insights into source depths, magma supply, intrusions and effusive/explosive eruptions (Part 2: Predicted emplacement processes and observations). Icarus 283:176–223

Head J, Hess P, McCord T (1978) Geologic characteristics of lunar highland volcanic domes (Gruithuisen and Mairan region) and possible eruption conditions. 9th Lunar Planet Sci Conf, p 488–490

Head III JW, Wilson L, Hiesinger H, van der Bogert C, Chen Y, Dickson JL, Gaddis LR, Haruyama J, Jawin ER, Jozwiak LM, Li C, Liu J, Morota T, Needham DH, Ostrach LR, Pieters CM, Prissel TC, Qian Y, Qiao L, Rutherford MR, Scott DR, Whitten JL, Xiao L, Zhang F, Ziyuan O (2023) Lunar mare basaltic volcanism: Volcanic features and emplacement processes. Rev Mineral Geochem 89:453–507

Herzog GF, Moynier F, Albarede F, Berezhnoy AA (2009) Isotopic and elemental abundances of copper and zinc in lunar samples, Zagami, Pele's hairs, and a terrestrial basalt. Geochim Cosmochim Acta 73:5884–5904

Hiesinger H, Jaumann R, Neukum G, Head JW (2000) Ages of mare basalts on the lunar nearside. J Geophys Res: Planets 105:29239–29275

Hiesinger H, Head J, Wolf U, Jaumann R, Neukum G (2011) Ages and stratigraphy of lunar mare basalts: A synthesis. Recent Advances and Current Research Issues in Lunar Stratigraphy 477:1–51

Hiesinger H, van der Bogert CH, Michael G, Schmedemann N, Iqbal W, Robbins SJ, Ivanov B, Williams J-P, Zanetti M, Plescia J, Ostrach LR, Head III JW (2023) The lunar cratering chronology. Rev Mineral Geochem 89:401–451

Hill E, Taylor LA, Floss C, Liu Y (2009) Lunar meteorite LaPaz Icefield 04841: Petrology, texture, and impact-shock effects of a low-Ti mare basalt. Meteorit Planet Sci 44:87–94

Hu S, He H, Ji J, Lin Y, Hui H, Anand M, Tartèse R, Yan Y, Hao J, Li R, Gu L (2021) A dry lunar mantle reservoir for young mare basalts of Chang'E-5. Nature 600:49–53

Hui H, Peslier AH, Zhang Y, Neal CR (2013) Water in lunar anorthosites and evidence for a wet early Moon. Nat Geosci 6:177–180

Hui H, Guan Y, Chen Y, Peslier AH, Zhang, Y, Liu, Y, Flemming RL, Rossman GR, Eiler JM, Neal CR, Osinski GR (2017) A heterogeneous lunar interior for hydrogen isotopes as revealed by the lunar highlands samples. Earth Planet Sci Lett 473:14–23

Hurley DM, Siegler MA, Cahill JTS, Colaprete A, Costello E, Deutsch AN, Elphic RC, Fa W, Grava C, Hayne PO, Heldmann J, Hendrix AR, Jordan AP, Killen RM, Klima RL, Kramer G, Li S, Liu Y, Lucey PG, Mazarico E, Pendleton Y, Poston M, Prem P, Retherford KD, Schaible M (2023) Surface volatiles on the Moon. Rev Mineral Geochem 89:787–827

Hurwitz DM, Kring DA (2014) Differentiation of the South Pole-Aitken basin impact melt sheet: Implications for lunar exploration. J Geophys Res: Planets 119:1110–1133

Isaacson PJ, Pieters CM (2009) Northern imbrium noritic anomaly. J Geophys Res: Planets 114:E09007

Isaacson PJ, Pieters CM, Besse S, Clark RN, Head JW, Klima RL, Mustard JF, Petro NE, Staid MI, Sunshine JM (2011) Remote compositional analysis of lunar olivine-rich lithologies with Moon Mineralogy Mapper (M^3) spectra. J Geophys Res: Planets 116:E00G11

Ivanov M, Head J, Bystrov A (2016) The lunar Gruithuisen silicic extrusive domes: Topographic configuration, morphology, ages, and internal structure. Icarus 273:262–283

James OB, Hammarstrom JG (1977) Petrology of four clasts from consortium breccia 73215. Proc 8th Lunar Planet Sci Conf 2459–2494

Jiang Y, Chen H, Fegley B, Lodders K, Hsu WB, Jacobsen SB, Wang K (2019) Implications of K, Cu and Zn isotopes for the formation of tektites. Geochim Cosmochim Acta 259:170–187

Jolliff BL, Haskin LA, Colson RO, Wadhwa M (1993) Partitioning in REE-saturating minerals: theory, experiment, and modelling of whitlockite, apatite, and evolution of lunar residual magmas. Geochim Cosmochim Acta 57:4069–4094

Jolliff BL, Gillis JJ, Haskin LA, Korotev RL, Wieczorek MA (2000) Major lunar crustal terranes: surface expressions and crust–mantle origins. J Geophys Res: Planets 105:4197–4216

Jolliff BL, Wiseman SA, Lawrence SJ, Tran TN, Robinson MS, Sato H, Hawke BR, Scholten F, Oberst J, Hiesinger H (2011) Non-mare silicic volcanism on the lunar farside at Compton–Belkovich. Nat Geosci 4:566

Joy KH, Crawford IA, Downes H, Russell SS, Kearsley AT (2006) A petrological, mineralogical, and chemical analysis of the lunar mare basalt meteorite LaPaz Icefield 02205, 02224, and 02226. Meteorit Planet Sci 41:1003–1025

Joy KH, Crawford IA, Anand M, Greenwood RC, Franchi IA, Russell SS (2008) The petrology and geochemistry of Miller Range 05035: A new lunar gabbroic meteorite. Geochim Cosmochim Acta 72:3822–3844

Joy KH, Gross J, Korotev RL, Zeigler RA, McCubbin FM, Snape JF, Curran NM, Pernet-Fisher JF, Arai T (2023) Lunar meteorites. Rev Mineral Geochem 89:509–562

Jozwiak LM, Head JW, Zuber MT, Smith DE, Neumann GA (2012) Lunar floor-fractured craters: Classification, distribution, origin and implications for magmatism and shallow crustal structure. J Geophys Res: Planets 117:E11005

Jozwiak LM, Head JW, Wilson L (2015) Lunar floor-fractured craters as magmatic intrusions: Geometry, modes of emplacement, associated tectonic and volcanic features, and implications for gravity anomalies. Icarus 248:424–447
Kato C, Moynier F (2017) Gallium isotopic evidence for extensive volatile loss from the Moon during its formation. Sci Adv 3:e1700571
Kato C, Moynier F, Valdes MC, Dhaliwal JK, Day JMD (2015) Extensive volatile loss during formation and differentiation of the Moon. Nat Commun 6:7617
Kato C, Moynier F, Foriel J, Teng F-Z, Puchtel IS (2017a) The gallium isotopic composition of the bulk silicate Earth. Chem Geol 448:164–172
Kato S, Morota T, Yamaguchi Y, Watanabe Si, Otake H, Ohtake M (2017b) Magma source transition of lunar mare volcanism at 2.3 Ga. Meteorit Planet Sci 52:1899–1915
Kerridge J, Kaplan I, Petrowski C, Chang S (1975) Light element geochemistry of the Apollo 16 site. Geochim Cosmochim Acta 39:137–162
Klima RL, Pieters CM, Boardman JW, Green RO, Head JW, Isaacson PJ, Mustard JF, Nettles JW, Petro NE, Staid MI (2011) New insights into lunar petrology: Distribution and composition of prominent low-Ca pyroxene exposures as observed by the Moon Mineralogy Mapper (M^3). J Geophys Res: Planets 116:E00G06
Klima R, Buczkowski D, Ernst C, Greenhagen B (2017) Geological and spectral analysis of low-calcium pyroxenes around the Imbrium Basin on the Moon. 48th Lunar Planet Sci Conf Abst #2502
Kobayashi S, Hasebe N, Shibamura E, Okudaira O, Kobayashi M, Yamashita N, Karouji Y, Hareyama M, Hayatsu K, d'Uston C (2010) Determining the absolute abundances of natural radioactive elements on the lunar surface by the Kaguya gamma-ray spectrometer. Space Sci Rev 154:193–218
Kobayashi S, Karouji Y, Morota T, Takeda H, Hasebe N, Hareyama M, Kobayashi M, Shibamura E, Yamashita N, d'Uston C (2012) Lunar farside Th distribution measured by Kaguya gamma-ray spectrometer. Earth Planet Sci Lett 337:10–16
Koeberl C, Kurat G, Brandstaetter F (1993) Gabbroic lunar mare meteorites Asuka-881757 (Asuka-31) and Yamato-793169: geochemical and mineralogical study. Proc NIPR Symp Antarctic Meteorites 6:14–34
Kommescher S, Fonseca ROC, Kurzweil F, Thiemens MM, Munker C, Sprung P (2020) Unravelling lunar mantle source processes via the Ti isotope composition of lunar basalts. Geochem Perspect Let 13:13–18
Korotev RL (2000) The great lunar hot spot and the composition and origin of the Apollo mafic ("LKFM") impact-melt breccias. J Geophys Res: Planets 105:4317–4345
Korotev RL (2005) Lunar geochemistry as told by lunar meteorites. Chemie Der Erde-Geochemistry 65:297–346
Korotev R, Jolliff B (2001) The curious case of the lunar magnesian granulitic breccias. 32nd Lunar Planet Sci Conf Abst #1455
Korotev RL, Jolliff BL, Zeigler RA, Gillis JJ, Haskin LA (2003) Feldspathic lunar meteorites and their implications for compositional remote sensing of the lunar surface and the composition of the lunar crust. Geochim Cosmochim Acta 67:4895–4923
Korotev RL, Zeigler RA, Jolliff BL (2006) Feldspathic lunar meteorites Pecora Escarpment 02007 and Dhofar 489: Contamination of the surface of the lunar highlands by post-basin impacts. Geochim Cosmochim Acta 70:5935–5956
Korotev R, Jolliff B, Zeigler R (2010) On the origin of the Moon's feldspathic highlands, pure anorthosite, and the feldspathic lunar meteorites. 41st Lunar Planet Sci Conf Abst #1440
Korotev R, Jolliff B, Zeigler R (2012) What lunar meteorites tell us about the lunar highlands crust. 2nd Conf Lunar Highlands Crust Abst #1677
Kramer GY, Kring DA, Nahm AL, Pieters CM (2013) Spectral and photogeologic mapping of Schrodinger Basin and implications for post-South Pole-Aitken impact deep subsurface stratigraphy. Icarus 223:131–148
Laneuville M, Wieczorek MA, Breuer D, Tosi N (2013) Asymmetric thermal evolution of the Moon. J Geophys Res: Planets 118:1435–1452
Lawrence DJ, Feldman WC, Barraclough BL, Binder AB, Elphic RC, Maurice S, Thomsen DR (1998) Global elemental maps of the moon: The Lunar Prospector gamma-ray spectrometer. Science 281:1484–1489
Lawrence D, Feldman W, Barraclough B, Binder A, Elphic R, Maurice S, Miller M, Prettyman T (1999) High resolution measurements of absolute thorium abundances on the lunar surface. Geophys Res Lett 26:2681–2684
Lawrence D, Feldman W, Barraclough B, Binder A, Elphic R, Maurice S, Miller M, Prettyman T (2000) Thorium abundances on the lunar surface. J Geophys Res: Planets 105:20307–20331
Lawrence D, Elphic R, Feldman W, Prettyman T, Gasnault O, Maurice S (2003) Small-area thorium features on the lunar surface. J Geophys Res: Planets 108:5102
Lawrence D, Puetter R, Elphic R, Feldman W, Hagerty J, Prettyman T, Spudis P (2007) Global spatial deconvolution of Lunar Prospector Th abundances. Geophys Res Lett 34:L03201
Lawrence SJ, Hawke BR, Gillis-Davis JJ, Taylor GJ, Lawrence DJ, Cahill JT, Hagerty JJ, Lucey PG, Smith GA, Keil K (2008) Composition and origin of the Dewar geochemical anomaly. J Geophys Res: Planets 113:E02001
Lemelin M, Lucey PG, Song E, Taylor GJ (2015) Lunar central peak mineralogy and iron content using the Kaguya Multiband Imager: Reassessment of the compositional structure of the lunar crust. J Geophys Res: Planets 120:869–887
Li H, Hermann J (2015) Apatite as an indicator of fluid salinity: An experimental study of chlorine and fluorine partitioning in subducted sediments. Geochim Cosmochim Acta 166:267–297
Li HJ, Hermann J (2017) Chlorine and fluorine partitioning between apatite and sediment melt at 2.5 GPa, 800 °C: A new experimentally derived thermodynamic model. Am Mineral 102:580–594

Li S, Milliken RE (2017) Water on the surface of the Moon as seen by the Moon Mineralogy Mapper: Distribution, abundance, and origins. Sci Adv 3:e1701471

Li SL, Hsu WB, Guan YB, Wang LY, Wang Y (2016) Petrogenesis of the Northwest Africa 4898 high-Al mare basalt. Meteorit Planet Sci 51:1268–1288

Li QL, Zhou Q, Liu Y, Xiao Z, Lin Y, Li JH, Ma HX, Tang GQ, Guo S, Tang X, Yuan JY (2021) Two-billion-year-old volcanism on the Moon from Chang'e-5 basalts. Nature 600:54–58

Lindsley DH (1969) Melting relations of plagioclase at high pressures. *In*: Origin of Anorthosite and Related Rocks. Vol 18. New York State Mus Sci Serv Mem, p 39–46

Lindstrom MM, Lindstrom DJ (1986) Lunar granulites and their precursor anorthositic norites of the early lunar crust. J Geophys Res: Solid Earth 91:D263–D276

Lindstrom MM, Salpas PA (1983) Geochemical studies of feldspathic fragmental breccias and the nature of North Ray crater ejecta. Proc 13th Lunar Planet Sci Conf A671–A683

Lindstrom MM, Knapp SA, Shervais JW, Taylor LA (1984) Magnesian anorthosites and associated troctolites and dunite in Apollo 14 breccias. J Geophys Res 89 Suppl 1:C41-C49

Ling Z, Jolliff BL, Wang A, Li C, Liu J, Zhang J, Li B, Sun L, Chen J, Xiao L (2015) Correlated compositional and mineralogical investigations at the Chang′ e-3 landing site. Nat Commun 6:8880

Liu Y, Floss C, Day JMD, Hill E, Taylor LA (2009) Petrogenesis of lunar mare basalt meteorite Miller Range 05035. Meteorit Planet Sci 44:261–284

Liu Y, Spicuzza MJ, Craddock PR, Day JMD, Valley JW, Dauphas N, Taylor LA (2010) Oxygen and iron isotope constraints on near-surface fractionation effects and the composition of lunar mare basalt source regions. Geochim Cosmochim Acta 74:6249–6262

Liu Y, Guan YB, Zhang YX, Rossman GR, Eiler JM, Taylor LA (2012) Direct measurement of hydroxyl in the lunar regolith and the origin of lunar surface water. Nat Geosci 5:779–782

Lock SJ, Stewart ST, Petaev MI, Leinhardt Z, Mace MT, Jacobsen SB, Ćuk M (2018) The origin of the Moon within a terrestrial synestia. J Geophys Res: Planets 123:910–951

Loper DE, Werner CL (2002) On lunar asymmetries 1. Tilted convection and crustal asymmetry. J Geophys Res: Planets 107(E6):5046

Lucey P, Korotev RL, Gillis JJ, Taylor LA, Lawrence D, Campbell BA, Elphic R, Feldman B, Hood LL, Hunten D, Mendillo M, Noble S, Papike JJ, Reedy RC, Lawson S, Prettyman T, Gasnault O, Maurice S (2006) Understanding the lunar surface and space–moon interactions. Rev Mineral Geochem 60:83–220

Lucey PG, Norman JA, Crites ST, Taylor GJ, Hawke BR, Lemelin M, Melosh HJ (2014) A large spectral survey of small lunar craters: Implications for the composition of the lunar mantle. Am Mineral 99:2251–2257

Magna T, Wiechert U, Halliday AN (2006) New constraints on the lithium isotope compositions of the Moon and terrestrial planets. Earth Planet Sci Lett 243:336–353

Malin MC (1974) Lunar red spots: Possible pre-mare materials. Earth Planet Sci Lett 21:331–341

Mathez EA, Webster JD (2005) Partitioning behavior of chlorine and fluorine in the system apatite–silicate melt–fluid. Geochim Cosmochim Acta 69:1275–1286

Matsunaga T, Ohtake M, Haruyama J, Ogawa Y, Nakamura R, Yokota Y, Morota T, Honda C, Torii M, Abe M (2008) Discoveries on the lithology of lunar crater central peaks by SELENE spectral profiler. Geophys Res Lett 35(23)

Maurice M, Tosi N, Schwinger S, Breuer D, Kleine T (2020) A long-lived magma ocean on a young Moon. Sci Adv 6:eaba8949

McCubbin FM, Ustunisik G (2018) Experimental investigation of F and Cl partitioning between apatite and Fe-rich basaltic melt at 0 GPa and 950–1050 °C: Evidence for steric controls on apatite–melt exchange equilibria in OH-poor apatite. Am Mineral 103:1455–1467

McCubbin FM, Steele A, Hauri EH, Nekvasil H, Yamashita S, Hemley RJ (2010a) Nominally hydrous magmatism on the Moon. PNAS 27:11223–11228

McCubbin FM, Steele A, Nekvasil H, Schnieders A, Rose T, Fries M, Carpenter PK, Jolliff BL (2010b) Detection of structurally bound hydroxyl in fluorapatite from Apollo mare basalt 15058,128 using TOF-SIMS. Am Mineral 95:1141–1150

McCubbin FM, Jolliff BL, Nekvasil H, Carpenter PK, Zeigler RA, Steele A, Elardo SM, Lindsley DH (2011) Fluorine and chlorine abundances in lunar apatite: Implications for heterogeneous distributions of magmatic volatiles in the lunar interior. Geochim Cosmochim Acta 75:5073–5093

McCubbin FM, Elardo SM, Shearer Jr CK, Smirnov A, Hauri EH, Draper DS (2013) A petrogenetic model for the co-magmatic origin of chassignites and nakhlites: Inferences from chlorine-rich minerals, petrology, and geochemistry. Meteorit Planet Sci 48:819–853

McCubbin FM, Vander Kaaden KE, Tartèse R, Boyce JW, Mikhail, S, Whitson ES, Bell AS, Anand, M, Franchi IA, Wang JH, Hauri EH (2015a) Experimental investigation of F, Cl, and OH partitioning between apatite and Fe-rich basaltic melt at 1.0–1.2 GPa and 950–1000 °C. Am Mineral 100:1790–1802

McCubbin FM, Kaaden KEV, Tartèse R, Klima RL, Liu, Y, Mortimer, J, Barnes JJ, Shearer CK, Treiman AH, Lawrence DJ, Elardo SM, Hurley DM, Boyce JW, Anand M (2015b) Magmatic volatiles (H, C, N, F, S, Cl) in the lunar mantle, crust, and regolith: Abundances, distributions, processes, and reservoirs. Am Mineral 100:1668–1707

McCubbin FM, Boyce JW, Srinivasan P, Santos AR, Elardo SM, Filiberto J, Steele A, Shearer CK (2016) Heterogeneous distribution of H_2O in the martian interior: Implications for the abundance of H_2O in depleted and enriched mantle sources. Meteorit Planet Sci 51:2036–2060

McCubbin FM, Barnes JJ, Ni P, Hui H, Klima RL, Burney D, Day JMD, Magna T, Boyce JW, Tartèse R, Vander Kaaden KE, Steenstra E, Elardo SM, Zeigler RA, Anand M, Liu Y (2023) Endogenous lunar volatiles. Rev Mineral Geochem 89:729–786

McLeod CL, Brandon AD, Armytage RM (2014) Constraints on the formation age and evolution of the Moon from ^{142}Nd–^{143}Nd systematics of Apollo 12 basalts. Earth Planet Sci Lett 396:179–189

McLeod CL, Brandon AD, Fernandes VA, Peslier AH, Fritz J, Lapen T, Shafer JT, Butcher AR, Irving AJ (2016) Constraints on formation and evolution of the lunar crust from feldspathic granulitic breccias NWA 3163 and 4881. Geochim Cosmochim Acta 187:350–374

Melosh HJ, Kendall J, Horgan B, Johnson BC, Bowling T, Lucey PG, Taylor GJ (2017) South Pole-Aitken basin ejecta reveal the Moon's upper mantle. Geology 45:1063–1066

Milliken RE, Li S (2017) Remote detection of widespread indigenous water in lunar pyroclastic deposits. Nat Geosci 10:561–565

Mills RD, Simon JI, Alexander CMOD, Wang J, Hauri EH (2017) Water in alkali feldspar: The effect of rhyolite generation on the lunar hydrogen budget. Geochem Perspect Lett 3:115–123

Moriarty DP, Pieters CM (2015) The nature and origin of Mafic Mound in the South Pole-Aitken basin. Geophys Res Lett 42:7907–7915

Moriarty DP, Pieters CM (2018) The character of South Pole-Aitken basin: Patterns of surface and subsurface composition. J Geophys Res: Planets 123:729–747

Moriarty DP, Pieters CM, Isaacson PJ (2013) Compositional heterogeneity of central peaks within the South Pole-Aitken Basin. J Geophys Res: Planets 118:2310–2322

Moriarty DP, Watkins RN, Valencia SN, Kendall JD, Evans AJ, Dygert N, Petro NE (2021) Evidence for a stratified upper mantle preserved within the South Pole-Aitken basin. J Geophys Res: Planets 121:e2020JE006589

Nagaoka H, Takeda H, Karouji Y, Ohtake M, Yamaguchi A, Yoneda S, Hasebe N (2014) Implications for the origins of pure anorthosites found in the feldspathic lunar meteorites, Dhofar 489 group. Earth Planets Space 66:1–14

Nakajima M, Stevenson DJ (2018) Inefficient volatile loss from the Moon-forming disk: Reconciling the giant impact hypothesis and a wet Moon. Earth Planet Sci Lett 487:117–126

Nakamura R, Matsunaga T, Ogawa Y, Yamamoto S, Hiroi T, Saiki K, Hirata N, Arai T, Kitazato K, Takeda H (2009) Ultramafic impact melt sheet beneath the South Pole–Aitken basin on the Moon. Geophys Res Lett 36:L22202

Nakamura R, Yamamoto S, Matsunaga T, Ishihara Y, Morota T, Hiroi T, Takeda H, Ogawa Y, Yokota Y, Hirata N (2012) Compositional evidence for an impact origin of the Moon's Procellarum basin. Nat Geosci 5:775–778

Neal CR (2001) Interior of the Moon: The presence of garnet in the primitive deep lunar mantle. J Geophys Res 106:27865–27885

Neal CR, Kramer GY (2006) The petrogenesis of the Apollo 14 high-Al mare basalts. Am Mineral 91:1521–1535

Nekvasil H, Lindsley DH, DiFrancesco N, Catalano T, Coraor AE, Charlier B (2015) Uncommon behavior of plagioclase and the ancient lunar crust. Geophys Res Lett 42:10573–10579

Ni P, Zhang Y, Guan Y (2017) Volatile loss during homogenization of lunar melt inclusions. Earth Planet Sci Lett 478:214–224

Norman MD (1982) Petrology of suevitic lunar breccia 67016. Proc 12th Lunar Planet Sci Conf 12:235–252

Norman MD, Keil K, Griffin WL, Ryan CG (1995) Fragments of ancient lunar crust: Petrology and geochemistry of ferroan noritic anorthosites from the Descartes region of the Moon. Geochim Cosmochim Acta 59:831–847

Nyquist LE, Shih CY, Reese YD (2007) Sm-Nd and Rb-Sr ages for MIL 05035: Implications for surface and mantle sources. 38th Lunar Planet Sci Conf Abstract #1702

O'Leary JA, Gaetani GA, Hauri EH (2010) The effect of tetrahedral Al^{3+} on the partitioning of water between clinopyroxene and silicate melt. Earth Planet Sci Lett 297:111–120

Ogawa Y, Matsunaga T, Nakamura R, Saiki K, Ohtake M, Hiroi T, Takeda H, Arai T, Yokota Y, Yamamoto S, Hirata N, Sugihara T, Sasaki S, Haruyama J, Morota T, Honda C, Demura H, Kitazato K, Terazono J, Asada N (2011) The widespread occurrence of high-calcium pyroxene in bright-ray craters on the Moon and implications for lunar-crust composition. Geophys Res Lett 38:L17202

Ohtake M, Matsunaga T, Haruyama J, Yokota Y, Morota T, Honda C, Ogawa Y, Torii M, Miyamoto H, Arai T, Hirata N, Iwasaki A, Nakamura R, Hiroi T, Sugihara T, Takeda H, Otake H, Pieters CM, Saiki K, Kitazato K, Abe M, Asada N, Demura H, Yamaguchi Y, Sasaki S, Kodama S, Terazono J, Shirao M, Yamaji A, Minami S, Akiyama H, Josset JL (2009) The global distribution of pure anorthosite on the Moon. Nature 461:236–240

Ohtake M, Takeda H, Matsunaga T, Yokota Y, Haruyama J, Morota T, Yamamoto S, Ogawa Y, Hiroi T, Karouji Y, Saiki K, Lucey PG (2012) Asymmetric crustal growth on the Moon indicated by primitive farside highland materials. Nat Geosci 5:384–388

Ohtake M, Uemoto K, Yokota Y, Morota T, Yamamoto S, Nakamura R, Haruyama J, Iwata T, Matsunaga T, Ishihara Y (2014) Geologic structure generated by large-impact basin formation observed at the South Pole-Aitken basin on the Moon. Geophys Res Lett 41:2738–2745

Osinski GR, Tornabene LL, Grieve RAF (2011) Impact ejecta emplacement on terrestrial planets. Earth Planet Sci Lett 310:167–181

Paniello RC, Day JMD, Moynier F (2012) Zinc isotopic evidence for the origin of the Moon. Nature 490:376–379
Papike JJ, Taylor LA, Simon S (1991) Lunar minerals. *In*: Lunar Sourcebook: A user's guide to the Moon. Heiken G, Vaniman DT, French BM (eds) Cambridge University Press, Cambridge, p 121–181
Papike JJ, Fowler GW, Shearer CK (1994) Orthopyroxene as a recorder of lunar crust evolution: an ion microprobe investigation of Mg-suite norites. Am Mineral 79:796–800
Papike JJ, Fowler GW, Shearer CK, Layne GD (1996) Ion microprobe investigation of plagioclase and orthopyroxene from lunar Mg-suite norites: implications for calculating parental melt REE concentrations and for assessing postcrystallization REE redistribution. Geochim Cosmochim Acta 60:3967–3978
Papike JJ, Ryder G, Shearer CK (1998) Lunar samples. Rev Mineral 36:5-1–5-234
Parendo CA, Jacobsen SB, Wang K (2017) K isotopes as a tracer of seafloor hydrothermal alteration. PNAS: 201609228
Patiño Douce AE, Roden MF (2006) Apatite as a probe of halogen and water fugacities in the terrestrial planets. Geochim Cosmochim Acta 70:3173–3196
Peplowski PN, Lawrence DJ (2013) New insights into the global composition of the lunar surface from high-energy gamma rays measured by Lunar Prospector. J Geophys Res: Planets 118:671–688
Peplowski PN, Beck AW, Lawrence DJ (2016) Geochemistry of the lunar highlands as revealed by measurements of thermal neutrons. J Geophys Res: Planets 121:388–401
Pernet-Fisher JF, Joy KH (2022) Thermal metamorphism on the Moon as recorded by the granulite suite. J Geol Soc 179: jgs2021-044
Petro NE, Pieters CM (2008) The lunar-wide effects of basin ejecta distribution on the early megaregolith. Meteorit Planet Sci 43:1517–1529
Pieters C (1978) Mare basalt types on the front side of the moon—A summary of spectral reflectance data. Proc 9th Lunar Planet Sci Conf 2825–2849
Pieters CM (1986) Composition of the lunar highland crust from near-infrared spectroscopy. Rev Geophys 24:557–578
Pieters C (1993) Compositional diversity and stratigraphy of the lunar crust derived from reflectance spectroscopy. *In:* Remote Geochemical Analysis Elemental and Mineralogical Composition, p 309–339
Pieters C, McCord TB, Zisk S, Adams JB (1973) Lunar black spots and nature of the Apollo 17 landing area. J Geophys Res 78:5867–5875
Pieters CM, Head JW, Adams JB, McCord TB, Zisk SH, Whitford-Stark JL (1980) Late high-titanium basalts of the western maria: Geology of the Flamsteed region of Oceanus Procellarum. J Geophys Res 85:3913–3938
Pieters C, Head J, Gaddis L, Jolliff B, Duke M (2001) Rock types of South Pole-Aitken basin and extent of basaltic volcanism. J Geophys Res: Planets 106:28001–28022
Pieters C, Boardman J, Buratti B, Clark R, Combe J, Green R, Goswami J, Head III J, Hicks M, Isaacson P (2009) Mineralogy of the lunar crust in spatial context: First results from the Moon Mineralogy Mapper (M^3). 40th Lunar Planet Sci Conf Abst #2042
Pieters CM, Besse S, Boardman J, Buratti B, Cheek L, Clark RN, Combe JP, Dhingra D, Goswami JN, Green RO, Head JW, Isaacson P, Klima R, Kramer G, Lundeen S, Malaret E, McCord T, Mustard J, Nettles J, Petro N, Runyon C, Staid M, Sunshine J, Taylor LA, Thaisen K, Tompkins S, Whitten J (2011) Mg-spinel lithology: A new rock type on the lunar farside. J Geophys Res: Planets 116:E00G08
Pieters CM, Hanna KD, Cheek L, Dhingra D, Prissel T, Jackson C, Moriarty D, Parman S, Taylor LA (2014) The distribution of Mg-spinel across the Moon and constraints on crustal origin. Am Mineral 99:1893–1910
Pieters C, Hiroi T, Milliken R, Cheek L (2018) Abundance and distribution of lunar primary crust anorthosite: The featureless plagioclase challenge. 49th Lunar Planet Sci Conf Abst #1698
Pieters CM, Klima RL, Green RO (2019) Compositional analysis of the Moon in the visible and near-infrared regions. *In*: Remote Compositional Analysis: Techniques for Understanding Spectroscopy, Mineralogy, and Geochemistry of Planetary Surfaces. Bishop JL, Moersch JE, III (eds). Cambridge University Press, Cambridge UK, p 368–392
Piskorz D, Stevenson DJ (2014) The formation of pure anorthosite on the Moon. Icarus 239:238–243
Poitrasson F, Halliday AN, Lee DC, Levasseur S, Teutsch N (2004) Iron isotope differences between Earth, Moon, Mars and Vesta as possible records of contrasted accretion mechanisms. Earth Planet Sci Lett 223:253–266
Poitrasson F, Zambardi T, Magna T, Neal CR (2019) A reassessment of the iron isotope composition of the Moon and its implications for the accretion and differentiation of terrestrial planets. Geochim Cosmochim Acta 267:257–274
Potts NJ, Barnes JJ, Tartèse R, Franchi IA, Anand M (2018) Chlorine isotopic compositions of apatite in Apollo 14 rocks: Evidence for widespread vapor-phase metasomatism on the lunar nearside similar to 4 billion years ago. Geochim Cosmochim Acta 230:46–59
Prettyman TH, Hagerty JJ, Elphic RC, Feldman WC, Lawrence DJ, McKinney GW, Vaniman DT (2006) Elemental composition of the lunar surface: Analysis of gamma ray spectroscopy data from Lunar Prospector. J Geophys Res: Planets 111(E12):E12007
Pringle EA, Moynier F (2017) Rubidium isotopic composition of the Earth, meteorites, and the Moon: Evidence for the origin of volatile loss during planetary accretion. Earth Planet Sci Lett 473:62–70
Prissel TC, Parman SW, Jackson CRM, Rutherford MJ, Hess PC, Head JW, Cheek L, Dhingra D, Pieters CM (2014) Pink Moon: The petrogenesis of pink spinel anorthosites and implications concerning Mg-suite magmatism. Earth Planet Sci Lett 403:144–156

Prissel TC, Parman SW, Head JW (2016) Formation of the lunar highlands Mg-suite as told by spinel. Am Mineral 101:1624–1635
Prissel KB, Krawczynski MJ, Nie NX, Dauphas N, Couvy H, Hu MY, Alp EE, Roskosz M (2018) Experimentally determined effects of olivine crystallization and melt titanium content on iron isotopic fractionation in planetary basalts. Geochim Cosmochim Acta 238:580–598
Qian Y, Xiao L, Zhao S, Zhao J, Huang J, Flahaut J, Martinot M, Head J, Hiesinger H, Wang G (2018) Geology and scientific significance of the Rümker region in Northern Oceanus Procellarum: China's Chang'E-5 landing region. J Geophys Res: Planets 123:1407–1430
Qiao L, Head J, Wilson L, Xiao L, Kreslavsky M, Dufek J (2017) Ina pit crater on the Moon: Extrusion of waning-stage lava lake magmatic foam results in extremely young crater retention ages. Geology 45:455–458
Qiao L, Head JW, Xiao L, Wilson L, Dufek JD (2018) The role of substrate characteristics in producing anomalously young crater retention ages in volcanic deposits on the Moon: Morphology, topography, subresolution roughness, and mode of emplacement of the Sosigenes lunar irregular mare patch. Meteorit Planet Sci 53:778–812
Rankenburg K, Brandon AD, Neal CR (2006) Neodymium isotope evidence for a chondritic composition of the Moon. Science 312:1369–1372
Rankenburg K, Brandon AD, Norman MD (2007) A Rb-Sr and Sm-Nd isotope geochronology and trace element study of lunar meteorite LaPaz Icefield 02205. Geochim Cosmochim Acta 71:2120–2135
Rapp J, Draper D (2018) Fractional crystallization of the lunar magma ocean: Updating the dominant paradigm. Meteorit Planet Sci 53:1432–1455
Rees C, Thode H (1974) Sulfur concentrations and isotope ratios in Apollo 16 and 17 samples. Proc 5th Lunar Planet Sci Conf 1963–1973
Riker J, Humphreys MCS, Brooker RA, De Hoog JCM, EIMF (2018) First measurements of OH–C exchange and temperature-dependent partitioning of OH and halogens in the system apatite–silicate melt. Am Mineral 103:260–270
Robert F, Gautier D, Dubrulle B (2000) The solar system D/H ratio: Observations and theories. Space Sci Rev 92:201–224
Robinson KL, Taylor GJ (2014) Heterogeneous distribution of water in the Moon. Nat Geosci 7:401–408
Robinson KL, Barnes JJ, Nagashima K, Thomen A, Franchi IA, Huss GR, Anand M, Taylor GJ (2016) Water in evolved lunar rocks: Evidence for multiple reservoirs. Geochim Cosmochim Acta 188:244–260
Rufu R, Aharonson O, Perets HB (2017) A multiple-impact origin for the Moon. Nat Geosci 10:89
Ryder G, Wood J (1977) Serenitatis and Imbrium impact melts—Implications for large-scale layering in the lunar crust. Proc 8th Lunar Planet Sci Conf, p 655–668
Saal AE, Hauri EH, Lo Cascio M, Van Orman JA, Rutherford MC, Cooper RF (2008) Volatile content of lunar volcanic glasses and the presence of water in the Moon's interior. Nature 454:192–196
Saal AE, Hauri EH, Van Orman JA, Rutherford MJ (2013) Hydrogen isotopes in lunar volcanic glasses and melt inclusions reveal a carbonaceous chondrite heritage. Science 340:1317–1320
Sarafian AR, Nielsen SG, Marschall HR, McCubbin FM, Monteleone BD (2014) Early accretion of water in the inner solar system from a carbonaceous chondrite-like source. Science 346:623–626
Sarafian AR, John T, Roszjar J, Whitehouse MJ (2017a) Chlorine and hydrogen degassing in Vesta's magma ocean. Earth Planet Sci Lett 459:311–319
Sarafian AR, Hauri EH, McCubbin FM, Lapen TJ, Berger EL, Nielsen SG, Marschall HR, Gaetani GA, Righter K, Sarafian E (2017b) Early accretion of water and volatile elements to the inner Solar System: Evidence from angrites. Philos Trans R Soc A:375:20160209
Schultz PH, Staid MI, Pieters CM (2006) Lunar activity from recent gas release. Nature 444:184
Sedaghatpour F, Jacobsen SB (2019) Magnesium stable isotopes support the lunar magma ocean cumulate remelting model for mare basalts. PNAS 116:73–78
Sedaghatpour F, Teng F-Z, Liu Y, Sears DW, Taylor LA (2013) Magnesium isotopic composition of the Moon. Geochim Cosmochim Acta 120:1–16
Seddio SM, Jolliff BL, Korotev RL, Zeigler RA (2013) Petrology and geochemistry of lunar granite 12032,366–19 and implications for lunar granite petrogenesis. Am Mineral 98:1697–1713
Seitz H-M, Brey GP, Weyer S, Durali S, Ott U, Münker C, Mezger K (2006) Lithium isotope compositions of Martian and lunar reservoirs. Earth Planet Sci Lett 245:6–18
Shahar A, Hillgren VJ, Horan MF, Mesa-Garcia J, Kaufman LA, Mock TD (2015) Sulfur-controlled iron isotope fractionation experiments of core formation in planetary bodies. Geochim Cosmochim Acta 150:253–264
Sharp ZD, Barnes JD, Brearley AJ, Chaussidon M, Fischer TP, Kamenetsky VS (2007) Chlorine isotope homogeneity of the mantle, crust and carbonaceous chondrites. Nature 446:1062–1065
Sharp ZD, Shearer CK, McKeegan KD, Barnes JD, Wang YQ (2010) The chlorine isotope composition of the Moon and implications for an anhydrous mantle. Science 329:1050–1053
Sharp ZD, McCubbin FM, Shearer CK (2013a) A hydrogen-based oxidation mechanism relevant to planetary formation. Earth Planet Sci Lett 380:88–97
Sharp ZD, Mercer JA, Jones RH, Brearley AJ, Selverstone J, Bekker A, Stachel T (2013b) The chlorine isotope composition of chondrites and Earth. Geochim Cosmochim Acta 107:189–204
Shearer CK, Papike JJ (2005) Early crustal building processes on the Moon: models for the petrogenesis of the magnesian suite. Geochim Cosmochim Acta 69:3445–3461

Shearer CK, Hess PC, Wieczorek MA, Pritchard ME, Parmentier EM, Borg LE, Longhi J, Elkins-Tanton LT, Neal CR, Antonenko I, Canup RM, Halliday AN, Grove TL, Hager BH, Lee DC, Wiechert U, Jolliff BL (2006) Thermal and magmatic evolution of the Moon. Rev Mineral Geochem 60:365–518

Shearer CK, Burger PV, Guan Y, Papike JJ, Sutton SR, Atudorei NV (2012) Origin of sulfide replacement textures in lunar breccias. Implications for vapor element transport in the lunar crust. Geochim Cosmochim Acta 83:138–158

Shearer CK, Sharp ZD, Burger PV, McCubbin FM, Provencio PP, Brearley AJ, Steele A (2014) Chlorine distribution and its isotopic composition in "rusty rock" 66095. Implications for volatile element enrichments of "rusty rock" and lunar soils, origin of "rusty" alteration, and volatile element behavior on the Moon. Geochim Cosmochim Acta 139:411–433

Shearer CK, Elardo SM, Petro NE, Borg LE, McCubbin FM (2015a) Origin of the lunar highlands Mg-suite: An integrated petrology, geochemistry, chronology, and remote sensing perspective. Am Mineral 100:294–325

Shearer CK, Burger PV, Bell AS, Guan YB, Neal CR (2015b) Exploring the Moon's surface for remnants of the lunar mantle 1. Dunite xenoliths in mare basalts. A crustal or mantle origin? Meteorit Planet Sci 50:1449–1467

Shearer C, Neal CR, Glotch TD, Prissel TC, Bell AS, Assis Fernandes V, Gaddis LR, Jolliff BL, Laneuville M, Magna T, Simon J (2023) Magmatic evolution II: A new view of post-differentiation magmatism. Rev Mineral Geochem 89:147–205

Shervais JW, McGee JJ (1998) Ion and electron microprobe study of troctolites, norite, and anorthosites from Apollo 14: Evidence for urKREEP assimilation during petrogenesis of Apollo 14 Mg-suite rocks. Geochim Cosmochim Acta 62:3009–3023

Singer JA, Greenwood JP, Itoh S, Sakamoto N, Yurimoto H (2017) Evidence for the solar wind in lunar magmas: A study of slowly cooled samples of the Apollo 12 olivine basalt suite. Geochem J 51:95–104

Sio CK, Borg LE, Cassata WS (2020) The timing of lunar solidification and mantle overturn recorded in ferroan anorthosite 62237. Earth Planet Sci Lett 538:116219

Smith JV, Anderson AT, Newton RC, Olsen EJ, Wyllie PJ (1970) A petrologic model for the Moon based on petrogenesis, experimental petrology, and physical properties. J Geology 78:381–405

Snyder GA, Taylor LA, Neal CR (1992) A chemical model for generating the sources of mare basalts: combined equilibrium and fractional crystallization of the lunar magmasphere. Geochim Cosmochim Acta 56:3809–3823

Snyder GA, Neal CR, Taylor LA, Halliday AN (1995) Processes involved in the formation of the magnesian-suite plutonic rocks from the highlands of the Earth's Moon. J Geophys Res: Planets 100:9365–9388

Sossi PA, Moynier F (2017) Chemical and isotopic kinship of iron in the Earth and Moon deduced from the lunar Mg-Suite. Earth Planet Sci Lett 471:125–135

Sossi PA, Moynier F, van Zuilen K (2018) Volatile loss following cooling and accretion of the Moon revealed by chromium isotopes. PNAS 115:10920–10925

Spohn T, Konrad W, Breuer D, Ziethe R (2001) The longevity of lunar volcanism: Implications of thermal evolution calculations with 2D and 3D mantle convection models. Icarus 149:54–65

Spudis PD, Martin DJP, Kramer G (2014) Geology and composition of the Orientale Basin impact melt sheet. J Geophys Res: Planets 119:19–29

Staid MI, Pieters CM, Besse S, Boardman J, Dhingra D, Green RO, Head JW, Isaacson P, Klima RL, Kramer G (2011) The mineralogy of late stage lunar volcanism as observed by the Moon Mineralogy Mapper on Chandrayaan-1. J Geophys Res: Planets 116:E00G10

Stephant A, Robert F (2014) The negligible chondritic contribution in the lunar soils water. Proc Nat Acad Sci USA 111:15007–15012

Stöffler D, Ryder G, Ivanov BA, Artemieva NA, Cintala MJ, Grieve RA (2006) Cratering history and lunar chronology. Rev Min Geochem 60:519–596

Strain PL, El-Baz F (1980) The geology and morphology of Ina. Proc 11th Lunar Planet Sci Conf 2437–2446

Sun Y, Li L, Zhang YZ (2017) Detection of Mg-spinel bearing central peaks using M^3 images: Implications for the petrogenesis of Mg-spinel. Earth Planet Sci Lett 465:48–58

Sunshine J, Besse S, Petro N, Pieters C, Head J, Taylor L, Klima R, Isaacson P, Boardman J, Clark R (2010) Hidden in plain sight: Spinel-rich deposits on the nearside of the Moon as revealed by Moon Mineralogy Mapper (M^3). 41st Lunar Planet Sci Conf Abst #1508

Takeda H, Yamaguchi A, Bogard DD, Karouji Y, Ebihara M, Ohtake M, Saiki K, Arai T (2006) Magnesian anorthosites and a deep crustal rock from the farside crust of the moon. Earth Planet Sci Lett 247:171–184

Tartèse R, Anand M (2013) Late delivery of chondritic hydrogen into the lunar mantle: Insights from mare basalts. Earth Planet Sci Lett 361:480–486

Tartèse R, Anand M, Barnes JJ, Starkey NA, Franchi IA, Sano Y (2013) The abundance, distribution, and isotopic composition of Hydrogen in the Moon as revealed by basaltic lunar samples: implications for the volatile inventory of the Moon. Geochim Cosmochim Acta 122:58–74

Tartèse R, Anand M, McCubbin FM, Elardo SM, Shearer CK, Franchi IA (2014a) Apatites in lunar KREEP basalts: The missing link to understanding the H isotope systematics of the Moon. Geology 42:363–366

Tartèse R, Anand M, Joy KH, Franchi IA (2014b) H and Cl isotope systematics of apatite in brecciated lunar meteorites Northwest Africa 4472, Northwest Africa 773, Sayh al Uhaymir 169, and Kalahari 009. Meteorit Planet Sci 49:2266–2289

Taylor SR, Jakeš P (1974) The geochemical evolution of the Moon. Proc 5th Lunar Sci Conf 1287–1305

Taylor LA, Mao HK, Bell PM (1973) "Rust" in the Apollo 16 rocks. Proceedings 4th Lunar Sci Conf 829–839
Taylor LA, Mao H, Bell P (1974) Identification of the hydrated iron oxide mineral akaganéite in Apollo 16 lunar rocks. Geology 2:429–432
Taylor G, Warner R, Keil K, Ma M-S, Schmitt R (1980) Silicate liquid immiscibility, evolved lunar rocks and the formation of KREEP. Conf Lunar Highlands Crust, p 339–352
Teng F-Z (2017) Magnesium isotope geochemistry. Rev Min Geochem 82:219–287
Tian Z, Jolliff BL, Korotev RL, Fegley B, Lodders K, Day JMD, Chen H, Wang K (2020) Potassium isotopic composition of the Moon. Geochim Cosmochim Acta 280:263–280
Tian HC, Wang H, Chen Y, Yang W, Zhou Q, Zhang C, Lin HL, Huang C, Wu ST, Jia LH, Xu L (2021) Non-KREEP origin for Chang'e-5 basalts in the Procellarum KREEP Terrane. Nature 600:59–63
Tomascak PB, Magna T, Dohmen R (2016) Advances in Lithium Isotope Geochemistry. Springer
Tompkins S, Pieters CM (1999) Mineralogy of the lunar crust: Results from Clementine. Meteorit Planet Sci 34:25–41
Tompkins S, Pieters CM (2010) Spectral characteristics of lunar impact melts and inferred mineralogy. Meteorit Planet Sci 45:1152–1169
Tran T, Robinson M, Lawrence S, Braden S, Plescia J, Hawke B, Jolliff B, Stopar J, Team L (2011) Morphometry of lunar volcanic domes from LROC. 42nd Lunar Planetary Sci Conf Abst #2228
Treiman AH, Gross J (2015) A rock fragment related to the magnesian suite in lunar meteorite Allan Hills (ALHA) 81005. Am Mineral 100:414–426
Treiman AH, Maloy AK, Shearer CK, Gross J (2010) Magnesian anorthositic granulites in lunar meteorites Allan Hills A81005 and Dhofar 309: Geochemistry and global significance. Meteorit Planet Sci 45:163–180
Treiman AH, Boyce JW, Gross J, Guan YB, Eiler JM, Stolper EM (2014) Phosphate—halogen metasomatism of lunar granulite 79215: Impact-induced fractionation of volatiles and incompatible elements. Am Mineral 99:1860–1870
Treiman AH, Boyce JW, Greenwood JP, Eiler JM, Gross J, Guan YB, Ma C, Stolper EM (2016) D-poor hydrogen in lunar mare basalts assimilated from lunar regolith. Am Mineral 101:1596–1603
Treiman AH, Kulis MEJ, Glazner AF (2019) Spinel-anorthosites on the Moon: Impact melt origins suggested by enthalpy constraints. Am Mineral 104:370–384
Uemoto K, Ohtake M, Haruyama J, Matsunaga T, Yamamoto S, Nakamura R, Yokota Y, Ishihara Y, Iwata T (2017) Evidence of impact melt sheet differentiation of the lunar South Pole-Aitken basin. J Geophys Res: Planets 122:1672–1686
Ustunisik G, Nekvasil H, Lindsley DH (2011) Differential degassing of H_2O, Cl, F, and S: Potential effects on lunar apatite. Am Mineral 96:1650–1653
Ustunisik G, Nekvasil H, Lindsley DH, McCubbin FM (2015) Degassing pathways of Cl-, F-, H-, and S-bearing magmas near the lunar surface: Implications for the composition and Cl isotopic values of lunar apatite. Am Mineral 100:1717–1727
Valley JW, Cavosie AJ, Ushikubo T, Reinhard DA, Lawrence DF, Larson DJ, Clifton PH, Kelly TF, Wilde SA, Moser DE (2014) Hadean age for a post-magma-ocean zircon confirmed by atom-probe tomography. Nat Geosci 7:219–223
Vander Kaaden KE, McCubbin FM (2015) Exotic crust formation on Mercury: Consequences of a shallow, FeO-poor mantle. J Geophys Res: Planets 120:195–209
Vaughan WM, Head JW (2014) Impact melt differentiation in the South Pole-Aitken basin: Some observations and speculations. Planet Space Sci 91:101–106
Vaughan WM, Head JW, Wilson L, Hess PC (2013) Geology and petrology of enormous volumes of impact melt on the Moon: A case study of the Orientale basin impact melt sea. Icarus 223:749–765
Wagner R, Head J, Wolf U, Neukum G (2002) Stratigraphic sequence and ages of volcanic units in the Gruithuisen region of the Moon. J Geophys Res: Planets 107:5104
Wagner R, Head J, Wolf U, Neukum G (2010) Lunar red spots: Stratigraphic sequence and ages of domes and plains in the Hansteen and Helmet regions on the lunar nearside. J Geophys Res: Planets 115(E11):E06015
Walcek H, Jolliff B, Zanetti M (2016) Volumes of volcanic constructs at the Compton-Belkovich Volcanic Complex on the Moon. 47th Lunar Planet Sci Conf Abst #2933
Wang K, Jacobsen SB (2016) Potassium isotopic evidence for a high-energy giant impact origin of the Moon. Nature 538:487–490
Wang K, Jacobsen SB, Sedaghatpour F, Chen H, Korotev RL (2015) The earliest Lunar Magma Ocean differentiation recorded in Fe isotopes. Earth Planet Sci Lett 430:202–208
Wang X, Zhang X, Wu K (2016) Thorium distribution on the lunar surface observed by Chang'E-2 gamma-ray spectrometer. Astrophys Space Sci 361:234
Warner J, Phinney W, Bickel C, Simonds C (1977) Feldspathic granulitic impactites and pre-final bombardment lunar evolution. Proc 8th Lunar Planet Sci Conf 2051–2066
Warren PH (1990) Lunar anorthosites and the magma-ocean plagioclase-flotation hypothesis—Importance of FeO enrichment in the parent magma. Am Mineral 75:46–58
Warren PH (1993) A Concise compilation of petrologic information on possibly pristine nonmare Moon rocks. Am Mineral 78:360–376
Warren PH (1994) Lunar and martian meteorite delivery services. Icarus 111:338–363
Warren PH, Kallemeyn GW (1993) Geochemical investigation of two lunar mare meteorites: Yamato-793169 and Asuka-881757. Antarctic Meteorit Res 6:35

Warren P, Wasson J (1980) Early lunar petrogenesis, oceanic and extraoceanic. Proc Conf Lunar Highlands Crust:81–99
Watson E, Harrison T (2005) Zircon thermometer reveals minimum melting conditions on earliest Earth. Science 308:841–844
Webster JD, Goldoff BA, Flesch RN, Nadeau PA, Silbert ZW (2017) Hydroxyl, Cl, and F partitioning between high-silica rhyolitic melts–apatite–fluid(s) at 50–200 MPa and 700–1000 °C. Am Mineral 102:61–74
Weitz CM, Head III JW, Pieters CM (1998) Lunar regional dark mantle deposits: Geologic, multispectral, and modeling studies. J Geophys Res: Planets 103:22725–22759
Weitz CM, Staid MI, Gaddis LR, Besse S, Sunshine JM (2017) Investigation of lunar spinels at Sinus Aestuum. J Geophys Res: Planets 122:2013–2033
Wetzel DT, Hauri EH, Saal AE, Rutherford MJ (2015) Carbon content and degassing history of the lunar volcanic glasses. Nat Geosci 8:755–758
Weyer S, Woodland A, Munker C, Arnold GL, Chakrabarti R, Anbar AD (2004) Iron isotope variations in the Earth's mantle and the terrestrial planets. Geochim Cosmochim Acta 68:A736–A736
Weyer S, Anbar AD, Brey GP, Munker C, Mezger K, Woodland AB (2005) Iron isotope fractionation during planetary differentiation. Earth Planet Sci Lett 240:251–264
Whitaker EA (1972a) Lunar color boundaries and their relationship to topographic features: A preliminary survey. The Moon 4:348–355
Whitaker EA (1972b) An unusual mare feature. Apollo 15: Preliminary Science Report 289
White LF, Cernok A, Darling JR, Whitehouse MJ, Joy KH, Cayron C, Dunlop J, Tait KT, Anand M (2020) Evidence of extensive lunar crust formation in impact melt sheets 4,330 Myr ago. Nat Astronom 4:974–978
Wieczorek MA, Phillips RJ (2000) The "Procellarum KREEP Terrane": Implications for mare volcanism and lunar evolution. J Geophys Res 105:20,417–20,430
Wieczorek MA, Jolliff BL, Khan A, Pritchard ME, Weiss BP, Williams JG, Hood LL, Righter K, Neal CR, Shearer CK, McCallum IS, Tompkins S, Hawke BR, Peterson C, Gillis JJ, Bussey B (2006) The constitution and structure of the lunar interior. Rev Min Geochem 60:221–364
Wieczorek MA, Neumann GA, Nimmo F, Kiefer WS, Taylor GJ, Melosh HJ, Phillips RJ, Solomon SC, Andrews-Hanna JC, Asmar SW, Konopliv AS, Lemoine FG, Smith DE, Watkins MM, Williams JG, Zuber MT (2013) The Crust of the Moon as Seen by GRAIL. Science 339:671–675
Wiesli RA, Beard BL, Taylor LA, Johnson CM (2003) Space weathering processes on airless bodies: Fe isotope fractionation in the lunar regolith. Earth Planet Sci Lett 216:457–465
Wilde SA, Valley JW, Peck WH, Graham CM (2001) Evidence from detrital zircons for the existence of continental crust and oceans on the Earth 4.4 Gyr ago. Nature 409:175
Wilson L, Head JW (2017) Eruption of magmatic foams on the Moon: Formation in the waning stages of dike emplacement events as an explanation of "irregular mare patches". J Volcano Geotherm Res 335:113–127
Wilson L, Head J (2018) Controls on lunar basaltic volcanic eruption structure and morphology: Gas release patterns in sequential eruption phases. Geophys Res Lett 45:5852–5859
Wilson J, Eke V, Massey R, Elphic R, Jolliff B, Lawrence D, Llewellin E, McElwaine J, Teodoro L (2015) Evidence for explosive silicic volcanism on the Moon from the extended distribution of thorium near the Compton–Belkovich Volcanic Complex. J Geophys Res: Planets 120:92–108
Wimpenny J, Borg L, Sanborn M, Yin Q-Z (2018) Investigating the Zn isotopic composition of mare basalts: Implications for Zn systematics on the Moon. 49th Lunar Planet Sci Conf Abst #2593
Wimpenny J, Marks N, Knight K, Rolison JM, Borg LE, Eppich G, Badro J, Ryerson FJ, Sanborn M, Huyskens MH, Yin QZ (2019) Experimental determination of Zn isotope fractionation during evaporative loss at extreme temperatures. Geochim Cosmochim Acta 259:391–411
Wing BA, Farquhar J (2015) Sulfur isotope homogeneity of lunar mare basalts. Geochim Cosmochim Acta 170:266–280
Wood JA, Dickey JS, Marvin UB, Powell BN (1970) Lunar anorthosites. Science 167:602–604
Xiao L, Zhu P, Fang G, Xiao Z, Zou Y, Zhao J, Zhao N, Yuan Y, Qiao L, Zhang X (2015) A young multilayered terrane of the northern Mare Imbrium revealed by Chang'E-3 mission. Science 347:1226–1229
Yamamoto S, Nakamura R, Matsunaga T, Ogawa Y, Ishihara Y, Morota T, Hirata N, Ohtake M, Hiroi T, Yokota Y, Haruyama J (2010) Possible mantle origin of olivine around lunar impact basins detected by SELENE. Nat Geosci 3:533–536
Yamamoto S, Nakamura R, Matsunaga T, Ogawa Y, Ishihara Y, Morota T, Hirata N, Ohtake M, Hiroi T, Yokota Y (2012a) Olivine-rich exposures in the South Pole-Aitken basin. Icarus 218:331–344
Yamamoto S, Nakamura R, Matsunaga T, Ogawa, Y, Ishihara, Y, Morota, T, Hirata, N, Ohtake, M, Hiroi, T, Yokota, Y, Haruyama, J (2012b) Massive layer of pure anorthosite on the Moon. Geophys Res Lett 39:L13201
Yamamoto S, Nakamura R, Matsunaga T, Ogawa Y, Ishihara Y, Morota T, Hirata N, Ohtake M, Hiroi T, Yokota Y (2013) A new type of pyroclastic deposit on the Moon containing Fe-spinel and chromite. Geophys Res Lett 40:4549–4554
Yamamoto S, Nakamura R, Matsunaga T, Ogawa Y, Ishihara Y, Morota T, Hirata N, Ohtake M, Hiroi T, Yokota Y, Haruyama J (2015) Featureless spectra on the Moon as evidence of residual lunar primordial crust. J Geophys Res: Planets 120:2190–2205
Yue Z, Johnson BC, Minton DA, Melosh HJ, Di K, Hu W, Liu Y (2013) Projectile remnants in central peaks of lunar impact craters. Nat Geosci 6:435–437

Zambardi T, Poitrasson F, Corgne A, Meheut M, Quitte G, Anand M (2013) Silicon isotope variations in the inner solar system: Implications for planetary formation, differentiation and composition. Geochim Cosmochim Acta 121:67–83

Zeigler RA, Korotev RL, Jolliff BL, Haskin LA (2005) Petrography and geochemistry of the LaPaz Icefield basaltic lunar meteorite and source crater pairing with Northwest Africa 032. Meteorit Planet Sci 40:1073–1101

Zhang Y, Ni H (2010) Diffusion of H, C, and O components in silicate melts. Rev Min Geochem 72:171–225

Zhang YX, Stolper EM (1991) Water diffusion in a basaltic melt. Nature 351:306–309

Zhang YX, Ni HW, Chen Y (2010) Diffusion data in silicate melts. Rev Min Geochem 72:311–408

Zhuqing X, Long L, Clive R (2018) Xenocryst origin of pyroxene and plagioclase in enriched high-Ti basalt clast from lunar meteorite Dhofar 1428. 49th Lunar Planet Science Conf Abst #1393

Ziethe R, Seiferlin K, Hiesinger H (2009) Duration and extent of lunar volcanism: Comparison of 3D convection models to mare basalt ages. Planet Space Sci 57:784–796